Synthesis and study of thiophene based semiconducting small molecules for photovoltaic application

THESIS SUBMITTED TO ACADEMY OF SCIENTIFIC AND INNOVATIVE

RESEARCH (**AcSIR**) FOR THE AWARD OF THE DEGREE OF

DOCTOR OF PHILOSOPHY IN CHEMISTRY

UNDER THE FACULTY OF SCIENCE

By
JAYANTHY S. PANICKER
Enrollment No: 10CC14J39004

Under the Supervision of
Dr. VIJAYAKUMAR C.

PHOTOSCIENCES AND PHOTONICS SECTION

CHEMICAL SCIENCES AND TECHNOLOGY DIVISION

CSIR-NATIONAL INSTITUTE FOR INTERDISCIPLINARY

SCIENCE AND TECHNOLOGY (CSIR-NIIST)

THIRUVANANTHAPURAM - 695019, KERALA

September 2019

DECLARATION

I hereby declare that the matter embodied in the Ph.D. thesis entitled: **"Synthesis and study of thiophene based semiconducting small molecules for photovoltaic application"** is the result of an independent work carried out by me at the Photosciences and Photonics Section, Chemical Sciences and Technology Division of the CSIR – National Institute for Interdisciplinary Science and Technology (CSIR-NIIST), Thiruvananthapuram, under the supervision of Dr. Vijayakumar C. and the same has not been submitted elsewhere for any other degree or diploma.

In keeping with the general practice of reporting scientific observations, research materials obtained from other investigations has been duly cited and acknowledged in the thesis.

Jayanthy S. Panicker

Thiruvananthapuram
August 23, 2019

i

National Institute for Interdisciplinary Science and Technology (NIIST)
Council of Scientific and Industrial Research, Thiruvananthapuram – 695 019, INDIA
Dr. Vijayakumar C., PhD
Senior Scientist, Photosciences and Photonics Section, CSTD
Tel: +91-471-2515-484; E-mail: cvijayakumar@niist.res.in

August 23, 2019

CERTIFICATE

This is to certify that the work embodied in the thesis entitled: "**Synthesis and study of thiophene based semiconducting small molecules for photovoltaic application**" has been carried out by Ms. Jayanthy S. Panicker under my supervision and guidance at the Photosciences and Photonics Section, Chemical Sciences and Technology Division of the CSIR – National Institute for Interdisciplinary Science and Technology, Thiruvananthapuram and the same has not been submitted elsewhere for a degree.

Dr. Vijayakumar C.

(Thesis Supervisor)

Jayanthy S. Panicker

ACKNOWLEDGEMENTS

CONTENTS

PREFACE

Organic semiconductors (OSCs) consists of π-conjugated small molecules and polymers have been a subject of great interest among the scientific community. Properties of OSCs such as processability and easy functionalization make them promising candidates for optical and electronic devices such as solar cells, field-effect transistors, light-emitting diodes, photodetectors, memories, etc. Structural engineering is the best way to tune the properties and improve the device performances of OSCs. The present thesis is a collection of works on thiophene based OSCs and their application in solar cell devices. The thesis is organized into five chapters. The first chapter gives an overview of the significance, design strategies, and applications of OSCs. The major scope and objectives of the thesis are briefly outlined at the end of the chapter.

Chapter 2 describes the design and synthesis of three novel semiconducting oligomers with n-type characteristics. Three oligomers were made of thiophene-based donors, bithiazole as spacer and rhodanine based acceptors using Suzuki and Stille coupling. Oligomers exhibited excellent absorption in the visible region because of the π-π* transition as well as intramolecular charge transfer between the donor and acceptor moieties. The packing of oligomers in the film state was studied using 2D grazing incidence X-ray diffraction (GIXRD) analysis and the percentage of edge-on orientation was found to be greater compared to face-on orientation in all three oligomers. HOMO and LUMO energy levels of the

oligomers in film state were calculated from ultraviolet photoelectron yield spectroscopy analysis and the onset of absorption spectrum, respectively. Detailed time-resolved microwave conductivity experiments proved that the oligomers can act as n-type materials making these oligomers are promising for optoelectronic device applications.

Third chapter deals with the design and synthesis of a dye, and two co-adsorbents for DSSC (dye sensitized solar cell) application. A new molecule consisting of a bithiazole chromophore sandwiched between two thiophenes, functionalized with benzothiophene unit at one end and cyanoacrylic acid acceptor at the other end was synthesized, photophysical properties were studied and employed as a photosensitizer in DSSC. The effect of various co-adsorbents on the device performance were investigated in detail.

The fourth chapter describes the synthesis of triphenylamine-bithiazole based two metal-free organic dyes employing D-π-A strategy for DSSCs. The dyes showed structural similarity with respect to donor and π bridge, but differed in the acceptor/anchoring group *viz*., cyanoacrylic acid and rhodanine 3-acetic acid. The photophysical, electrochemical and photovoltaic properties of the dyes were investigated in detail. The IPCE spectrum exhibited a wide range of absorption extending up to 600 nm. A co-adsorbent, CDCA, was employed to enhance the efficiency by preventing π-π stacking interactions. Fundamental insight into the charge

transfer processes occurring in the devices was studied by electrochemical impedance spectroscopy (EIS), which is in agreement with the device characteristics.

The last chapter deals with three triphenylamine-rhodanine acetic acid based metal-free organic dyes consisting of thiophene, bithiophene and thienothiophene spacers flanked by alkylated thiophenes on both sides and rhodamine-acetic acid as anchoring group. The dyes were designed and synthesized employing the D-π-A strategy. The effect of the electron donor spacer units on the optoelectronic properties of the dyes were studied in detail, and applied them in DSSCs devices. All the dyes showed broad absorption band in the UV-vis region from 250-750 nm. EIS measurements indicated that the device sensitized by the compound having thiophene as the spacer exhibited the largest resistance for recombination between the electrons injected to TiO_2 and electrolyte leading to a better photovoltaic efficiency compared to other two dyes.

LIST OF ABBREVIATIONS

1. AM – Air Mass

2. Å – Angstrom

3. Ar – Argon

4. AcOH – Acetic Acid

5. BDD – Benzodithiophenedione

6. BDT – Benzodithiophene

7. BHJ – Bulk heterojunction

8. B3LYP – Becke 3-parameter, Lee-Yang-Parr

9. BMII – 1-butyl-3-methylimidazolium iodide

10. CIGS – Copper indium gallium selenide

11. CV – Cyclic voltammetry

12. ^{o}C – Degree Celsius

13. $CDCl_3$ – Deuterated chloroform

14. CH_3CN – Acetonitrile

15. Calcd. – Calculated

16. CDCA – Chenodeoxycholic acid

17. DIO – 1,8-Diiodooctane

18. DPP – Diketopyrrolopyrrole

19. DFT – Density Functional Theory

20. DCM – Dichloromethane

21. DMSO – Dimethyl sulfoxide

22. DMF – Dimethylformamide

23.   EIS – Electrochemical impedance spectroscopy

24.   Eg – Bandgap

25.   ETL – Electron transport layer

26.   EQE – External quantum efficiency

27.   *et al. – Et allii/alia*

28.   ε – Molar extinction coefficient

29.   eV – Electron Volt

30.   FET – Field-effect transistor

31.   FTIR – Fourier-transform infrared spectroscopy

32.   FTO – Fluorine-doped tin oxide

33.   FP-TRMC – Flash photolysis time-resolved microwave conductivity

34.   *FF* – Fill factor

35.   g – Gram

36.   GIXRD – Grazing incidence X-ray diffraction

37.   GuSCN – Guanidinium thiocyanate

38.   HR-MS – High resolution mass spectrometry

39.   h – Hour

40.   HOMO – Highest occupied molecular orbital

41.   HCl – Hydrochloric acid

42.   HTL – Hole transport layer

43. I_2 – Iodine

44.   ICT – Intramolecular charge transfer

45.   IPCE – Incident photon-to-current conversion efficiency

46.   IR – Infrared

47. I_{SC} – Short circuit current

48.   ITO – Indium tin oxide

49. J_{SC} – Short circuit current density

50.   K – Kelvin

51.   LiI – Lithium iodide

52.   LUMO – Lowest unoccupied molecular orbital

53.   LC – Liquid crystalline

54. λ_{max} – Wavelength maximum

55.   MW – Molecular weight

56.   MALDI-TOF – Matrix-assisted laser desorption/ionization time of flight

57.   M – Molar

58.   MIS – Metal-insulator-semiconductor

59.   mg – Milligram

60.   mL – Millilitre

61.   MLCT – Metal to ligand charge transfer

62.   µM – Micromolar

63.   µs – Microseconds

64.   µm – Micrometer

65.   mM – Millimolar

66.   mmol – Millimole

67.   NT – Naphtho[1,2-*c*:5.6-*c'*] bis [1,2,5]thiadizole

68.   NBS – *N*-bromosuccinimide

69.   NIR – Near infrared

70.   nm – Nanometer

71. NMR – Nuclear magnetic resonance

72. ns – Nanosecond

73. OCVD – Open circuit voltage decay

74. OSC – Organic semiconductors

75. P3AT – Poly-3-alkyl thiophene

76. P3HT – Poly-3-hexyl thiophene

77. PBI – Perylenebismide

78. PS – Polystyrene

79. P_{max} – Maximal power

80. P_{in} – Power input

81. PEDOT:PSS – Poly(3,4- ethylenedioxythiophene)polystyrenesulfonate

82. PCE – Power conversion efficiency

83. $PC_{71}BM$ – [6,6]-Phenyl-C_{71}-butyric acid methyl ester

84. $PC_{61}BM$ – [6,6]-Phenyl-C_{61}-butyric acid methyl ester

85. PDI – Perylene diimide

86. PV – Photovoltaic

87. PYS – Photoelectron yield spectroscopy

88. PHJ – Planar heterojunction

89. PL – Photoluminescence

90. Φ_F – Quantum yields of fluorescence

91. s – Seconds

92. Si – Silicon

93. SQ – Squaraine

94. TBP – 4-*tert*-butyl pyridine

Chapter 1

Organic semiconductors for photovoltaic applications: An overview

1.1. Abstract

Organic semiconductors (OSCs) are one of the promising candidates for optoelectronic devices such as solar cells, field-effect transistors, light-emitting diodes, photodetectors, memories, etc. The main advantage of these materials is that they can be easily functionalized to make them solution processable for device fabrication instead of expensive techniques like vacuum deposition or lithography being used for silicon-based materials, thus making the devices highly cost-effective. The essential criterion for the good performance of the OSCs in devices is the high charge carrier mobility. The charge carrier mobility of the OSCs has been improved by five orders of magnitude over the last few years. Development of new materials is needed in this field for the further advancements, which can be achieved by the rational molecular designing. The first chapter gives an overview of OSCs and their application in photovoltaic devices.

1.2. Introduction

Organic materials with carbon-carbon bonds conduct electrons in the same way as inorganic semiconductors are termed as organic semiconductors. OSCs have been a subject of intense academic interest for the past few decades because of their applications in optical and electronic devices such as solar cells, field-effect transistors, light-emitting diodes, photodetectors, memories, etc.[1-6] The π-conjugated backbone forms the active component of the OSC devices. Delocalised π-orbitals originates from the π-conjugated bonds remarkably affect the optoelectronic properties. Structure-property relationships determine the performance of these materials in photovoltaic devices, which governs the physics and chemistry of OSCs. The major breakthrough in the field of OSCs was the discovery of high conductivity in doped polyacetylene in 1977 by Heeger, Macdiarmid and Shirakawa.[7] They have honoured with Nobel prize in Chemistry in the year 2000 for this. Their studies revealed that organic molecules are competant materials for transporting current and doping can significantly improve the conductivity, which make them suitable for device applications.

Structural engineering of OSCs alllows the incorporation of various functinalities into the molecular design leading to the structural versatility, which in turn enhance the performance of electronic devices.[8-10] Simple solution

processability of OSCs make them suitable for fabricatiing low-cost, large area devices with structural flexibility. Performance of OSC based devices mainly depends on the generation and movement of charge carriers (electrons and holes) along the π-conjugated bonds. Development of OSCs with functional applications can be achieved through synthetic organic chemistry. In the context of photovoltaics, OSCs are mostly used in the third generation technology. In this chapter, we describe the basics of third generation solar cells and an overview of OSCs used in these devices.

1.3. Third generation solar cell devices

Large scale production of clean energy is the major challenge faced by the current society. In the coming years, the modern standard of living in a raising world population would increase the consumption of energy dramatically. Generating power from the sun through photovoltaics is found to be an attractive solution to address this issue. It was assessed that the amount of solar energy radiations fall on the earth per hour (1.4×10^{30} J) is greater than the energy required by the world population per year.[1]

Alexandre Edmond Becquerel discovered the phenomenon of photovoltaic effect in 1839.[11] He observed the generation of photocurrent when a platinum electrode covered with silver halide was illuminated in aqueous solution

(electrochemical cell). Observations of photovoltaic effect forms the basis for different concepts of solar energy conversion methods and create a new era of clean energy generation. For efficient functioning of the solar cells, it should absorb a range of the solar spectrum. The wavelength of the solar spectrum ranges from 100 nm to 1 mm. But highest solar irradiance occurs in the visible region (400-740 nm; **Figure 1.1a**). Thus for harvesting maximum photons, materials used in the solar cells should cover the visible and the near-IR region.[12] The path length taken by the light passes through the atmosphere normalized to the shortest possible path length is called the Air Mass (AM). Definition of AM is given by, $AM = \dfrac{1}{\cos\theta}$ where θ is called the zenith angle (the angle from the vertical). The AM is 1 when the sun is directly overhead (**Figure 1.1b**).

a)

b)
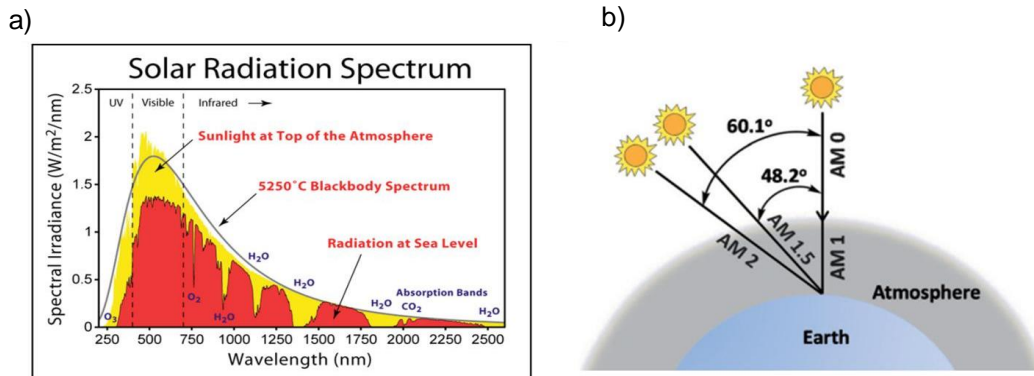
Figure 1.1 a) Solar irradiance spectrum, b) Schematic representation of the path length, in units of Air Mass, and its dependence on the zenith angle. (adapted from ref.1)

Conventional solar cells or the first generation of solar cells are based on silicon (Si). The first Si solar cell was developed by Bell Laboratories in 1954 with an efficiency of 6%. In terms of single-junction photovoltaic devices, silicon solar cells are the most efficient, and silicon is the second most abundant element on earth. The band gap of Si is 1.1 eV, suitable for photovoltaic application. The current photovoltaic market is dominated by Si-based solar cells (about 90% of market share). Second generation solar cells are based on amorphous Si, CIGS and CdTe. These cells are also called thin-film solar cells. Solar cells of the first and second generation are based on single junction devices. Thermodynamic efficiency in a single junction device is found to be about 31%, which is called the Shockley - Queisser limit. In single junction device, absorption of individual photon results in the formation of a single electron-hole pair and all photons exceeding the energy gap lost as heat energy. In the case of first and second generation solar cells, the production cost is very high. In the case of second generation solar cells, additional drawbacks are the toxicity and low abundance of the materials.[13]

The first two generations of solar cells don't transform the solar energy with the expected qualities such as lower production and energy cost. To overcome these issues, researchers developed the third generation solar cells. The concept of third generation photovoltaic is to considerably increase the device efficiency

while using thin film processes and low cost materials having no toxicity. Using multiple energy threshold approaches, this can be achieved by overcoming the Shockley - Queisser limit for single-band gap devices.[14] Different approaches to improve the efficiency above 31% are tandem cells, hot carrier cells, multi-exciton generation, multiband cells, and thermo-photovoltaics.

The main objective of solar cells of the third generation is to supply electricity at a competitive cost on a big scale. This implies the use efficient solar cells that can be generated through methods which allow easy mass production. By implementation of these concepts, production of photovoltaic devices would be the cheapest technique for clean energy production. The present state of the art shows a vibrant growth in recent years in terms of evolving photovoltaic techniques. Third generation solar cells include organic, dye-sensitized and perovskite photovoltaics. Organic and dye-sensitized solar cells are the main players in the context of commercialization of third generation technologies.

In organic solar cells, active layer used is organic small molecule or oligomer or polymer materials which facilitate solution processability and device flexibility. The major reason for increasing interest from both academy and industry in organic based third generation technology is attributed to the ability to significantly modify the chemical and physical properties of organic

compounds through rational molecular designing. Organic solar cells may have a bilayer structure or a bulk- heterojunction (BHJ) structure. DSSC can be regarded as hybrid device because the organic materials adsorbed on an inorganic semiconductor thin film. This thesis deals with third generation solar cell devices, particularly bulk-heterojunctions and dye-sensitized solar cells.

1.3.1. Bulk-heterojunction Solar cells
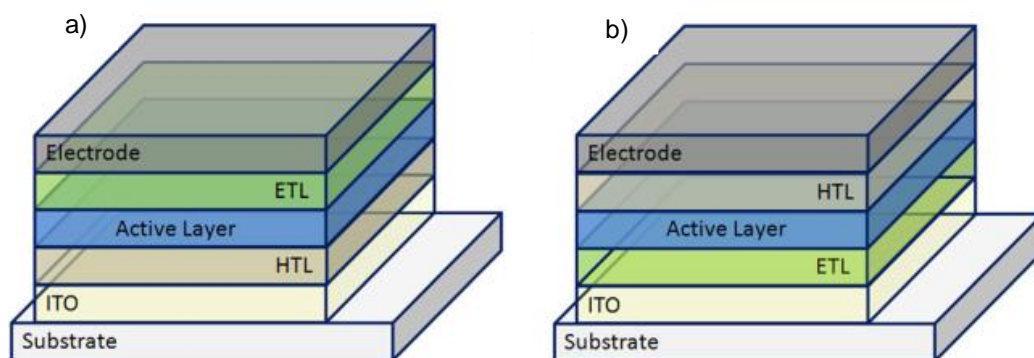
Figure 1.2 Different device architectures of BHJ solar cells. (a) Standard device design with cathode on top of the device stack and (b) inverted device architecture with cathode located on the transparent substrate. (adapted from ref. 14)

As an attractive alternative to the conventional inorganic photovoltaic devices, solution processable organic solar cells have attracted a remarkable interest. Light-weightiness, flexibility, semi-transparency, low cost, shorter processing time etc. are the main advantages of these devices.[15] In BHJ architecture, the device contains multiple layers and individually each layer can be deposited. The photoactive layer consists of two OSC materials with different

electron affinities and ionization potentials. The materials with higher electron affinity will accept the electrons and those with smaller ionization potential will accept the holes, if the potential energy difference is higher than the energy required for dissociating excitons. For effective exciton dissociation in BHJ architecture, donor and acceptor components are to create a bicontinuous interpenetration network with big interfacial sites.

For better conductivity and transparency, electrodes used in most of the reported BHJ devices are made of indium tin oxide (ITO). ITO is usually coated with poly(3,4-ethylenedioxythiophene): poly(styrenesulfonate) (PEDOT: PSS), a highly conducting organic semiconductor for charge transport. The absorber layer is placed between the anode and cathode. In BHJ device, cathode materials used are low work function metals such as calcium, aluminum, etc. To improve the performance and stability of the BHJ devices, interfacial layers such as hole transport layer (HTL) and the electron transport layer (ETL) often inserted between electrode-photoactive layer interfaces. There are two types of architectures established for BHJ: standard structure and inverted structure (shown in **Figure 1.2**). In standard device structure, the positive electrode placed on the top of the multilayer structure while in the inverted architecture, it is placed on the transparent substrate. Inverted architecture has some advantages including improved stability in ambient conditions and processing feasibility.

The first report on BHJ architecture for solar cells was by Heeger and coworkers in 1995.[16] For improving the photovoltaic properties, they have utilized the idea of intimate blending of two organic semiconductors. The material used as donor in this study was a strong light absorbing conjugated polymer, poly(2-methoxy-5-(2'-ethyl-hexyloxy)-1,4-phenylene vinylene) (MEH-PPV), **16** and the acceptor was a soluble fullerene derivative, [6]-phenyl-C61 butyric acid methyl ester (PC61BM). The blend of donor and acceptor moieties constitute the photoactive layer of BHJ solar cell. The composition of these blends have great impact on the performance of the solar cells. The concept of blending is based on the assumption that efficient electron transfer from polymer to fullerene happens in a femtosecond time scale.
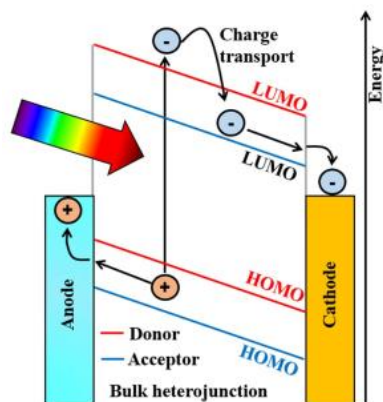
Figure 1.3 Schematic energy level diagram showing BHJ mechanism. (adapted from ref. 16)

In BHJ solar cells, fundamental steps involved in the conversion of light into electricity described as follows: (i) light absorption leading to the generation of

exciton, (ii) exciton diffusion, (iii) exciton dissociation resulting in charge carriers' generation, (iv) transport of charge carriers and (v) collection of charges at respective electrodes. Organic molecules have high absorption coefficients in the order of 10^5 cm^{-1}, so with a lower thickness of around 100-200 nm is sufficient to harvest light from the sun.[17] Light absorption by photoactive layer promotes the electron from HOMO to the LUMO and excitons (bound electron-hole pairs) are generated in the D-A blend. Diffusion of generated excitons through the photoactive layer interrupted only after reaching the interface of the D-A blend. Photoinduced charge transfer from LUMO of the donor to the LUMO of the acceptor facilitates the dissociation of the generated exciton. These photogenerated charge carriers diffused and collected at the respective electrodes rather than recombination. The binding energy of excitons is in the range of 0.3-0.4 eV. So the LUMO of the acceptor should be 0.3-0.4 eV lower than the LUMO of the donor for better charge separation. Starting from photon absorption to the charge carrier collection steps of organic solar cells is depicted in **Figure 1.3**.

1.3.2. Dye sensitized solar cells

DSSC, a highly promising third generation photovoltaic technology got its inspiration from the natural process, photosynthesis.[18] In photosynthesis,

antenna complexes harvest the sunlight and then convert it into energy by efficient charge separation through various protein centers.[19] DSSCs also absorb solar energy and transform it into electricity through a similar mechanism. A DSSC device typically consists of a transparent conductive oxide (TCO), semiconductor oxide, sensitizer dye, electrolyte and counter electrode.[20] Titanium dioxide (TiO_2) is usually used as the semiconductor in these devices. In 1960, Spitler and Calvin initially reported that the photoexcited dye molecules inject an electron into the conduction band of the n-type semiconductor substrate.[21] This gave the first experimental proof for the mechanism of DSSC. The seminal paper by O'Regan and Grätzel in 1991 first reports the modern version of DSSC.[22]
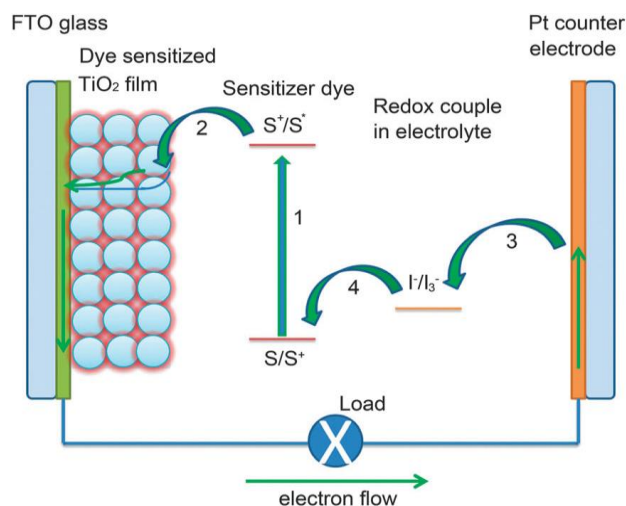
Figure 1.4 Schematic energy level diagram showing mechanism of DSSC device. (adapted from ref: 23)

In DSSC, light illumination excites the dye molecules adsorbed on TiO_2 from the ground state to the excited state.[23] The excited electrons transferred to the LUMO of the dye are injected into the TiO_2 conduction band. Electrons are then transported through the TiO_2 layer and the outer circuit to the cathode (e.g., Pt) of the DSSC. The conventionally used redox couple I^-/I_3^- reduces the oxidized dye molecule, and the cathode can regenerate the oxidized redox couple. This repeating cycle enables the DSSC to generate electric power continuously. Although p-type DSSCs have the same working principle as n-type DSSCs, a p-type semiconductor such as NiO is used as the photoelectrode (photocathode) for dye loading. Upon photo-excitation, the sensitizer injects a hole into the valence band of NiO leading to the reduction of the sensitizer. The sensitizer is regenerated from the reduced form by the redox mediator. The injected holes then diffuse through the electrode into the outer circuit and reach the counter electrode where they regenerate the reduced redox mediator. Various electron transfer processes involved in DSSC is schematically represented in **Figure 1.4**.

Sensitizers play a very significant role in the development of DSSCs because the light harvesting ability of them determines the photoelectric efficiency of the cells.[22] Organic sensitizers can be broadly classified as two major types as metal containing dyes and metal-free dyes. The dye requires some chemical group which enables its adsorption on to a metal oxide substrate (which is usually

TiO$_2$). This anchoring provides a means for electron injection from the dye to the substrate. The most important type of bonding involved between the dye and TiO$_2$ surface atoms is the covalent bond which can ensure strong coupling, a homogeneous dye distribution and device stability. More details about sensitizer dyes are included in the following section.

Redox electrolytes or redox mediators play an important role in DSSCs because they affect dye regeneration, charge recombination and consequently cell performance.[24] I$^-$/I$_3^-$ redox mediator has been widely used as the electrolyte of high performance DSSCs. The counter electrode acts as the reducing site for redox couples in the electrolyte solution or hole transporting layer in the solid-state electrolyte. The important requirement for a good counter electrode is that it should possess high conductivity for the electrons and good electro-catalytic activity for reducing the redox mediator. Platinum is the most commonly used counter electrode in DSSCs. Nowadays, other materials such as carbon, graphene and conductive polymers are also being used.[19]

High efficiency, long term stability, and low cost are the main properties required for commercializing a photovoltaic technology.[25,26] Now DSSC technology is in a position to compete with other technologies in terms of the above mentioned properties. Lab level prototypes of DSSCs shows efficiency up to 14% (32% under low-light illumination) and modules perform around 12%.[27]

For more than 20,000 h of ongoing illumination, thermal cycling and several years of indoor experiments, DSSCs showed stable efficiency. G24i Company launched the first DSSC module in the UK with a capability of 25 MW having expandable targets up to 200 MW by the end of 2008. Companies like G24i and 3GSolar are the pioneers in the field of DSSC commercializing. The outdoor aging test for DSSC shows the highest value of 2.5 years.

1.4. Organic Semiconductors

OSCs are mainly classified into two types: low molecular weight materials and polymers. In both cases, the conjugated π-electron system is formed from the trigonal hybridized p-orbitals (p_z of sp^2 hybridized orbital). The backbone of the molecular systems is constituted by the σ-bonds which are stronger than π-bonds. The π-π^* transition being the lowest energy transition with an energy gap between 1.5-3 eV results in light absorption or visible spectral emission.[28] The energy gap is the difference between energy states of HOMO and LUMO. The energy gap can be tuned by the degree of conjugation of the system or by introducing electron donating or withdrawing groups in the system. Organic chemistry, therefore, offers various of possibilities for modifying optoelectronic properties of OSCs. Molecular structures of some of the highly useful OSC materials are given in **Figure 1.5.**
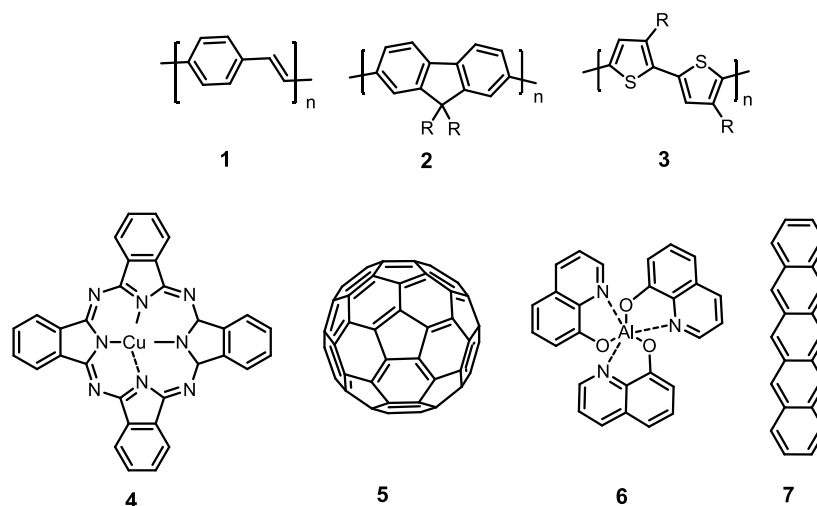
Figure 1.5 Molecular structure of OSC; **1**: PPV, **2**: PFO (R= C_6H_{13}), **3**: P3AT (R= C_6H_{13}), **4**: CuPc, **5**: C60, **6**: Alq3, **7**: Pentacene.

In organic materials, the charge transport depends on intramolecular carrier movement and intermolecular charge transfer within the materials. Researchers explained the charge carrier transport with the help of the hopping model and multiple trapping and release model.[29] According to the hopping model, charge transport in organic materials occur through hopping of charge carriers between adjacent molecules. This happens through the excited state electrons which pass over the barrier to transport charges in between neighboring molecules.[30-32] In multiple trapping and release model, localized levels are responsible for the traps and charge carriers are transported along with the traps through trapping and releasing.[33] In the case of OSC, the multiple trapping and release model is more accepted.

1.4.1. Polymer based Organic Semiconductors
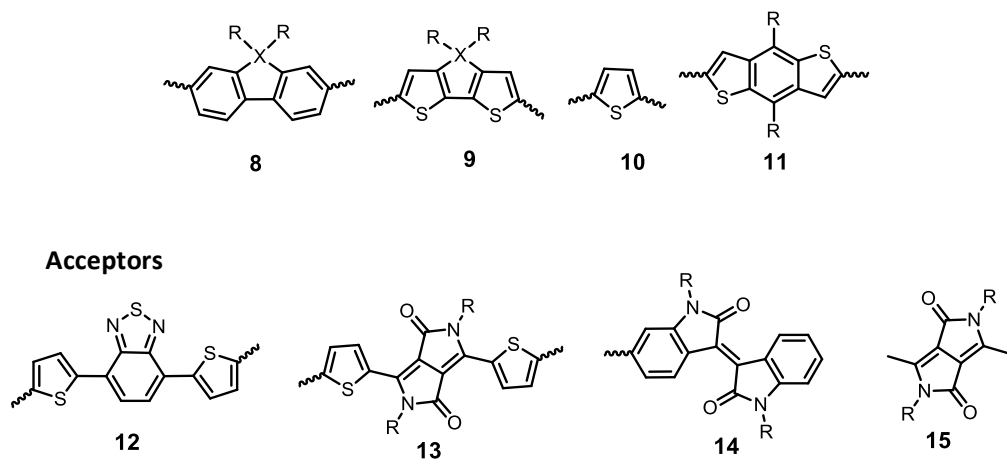
Figure 1.6 Molecular structure of OSC; **8**: Fluorene; X = C, Si, Ge, **9**: Cyclopenta[2,1-b:3,4-b']
dithiophene; X= C, Si, Ge, **10**: Oligothiophene, **11**: Benzo[1,2-b:4,5-b'] dithiophene(BDT), **12**:
4,7-Di(2-thienyl)-2,1,3-benzodithiazole, **13**: 3,6-Di(2-thienyl)-pyrrolo [3,4-c]pyrrole-1,4-dione, **14**:
Isoindigo, **15**: Diketopyrrolopyrrole (DPP).

In recent years, photovoltaic devices based on conjugated polymers have been studied extensively. Properties of polymers like solution processability, good film quality, thermal stability and excellent optoelectronic properties make them suitable for photovoltaic devices.[34-37] Type of charge carrier generated or transported by the semiconducting polymer mainly depends on the HOMO and LUMO levels. Polymer semiconductors possessing high HOMO energy level promotes holes and those with lower LUMO energy level promotes electron for charge transport. Under an electrical bias, the former type of polymer behaves as an electron donor (p-type) material and the latter behaves as an electron

accepter (n-type) material. Polymers containing donor (D) and acceptor (A) moieties in the backbone found to be one of the most promising design strategy for polymer based OSCs.[38,39] The existence of quinoid structure is an important consequence of the D-A repeating units in low bandgap polymers. Some of the widely explored donor and acceptor moieties are depicted in **Figure 1.6**.
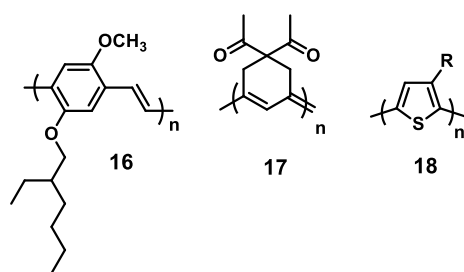
Figure 1.7 Molecular structure of polymers used in Ref: 26.

In 1982, Ebisawa *et. al* reported π-conjugated polymer based organic thin film transistor (OTFT) for the first time.[40] They have used a polyacetylene/ polysiloxane interface for metal-insulator-semiconductor (MIS) diodes. In MIS diodes, depletion occurs at the interface of polymeric semiconductor and insulating polysiloxane. With polyacetylene/ polysiloxane field defect, attempted to fabricate an MIS FET which performed as a depletion-type transistor. The first report on organic photovoltaics appeared in 1993 by A. J. Heeger and coworkers. They have demonstrated the photoinduced electron transfer between three semiconducting polymers (**16,17,18**) and

buckminsterfullerene.[41] They have fabricated a diode bilayer with semiconducting polymer as the donor and fullerene as the acceptor. This diode bilayer can perform as photodiodes and photovoltaic cells.
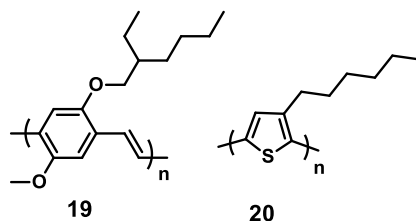
Figure 1.8 Molecular structure of polymers used in Ref: 26.

Generally, increased conjugation length enhances the absorption capability of the polymers. Poly[2-methoxy-5-(2'ethylhexyloxy)-1,4-phenylenevinylene] (MEH-PPV), **16** and poly[2-methoxy-5-(3',7'-dimethyloctyloxy)-1,4-phenylene] (MDMO-PPV), **19** are dialkoxy-substituted poly(*para*-phenylene) derivatives. These polymers exhibited strong absorption profile in the visible region of the solar spectrum and performed as the photoactive material in solar cells with good power conversion efficiency in a reproducible manner.[42-44] P3HT, **20** a polythiophene derivative is a well-known polymer donor molecule widely explored in BHJ cells. Better solubility and electric properties of P3HT make them a suitable candidate for solar cell applications.[45,46] Presence of alkyl groups as side chains in MEH-PPV, MDMO-PPV and P3HT improves the solubility in common organic solvents. This allows the feasibility of these

materials for solution processing techniques like spin casting, dip coating, ink jet printing, screen printing, and micromoulding.[47-50] BHJ solar cells using these polymers as donor moiety showed a remarkable increase in photovoltaic performance with various optimization techniques in the device level.
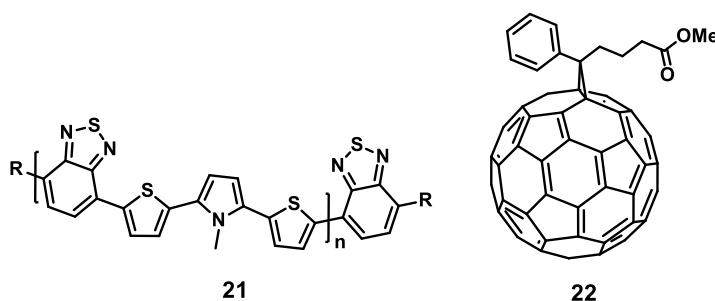
Figure 1.9 Molecular structure of polymer **21** and PCBM derivative **22**.

Benzothiadiazole (BT) is a heterocyclic moiety with electron-accepting capabilities. The polymers containing BT unit exhibit high hole mobility and wide sunlight absorption. Duren *et al.* synthesized a novel conjugate polymer, **21** with a lower bandgap of 1.6 eV which contains alternating electron rich *N*-dodecyl-2,5-bis(2'-thienyl)pyrrole (TPT) and electron rich 2,1,3-benzothiadiazole.[51] With this copolymer as donor and PCBM, **22** as an acceptor in blends found to be effective in photogeneration of charge-separated state which was confirmed through photoinduced absorption and fluorescence spectroscopy. Preliminary photovoltaic results show that **21** based BHJ device showed power conversion efficiency of 0.34%.
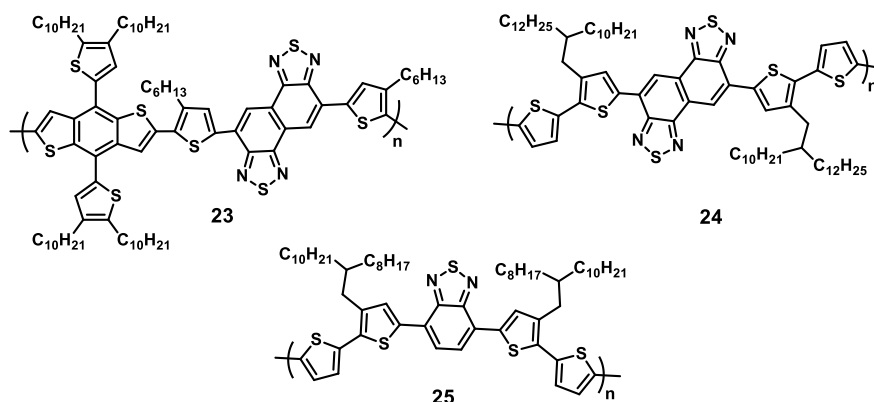
Figure 1.10 Molecular structure of polymers **23 - 25.**

Naphtho[1,2-*c*:5.6-*c'*] bis [1,2,5]thiadizole (NT) is a fused structure of two BT units, which possesses more conjugation and slightly stronger electron withdrawing capacity. Wang *et al*. synthesized NT based conjugate polymer, **23** with a bandgap of 1.58 eV, which exhibited PCE of 6% (J_{SC} = 11.71 mA/cm2, V_{OC} = 0.80 V, *FF* = 0.61).[52] Osaka *et al*. synthesized NT based D-A based conjugate polymer, **24** for organic field-effect transistors and bulk heterojunction solar cells applications.[53] **24** showed PCE of 6.3% for BHJ solar cells and high field effect mobility of 0.56 cm^2/Vs.
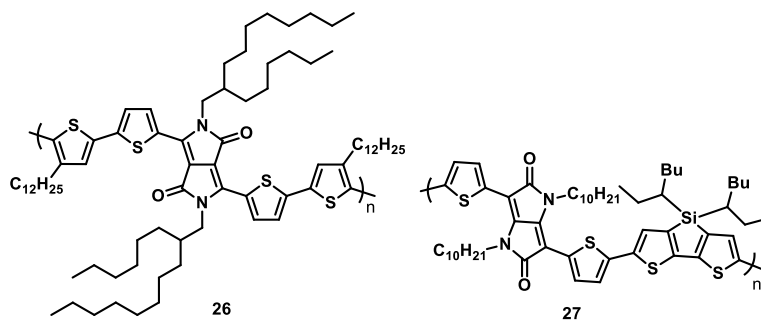
Figure 1.11 Molecular structure of polymers **26** and **27**.

Construction of D-A type semiconductor with diketopyrrolo[3,4-*c*]pyrrole (DPP) as acceptor has been receiving considerable attention for photovoltaic applications.[54-56] The first report on DPP based polymer for OFET and OPV applications was reported by Winnewisser and coworkers.[56] They have synthesized a new polymer (**26**), homopolymerised from a monomer which contains 2-hexyldecyl substituted DPP anchored with 3-dodecylthiophene on both ends. This polymer used as an ambipolar transporter with balanced hole and electron mobilities. Incorporation of diketopyrrolo[3,2-*b*]pyrrole, a stereoisomer of diketopyrrolo[3,4-*c*]pyrrole,[57] as an acceptor building block in polymers exhibits better performance with hole mobilities of 0.03 cm^2/Vs). BHJ solar cells with ITO/ PEDOT:PSS/ **27**:PC$_{71}$BM/Al showed PCE of 5.1%.[58]
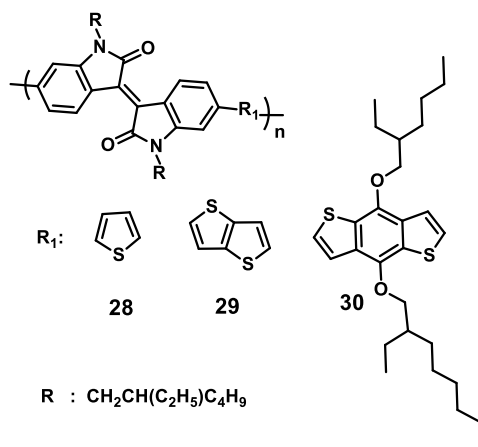
Figure 1.12 Molecular structure of polymers in Ref. 60.

Isoindigo, a structural isomer of indigo used as an electron acceptor in OSCs. It possesses a symmetrical structure with two indoline units and strongly electron

withdrawing in nature.[59] Generally, planar π-conjugated isoindigo based conjugate polymers possess low bandgap. In 2011, Zhang *et al.* synthesized a series of isoindigo based low bandgap polymers (**28**, **29** and **30**).[60] The properties of polymers such as broad absorption, optimal bandgap, and suitable energy levels with PCBM make them suitable for photovoltaic applications.
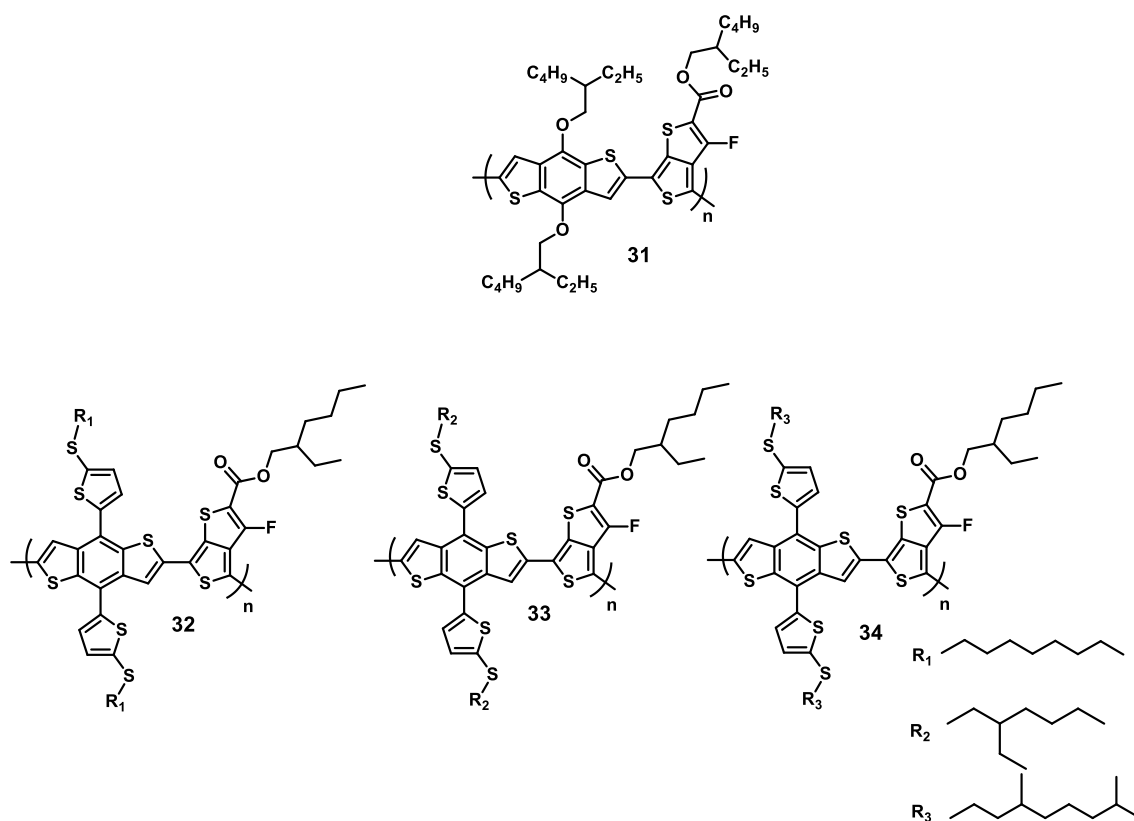
Figure 1.13 Molecular structures of polymers **31-34**.

Polymer, **31** is one of the widely explored donor material developed by Yu *et al.* in 2010, which consists of electron rich 4,8-bis(2-ethylhexyloxy) benzo[1,2-*b*:4,5-*b'*]dithiophene and (2-ethylhexylester)-(fluoro)thieno [3,4-

b]thiophene.[59,61,62] The presence of the side chain on the two moieties improved the processability of these type of polymers for solar cell applications. Hou *et al.* synthesized new modified polymers (**32**-**34**) from **31** by introducing linear side chains.[63] Under optimized conditions, **32** achieved a PCE of nearly 10%. In 2015, the same group have reported three new donor materials for solar cell applications.[64] They have incorporated octyl, 2-ethylhexyl and 3,7-dimethyl octyl side chains on **31** based polymers to make **32-34**, respectively. Influence of alkyl chain on the π–π stacking plays a major role in the morphological and photovoltaic properties. Among the three polymers, **32** shows better performance (9.48%) due to strong π–π inter-chain packing.
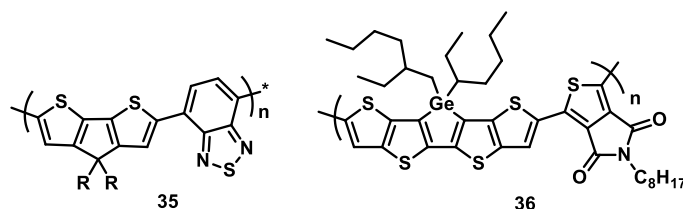
Figure 1.14 Molecular structure of **35** and **36**.

Fused thiophene based polymers are well explored as donors and hole transporting materials in photovoltaic cells.[65,66] Synthetic feasibility for creating the desirable bandgap, solution processability and higher stability make them suitable for photovoltaic application. First reported fused thiophene based low bandgap polymer with high PCE having absorption extending to the IR region.[67]

The low bandgap polymer poly[2,6-(4,4-bis-(2-ethylhexyl)-4*H*-cyclopenta[2,1-b;3,4-b′]-dithiophene)-alt-4,7-(2,1,3-benzothiadiazole)] (**35**) exhibited a bandgap of 1.46 eV and PCE of 2.7%. Heeney and coworkers reported a novel ladder type fused ring donor dithienogermolodithiophene in which two thieno[3,2-b]thiophene units are held coplanar by bridging dialkyl germanium.[68] Polymerizing this monomer with N-octylthienopyrrolodione via Stille polycondensation results in the polymer (**36**) having an optical band gap of 1.75 eV. BHJ solar cells based on this polymer exhibits efficiencies up to 7.2%.
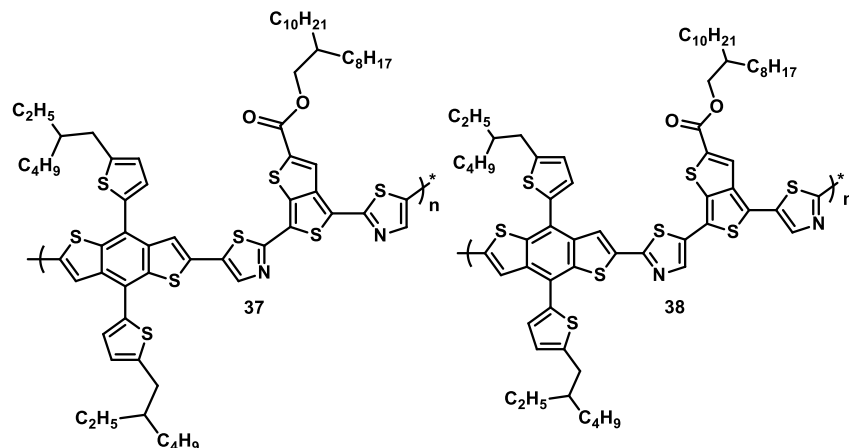
Figure 1.15 Molecular structure of **37** and **38.**

In 2017, Yang and coworkers reported two novel polymers (**37** and **38**) with thieno[3,4-b] thiophene and thiazole units as building blocks.[69] In these polymers, thiazole moiety was employed as the π-bridge incorporating into the backbone of quinoid polymers. Different orientations of the thiazole relative to

thienothiophene were systematically studied. Among the two polymers, **37** exhibits lower HOMO energy level and a PCE of 9.72%.
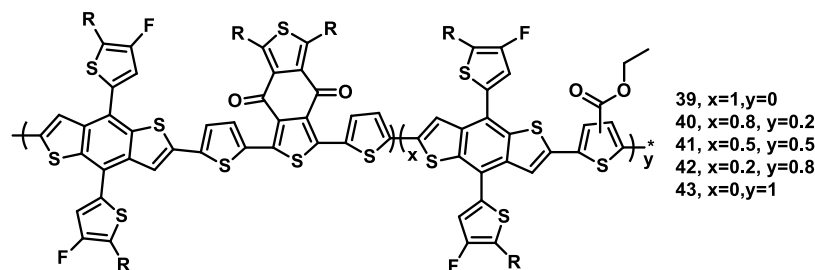
Figure 1.16 Molecular structure of **39-43.**

Hou and coworkers introduced ternary blending and copolymerization strategy for improving the photovoltaic properties.[70] They have utilized ester substituted thiophene as the electron-withdrawing unit, which incorporated into the polymers (**39-43**) having benzo[1,2-b:4,5-b']dithiophene (BDT) and benzo[1,2-c:4,5-c']dithiophene-4,8-dione(BDD). Introduction of ester functionality into the polymer backbone broadened the absorption spectrum and lower its HOMO level results in a simultaneous increase in *Jsc* and *Voc* in the device. The device processed by the THF yields a high PCE of 14.2%.

1.4.2. Small molecule based Organic Semiconductors

Small molecules or oligomers have been increasingly used as an active component in organic electronic devices in recent times. Compared to polymer counterparts, small molecules have a well-defined molecular structure,

molecular weight, and high purity without batch to batch variations, which make them ideal for device applications.[71] Compared to polymers, small molecules lack the chain entanglement which facilitates the formation of single-crystals. Single crystal analysis provides more insight into the solid-state chain packing, which plays an important role in the device properties. Monodisperse small molecules can tune the physical properties (such as optical, charge carrier mobility, HOMO/LUMO energy levels, and structural ordering) through chemical modifications. Molecular design of almost all small molecules is based on well-established semiconducting moieties such as thiophenes,[1] triarylamines,[72] and acenes.[73]

1.4.2. 1. Thiophene based small molecules

Oligothiophenes without substituents have electron transporting and hole transporting properties.[74] Chemical stability and easy functionality allow them to tune their relevant properties. On increasing the thiophene conjugation leads to better π-π stacking which in turn improves the charge carrier transport. A series of conjugated D-A small molecules consisting of electron-withdrawing groups coupled with different oligothiophene segments have been designed and synthesized in the last few years to provide new materials for device

applications. Bandgap tuning in oligothiophene can be achieved by incorporating electron-withdrawing groups in the α-position.
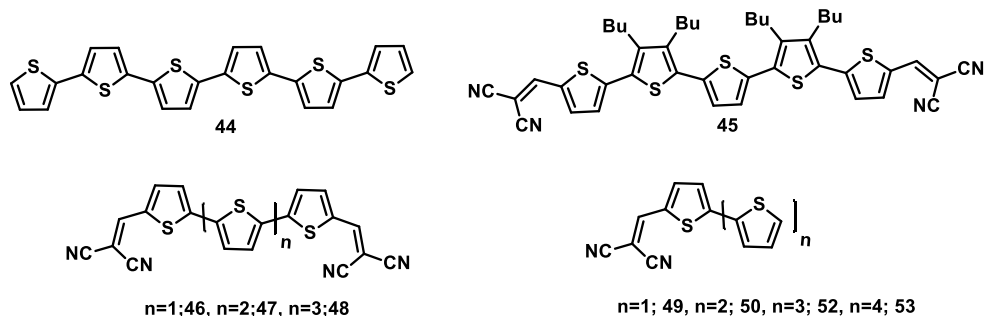
Figure 1.17 Molecular structure of thiophene based compounds (**44-53**).

α-sexithiophene,**44** was first introduced in OFET devices in 1989 by Garnier *et al*. In 2008, Sakai *et al*. utilized the same material as donor and C_{60} as an acceptor in solar cells and achieved a PCE of 0.8%.[75] Bäuerle and coworkers developed a series of D-A based oligothiophenes (**45-48**) with 2,2'-dicyanovinylene (DCV) as the acceptor.[76] DCV substitution results in intramolecular charge transfer (ICT) character, which facilitates the intense absorption in the visible range. Robertson and coworkers reported a series of 3-hexylthiophene derivatives (**49-53**) by varying the thiophene units from one to five, with a cyanoacrylic acid end group which allows the anchoring of these onto the TiO_2.[77] With increase in light harvesting capacity, PCE was also increased. **55**, having five thiophene units exhibits increased PCE of 0.24% compared to other derivatives.
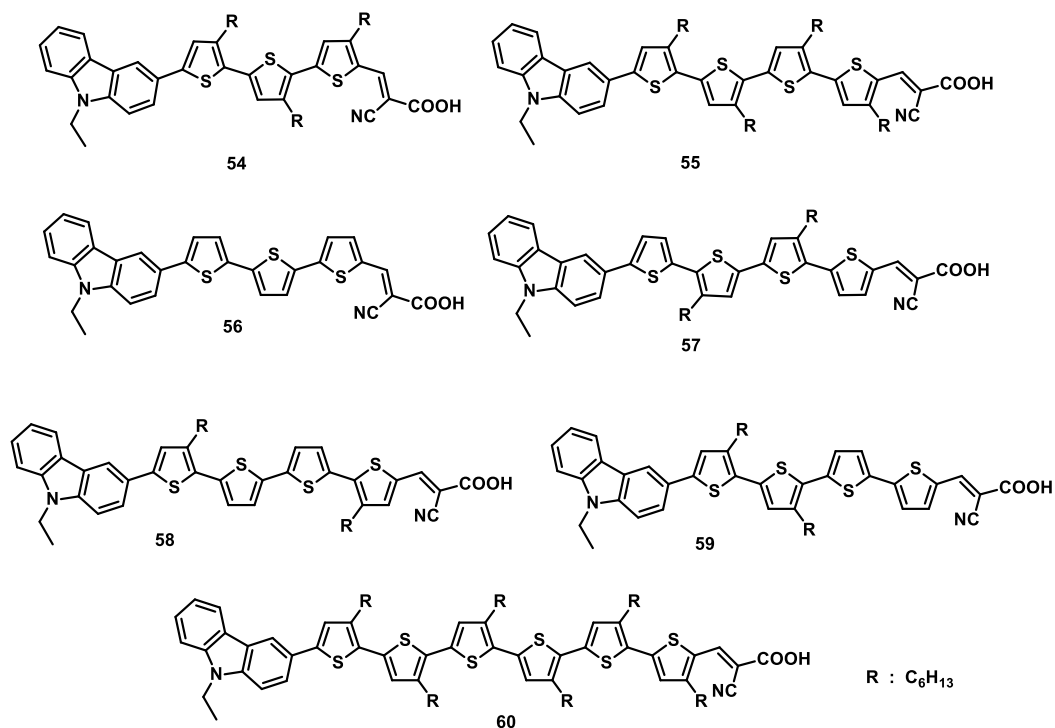
Figure 1.18 Molecular structure of thiophene based compounds (**54-60**).

Hara and coworkers synthesized a series of novel organic dyes (**54**-**60**) for DSSC application, with carbazole as the donor and cyanoacrylic acid as the electron acceptor, connected with oligothiophene as a π-conjugated system.[78,79] Photovoltaic performance of the device made out of them depends on the number and position of alkyl chains and also the number of thiophene moieties. On increasing the alkyl chain length, dyes exhibit increased electron lifetime which was favorable for solar cell performance.

Two dimensional oligothiophenes were also reported for photovoltaic applications. Zhu and coworkers initially reported X-shaped oligothiophenes

(**61**-**64**) as donors for BHJ solar cells.[80] On increasing the thiophene rings in each branch, absorption spectra shifted bathochromically and hence the light
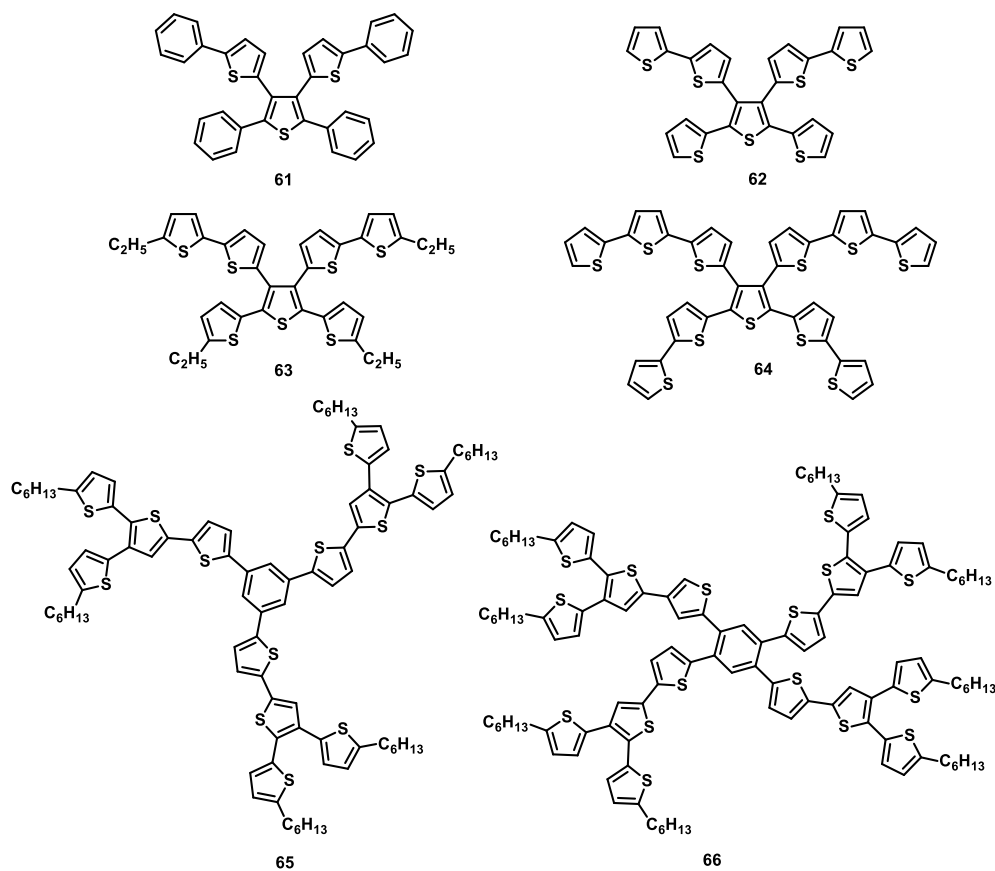
Figure 1.19 Molecular structures of oligothiophene derivatives (**61**-**66**).

harvesting efficiency was also increased. Higher photocurrent and IPCE was exhibited by compounds with a higher number of thiophene units. Kopidakis *et al.* reported two phenyl-cored thiophene dendrimers (**65** and **66**) for BHJ device fabricated with PCBM.[81] Second generation dendrimers having three and four thiophene arms were used. With an increase in chain length of the four-arm

dendron (**66**), better device performance was observed due to increased charge carrier mobility.
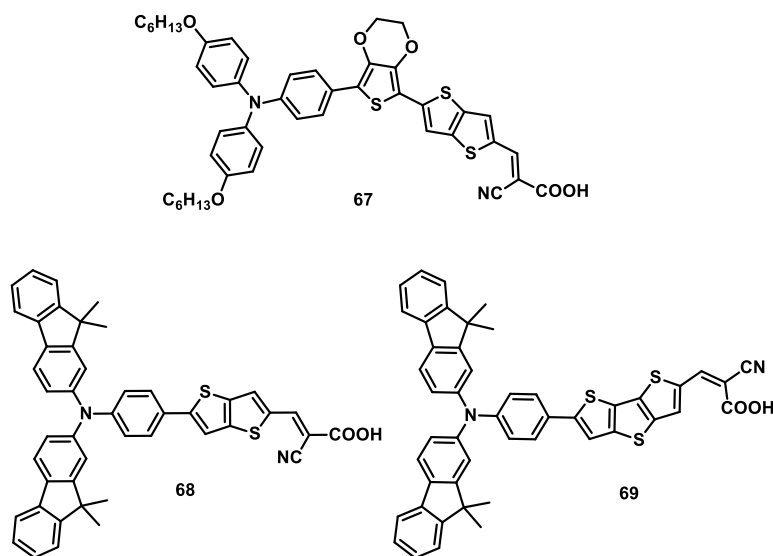
Figure 1.20 Molecular structures of fused thiophene based sensitizers employing for DSSC.

Fused thiophenes have extended conjugation than thiophenes due to more rigid structures. These materials can adjust the bandgap of organic materials and can enhance the intermolecular interactions in the solid state.[82] In D-π-A dye design for DSSC applications, π-spacer plays an important role in the bandgap tuning. In high polarity electrolytes, normally used in DSSCs, fused thiophenes have low free energy of solvation. Some DSSC sensitizers (**67**, **68** and **69**) utilizing fused thiophenes as the π-spacer is depicted in **Figure 1.20**.[83-85]

Peripheral positioning of the sulphur atoms in fused thiophene systems makes multiple short intermolecular S-S contacts which improve electronic

structure dimension. This results in enhanced charge transport properties. Highly planar tetrathienoacene (TTA), a fused thiophene core utilized as π-bridge for
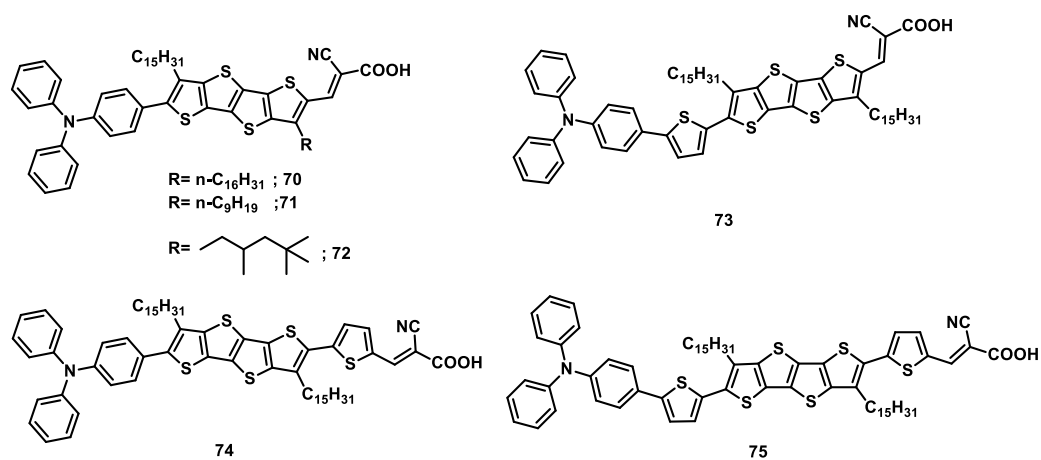
Figure 1.21 Molecular structures of photosensitizers (**70-75**).

some of the highly efficient photosensitizers (**Figure 1.21**).[86,87] Alkyl chains introduced in the π-spacer to suppress the dye aggregation and charge recombination of dyes on the TiO$_2$ surface. Incorporation of thiophene units between donor and planar TTA spacer increases the conjugation, absorption capacity, and HOMO energy levels. Some of the TTA based dyes are depicted in **Figure 1.21**.

1.4.2.2. Triphenylamine based small molecules

Properties like hole-transportation and electron donation make triphenylamine (TPA) a suitable material for OSC.[88] In TPA, the central nitrogen atom is sp^2 hybridized with a planar configuration and also the steric interaction

between the phenyl groups provides a propeller geometry which makes the
molecule a promising building block for three-dimensional donors.
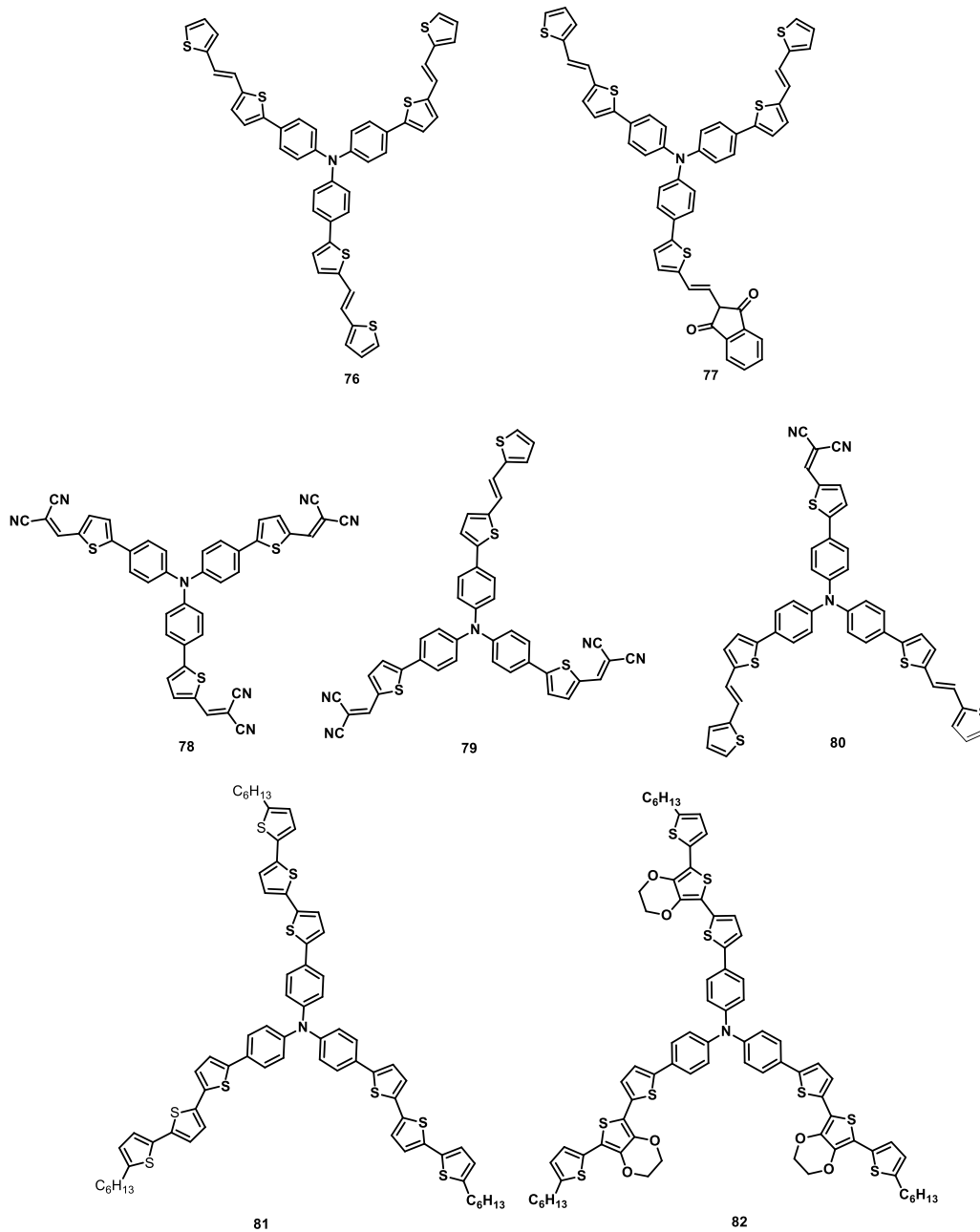
Figure 1.22 Molecular structures of TPA based compounds (**76**-**82**).

In 2006, Roncali's group reported a series of star shaped TPA based small molecules having excellent optoelectronic properties.[89-91] They synthesized a series of molecules (**76**-**82**) with TPA as the core connected with dithienylethylene π-conjugated chains and various electron-acceptor groups. End group functionalization with dicyanovinyl groups facilitates ICT leading to extended absorption towards longer wavelength region. Fabricated BHJ solar cells out of these molecules exhibited extended photoresponse and increased open-circuit voltage. These molecules can form amorphous thin films via wet preparation methods and devices made out of them exhibits photovoltaic effects and electroluminescence at low voltage
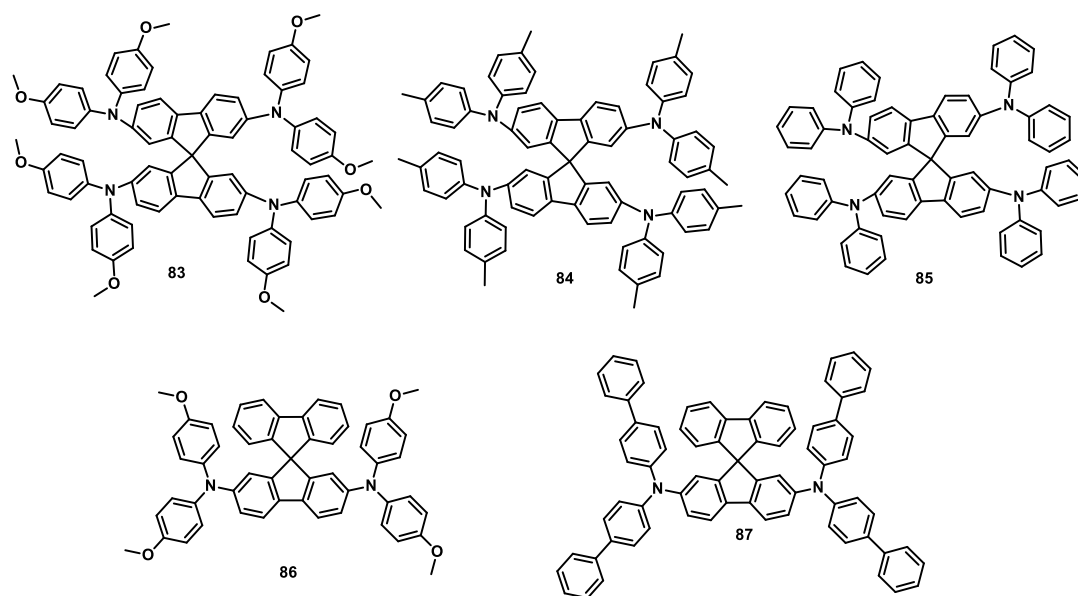
Figure 1.23 Molecular structures of TPA based HTM (**83**-**87**).

The main ongoing research in DSSC has focused on replacing liquid electrolytes with solid ones (Hole Transport Materials; HTM).[92] Aromatic amines are widely explored as HTM in which the hole transporting behavior arises due to the electron donating amine nitrogen atom. The first solid-state HTM was introduced in perovskite solar cell (PSC) by replacing the liquid electrolyte with spiro- OMeTAD, exhibits a PCE of 10%.[93] There are a large number of new HTM reported with TPA moieties in combination with various π-conjugated groups. Some of the representative examples are shown in Figure **1.23**.[94,95]
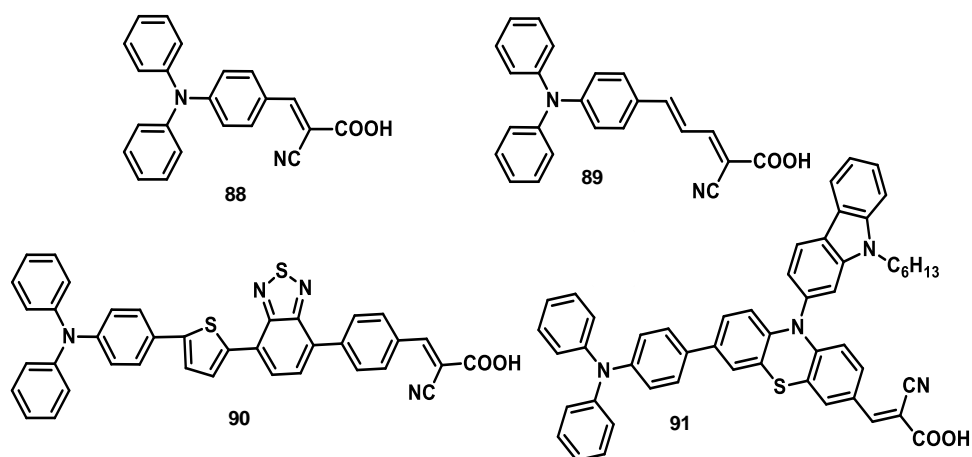
Figure 1.24 Molecular structures of TPA based dyes (**88-91**).

One of the most common donor moiety used in metal-free dyes is TPA.[96] Introduction of TPA moiety into the sensitizer can improve the hole-transporting ability, and also can effectively prevent the aggregation due to its non-planar

structure. TPA donor moiety is capable of separating and localizing cationic charge from TiO$_2$ surface, which remarkably restricts charge-recombination and other back electron transfer reactions. In 2004, Kitamura *et al.* reported TPA based two metal-free organic dyes (**88** and 8**9**), with a double bond as the π-bridge and cyanoacrilic acid as the acceptor and anchoring group.[97] The dye possessing longer π-bridge exhibits red shifted absorption and higher PCE. Structures of some TPA based sensitizers are illustrated in **Figure 1.24**.

1.4.2.3 Acene based small molecules

Organic compounds and polycyclic aromatic hydrocarbons having linearly fused benzene rings constitute the class of acenes or polyacenes. Acenes possess unique properties like fused aromatic structure with planarity.[73]They have high charge carrier mobility and broad absorption spectrum, which make them suitable donor materials for organic solar cells.
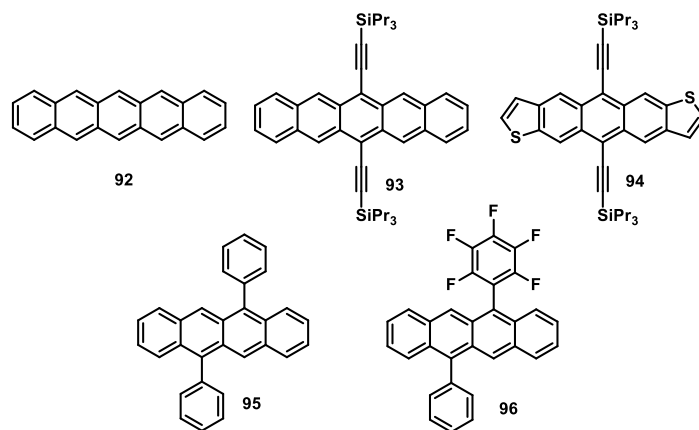
Figure 1.25 Molecular structure of acene based compounds (**92**-**96**).

The photovoltaic properties of pentacene (**92**) was initially reported by Kippelen and coworkers in 2004.[98] They fabricated a bulk heterojunction solar cell with C_{60} as acceptor, yielding a PCE of 1.5%. Functionalization of acenes increases the solubility in common organic solvents and facilitates solution processing. Structures of some acene based compounds were depicted in **Figure 1.25**. Functionalization can also enhance the capability of molecules to self-assemble with increased π-stacking which in turn enhances the intermolecular orbital overlap and charge carrier mobility.[99, 100]
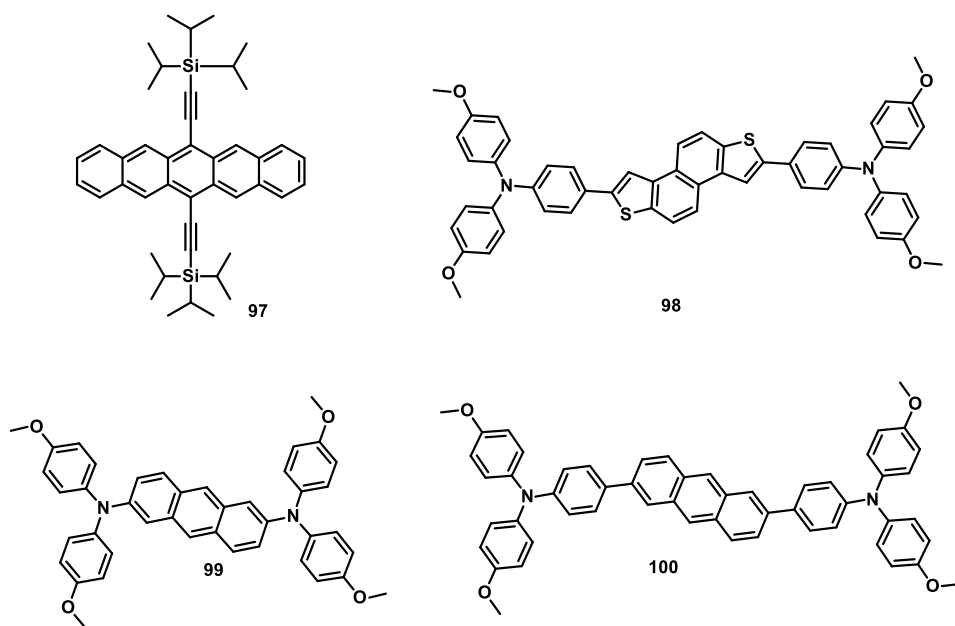
Figure 1.26 Molecular structure of Acene based compounds (**97-100**).

Recently, Ahmad and coworkers reported TIPS-pentacene (**97**) as a hole transport material for perovskite solar cells.[101] TIPS functionalization at the C-

6/C-13 of pentacene enhances the solubility and two-dimensional lamellar structure with brick walls style in the solid state. Structure of some acene based compounds depicted in **Figure 1.26**. Pham *et al.* reported a series of acene-based solution processable small molecules (**98-100**) with triphenylamine and diphenylamine end groups.[102] Anthracene and naphtha[1,2-b:5,6-b']dithiophene based cores were used due to their planar nature. These molecules were used as HTM without additive in perovskite solar cells.
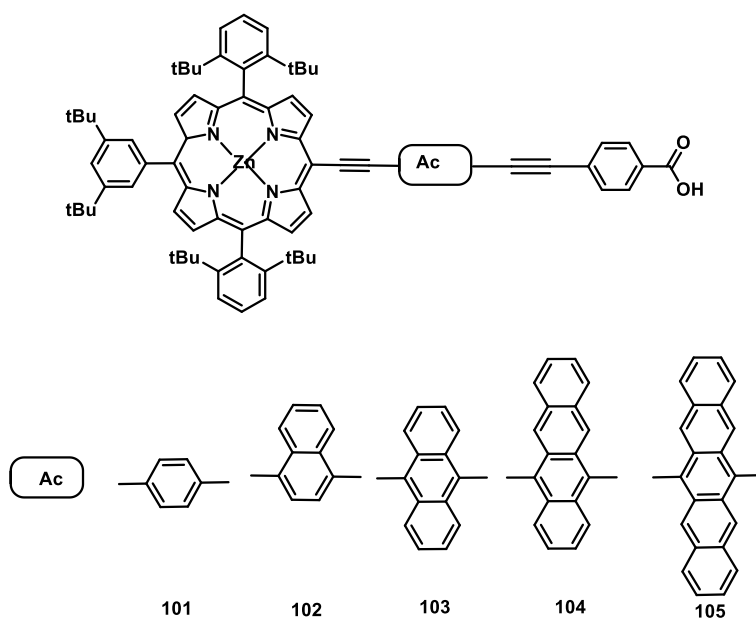
Figure 1.27 Molecular structures of acene-modified porphyrins (**101-105**).

Diau *et al.* reported a series of acene-modified zinc porphyrin dyes (**101**-**105**) for DSSC applications shown in **Figure 1.27**.[103] In these dyes, acenes placed between the porphyrin and carboxylic acid anchoring group. Dyes with

anthracene and pentacene groups (**103** and **105**) enhances the porphyrin B and Q bands respectively. Anthracene based dye (**103**) outperforms the other dyes in this series. IPCE and absorption spectra of **103** on TiO$_2$ exhibits broadened absorption bands which reduces the porphyrin Q-band. Pentacene based derivative (**105**) shows poor performance due to rapid non-radiative relaxation of the molecule in the singlet excited state.

1.4.2.4 Diketopyrrolopyrrole based small molecules

106
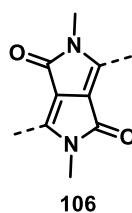
Figure 1.28 Molecular structures of DPP moiety.

Small molecules based on diketopyrrolopyrrole (DPP) core (**106**) have been widely explored as photovoltaic materials.[104] DPP is composed of bicyclic lactum rings with planar structure. In the solid state, strong intermolecular interactions such as hydrogen bonding (between N-H and O) and π-π interactions (between adjacent lactam rings) facilitates highly ordered molecular stacking favorable for intermolecular charge transfer hopping. Suraru *et al*. initially reported a p-channel OSC material possessing DPP core with efficient charge carrier mobilities.[105] Charge transport properties were determined by fabricating

bottom-gate top contact thin film transistor. The molecule exhibited a hole mobility of 0.7 $cm^2V^{-1}s^{-1}$.

107; R = n-C_6H_{13}
108; R = n-C_8H_{17}
109; R = n-$C_{12}H_{25}$
110; R = 2-ethyl hexyl

111; R = n-C_8H_{17}

112 ; R = n-C_8H_{17}
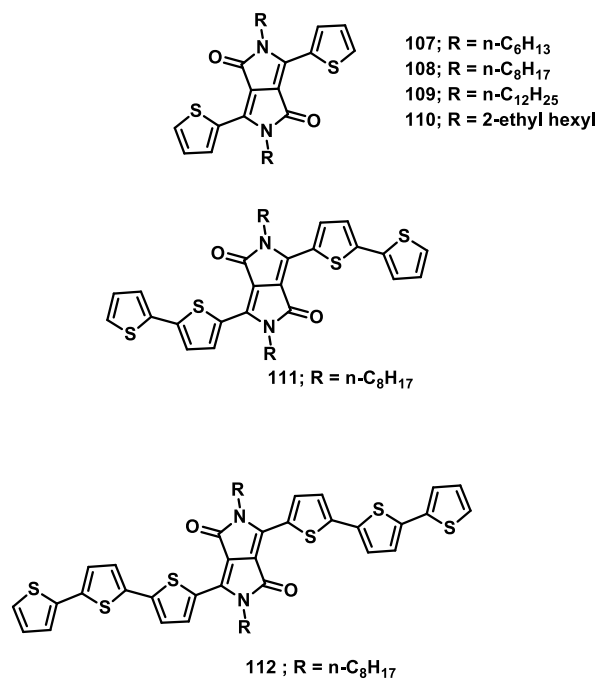
Figure 1.29 Molecular structures of DPP derivatives (**107**-**112**).

Nguyen and coworkers reported soluble DPP-based oligothiophenes (**107**-**112**) for BHJ application.[106] By changing the conjugation length and/or the substituents, optical, electronic and molecular packing of the materials were controlled. Among the DPP derivative studied, **112** based BHJ solar cells fabricated with PCBM as acceptor achieved a PCE of 2.3%.

The potential of DPP based dyes for DSSCs was also explored. Soluble dyes were synthesized by attaching long alkyl chains onto DPP cores, which also help

to inhibit charge recombination and other back electron transfer processes in the devices.[107,108] DPP core can enhance dye absorption to longer wavelength which in turn increases the IPCE action spectra. Structures of some DPP based sensitizers are illustrated in **Figure 1.30**.
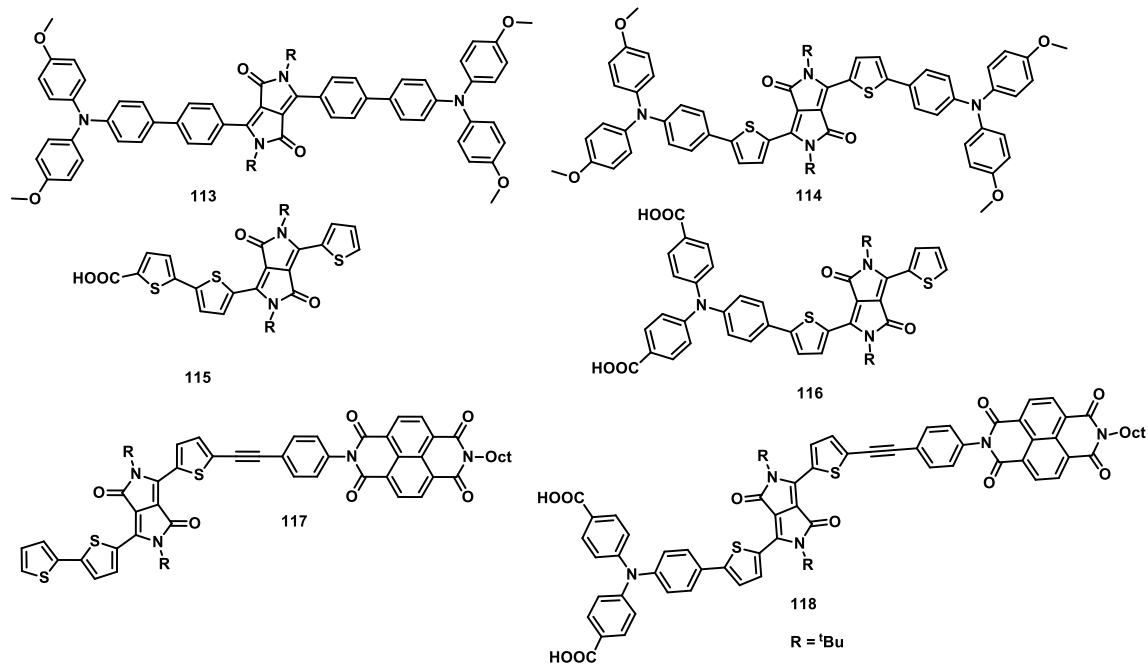
Figure 1.30 Molecular structures of DPP based dyes (**113**-**118**).

1.4.2.5. Porphyrin based small molecules
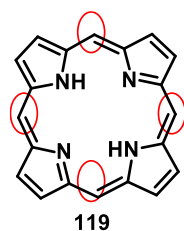
Figure 1.31 Structure of porphyrin core (*meso* positions marked with red circles).

Porphyrin, a structural analog of chlorophyll is electron donating in nature and possesses extended π-conjugation.[109] Porphyrins absorb light mainly in the blue and moderately in the green regions of the visible spectrum with high molar absorption coefficients. Porphyrin based systems were well explored in optoelectronic devices. Synthetic modification in the periphery of porphyrins (*meso-* and *β*-positions) and metal center variations can fine-tune the optical and electronic properties of the devices.
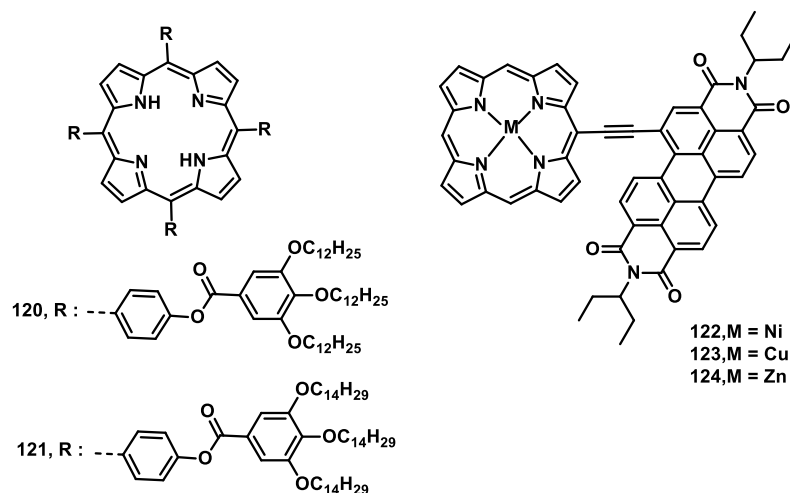
Figure 1.32 Molecular structures of Porphyrin dyes (**120-124**).

Sun *et al.* developed soluble porphyrins (**120** and **121**) with discotic liquid crystalline (LC) phases as donors in BHJ solar cells.[110] Energy harvesting from these materials occurs through homotropic alignment of LC columns normal to the electrode surface. After post-annealing, one of the porphyrin based device exhibits better performance. Shankar and coworkers reported the metallated

porphyrin – perylenebismide (PBI) derivatives (**122**-**124**) for BHJ solar cell applications and studied the photovoltaic properties of devices on changing the metal center.[111] Solution processed BHJ devices were fabricated with $PC_{71}BM$ as accepter and metallated porphyrin- PBI derivative as the donor. Porphyrins with Zn (**128**) showed higher PCE value 6.18%.

Panchromatic sensitizers consisting of porphyrin as π-spacer in D-π-A dyes were designed and developed for DSSC applications.[112] The most studied porphyrins for DSSC are free-base porphyrins and Zn porphyrins. In 2011, Gratzel's group reported record breaking efficiency for Zn-porphyrin (**125** and
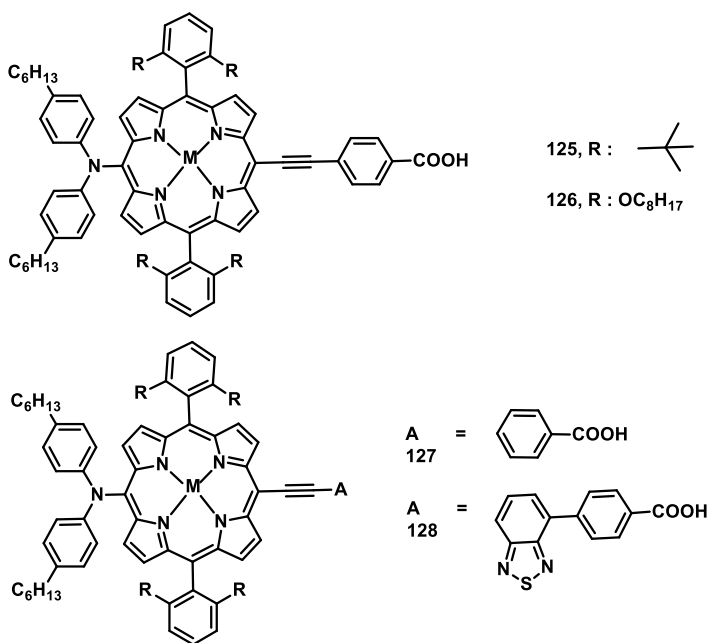
Figure 1.33 Molecular structures of Porphyrin dyes (**126-128**).

the visible spectrum and co-sensitization with another organic dye improves the efficiency to 12.3%. Nazeeruddin and co-workers reported push-pull porphyrin

dye (**128**), which exhibits unprecedented PCE of 13%.[114] The fabricated device used the redox couple electrolyte [Co(bpy)$_3$]$^{2+/3+}$.

1.4.2.6 Squaraine based small molecules

Squaraine (SQ) dyes, a class of polymethine dyes with zwitter ionic structures possess four-membered aromatic ring system derived from squaric acid. Properties like intense light absorption and quenched fluorescence emission of SQ dyes make them a potential candidate for photovoltaic applications.[115] These dyes have high molar extinction coefficients in the order of 10^{-5} M^{-1}cm^{-1} and ability to harvest light in the near infrared (NIR) region.
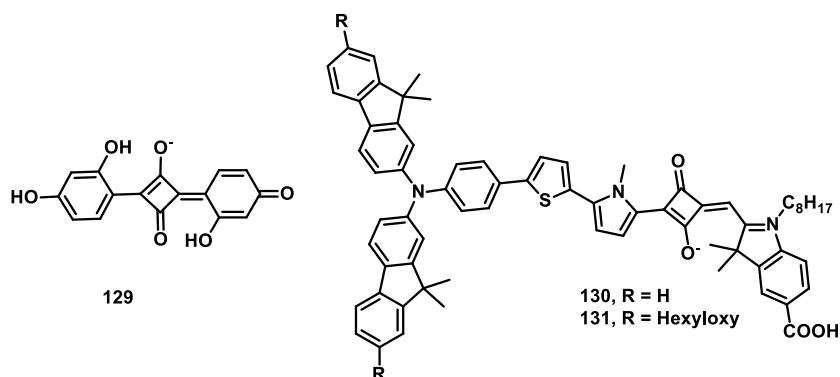
Figure 1.34 Molecular structures of SQ dyes (**129-131**).

First report on the ability of SQ dye (**129**) for photosensitization was by Kamat *et al* in 1993.[116] This dye showed a maximum photon-to-current efficiency of about 0.05%, which is lower than the fluorescence quantum efficiency obtained in solution state. NIR absorbing SQ dyes as sensitizers in

DSSC generally exhibit lower PCE values. The performance of SQ dyes can be improved by introducing the unsymmetrical SQ unit and non-planar moieties into the dye design. This helps to suppress the aggregation and improves the long-term stability of the device. Paek *et al.* reported two unsymmetrical SQ dyes (**134** and **135**) having thiophenyl pyrrolyl and indoline moieties.[117] These dyes exhibit panchromatic light absorption up to 780 nm and one of them shows a record efficiency (6.29%) for near-IR DSSC.
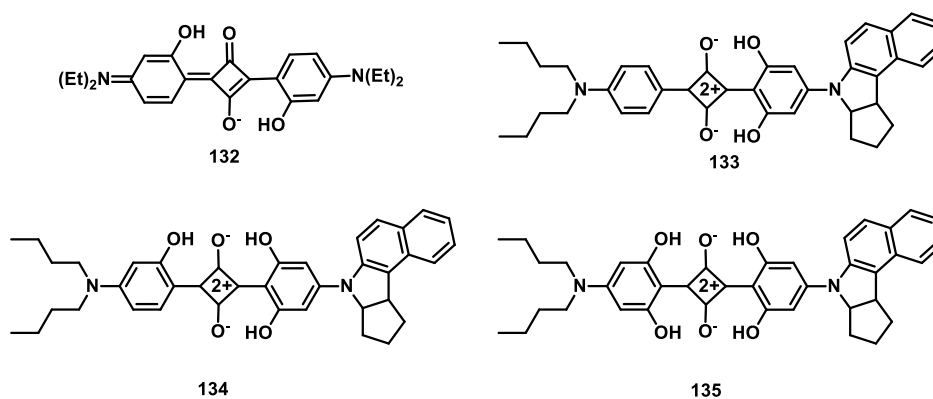
Figure 1.35 Molecular structures of SQ dyes (**132-135**).

Meritt *et al.* reported the first symmetric SQ dye (**132**) as photoactive material in organic photovoltaic cells.[118] Structures of some SQ based dyes were depicted in **Figure 1.35.** Polycrystalline films of SQ dyes were prepared by evaporation and solution processing exhibit absorption in the whole visible range. The PCE obtained under AM white light was 0.1%. A variety of SQ based dyes was reported so far and the efficiency also improved through rational

molecular designing. Huang and coworkers developed a series of highly efficient unsymmetrical SQ dyes having hydroxyl substituents (**133-135**).[119] Solution processed BHJ cell with **134** as electron donor outperforms with PCE of 6.07%.

1.5. Objectives of the present thesis

Harvesting and converting of solar energy through photovoltaic technology is the most successful way to address the energy crisis in the near future. Third generation solar cell devices, which utilizes organic semiconductors as the active components are promising in this context due to the abundant material resources.[120] Development of organic semiconductors can be achieved through synthetic organic chemistry that offers a wide variety of π-conjugated materials with attractive optoelectronic properties. In the present thesis work, several organic small molecules were designed and synthesized using donor-acceptor approach. The core units in our designs includes thiophene, thiophene analogs and triphenylamine. To check the applicability of these molecules as active material in the third generation solar cells, BHJ or DSSC devices were fabricated.

1.6. References

1.   Mishra, A.; Bäuerle, P. *Angew. Chem. Int. Ed.* **2012**, *51*, 2020–2067.

2. Pang, H.; Xu, H.; Tang, C.; Meng, L.; Ding, Y.; Xiao, J.; Liu, R.;Pang,Z.;Huang, W. *Org. Electron.* **2018**, *65*,275–299.

3. Yang, D.; Ma, D. *Adv. Opt. Mater.Mater.* **2018**, *1800522*, 1–23.

4. Zhang, J.; Xu, W.; Sheng, P.; Zhao, G.; Zhu, D. *Acc. Chem. Res.* **2017**, *50*,1654−1662.

5. Gsänger, M.; Bialas, D.; Huang, L.; Stolte, M.; Würthner, F. *Adv. Mater.* **2016**, *28*, 3615–3645.

6. Brophy, J. J; Buttery, J.W. *Nature*, **1963**, *197*, 932.

7. Shirakava, H.; Louis, J.; Macdiarmid, A. G. *J. Chem. Sci. Chem Comm.* **1977**, 578–580.

8. Wang, C.; Dong, H.; Hu, W.; Liu, Y.; Zhu, D.*Chem. Rev.* **2012**, *112*, 2208–2267.

9. Dimitrakopoulos, B. C. D.; Malenfant, P. R. L. *Adv. Mater.* **2002**, *14*, 99–117.

10. Mas-torrent, M.; Rovira, C. *Chem. Soc. Rev* **2008**, *37*, 827–838.

11. Becquerel, E. *Compt. Rend*. **1839**, 9, 561-567.

12. Sun, Q.; Dong, G.; Zhao, H.; Qiao, J.; Liu, X.; Duan, L.; Wang, L., *Org. Electron.* **2011**, *12*, 1674–1682.

13. Hammond, L. A. *Science* **1966**, *178*, 732–733.

14. Vos, A. D. *J. Phys. D Appl. Phys.* **1980**, *13*, 839–846.

15. Scharber, M. C.; Sariciftci, N. S. *Prog Polym Sci* **2013**, *38*, 1929–1940.

16. Yu, G.; Gao, J.; Hummelen, J. C.; Wudl, F.; Heeger, A. J., *Science* **1995**, *270*, 1789–1792.

17. Rafique, S.; Mah, S.; Sulaiman, K.; Iwamoto, M. *Renew. Sustain. Energy Rev.* **2018**, *84*, 43–53.

18. Mcconnell, I.; Li, G.; Brudvig, G. W. *Cell* **2010**, *17*, 434–447.

19. Adedokun, O.; Titilope, K.; Awodugba, A. O. *Int. J. Eng Tech.* **2016**, *2*, 34–41.

20. Preat, J.; Jacquemin, D.; Perp, E. A. *Energy Environ. Sci* **2010**, *22*, 891–904.

21. Yen, Y.; Chou, H.; Chen, Y.; Hsu, C.; Lin, J. T. *J*. *Mater. Chem.* **2012**, *22*, 8734–8747.

22. O' Regan, B.; Gratzel, M. *Nature* **1991**, *53*, 737–739.

23. Wu, Y.; Zhu, W. *Chem. Soc. Rev.* **2013**, *42*, 2039–2058.

24. Kanaparthi, R. K.; Kandhadi, J.; Giribabu, L. *Tetrahedron* **2012**, *68*, 8383–8393.

25. Moza, S.; Reza, M.; Borhani, M. *Renew. Sustain. Energy Rev.* **2016**, *71*, 675–686.

26. Baxter, J. B. *J. Vac. Sci. Technol. A* **2012**, *30*, 1–17.

27. Sharma, K.; Sharma, V.; Sharma, S. S. *Nanoscale Res. Lett.* **2018**, *6*, 1–46.

28. Sheats, J. R. *J. Mater. Res.* **2004**, *19*, 1974–1989.

29. Fichou, D. *J. Mater. Chem.* **2000**, *10*, 571–588.

30. Zaumseil, J.; Sirringhaus, H. *Chem. Rev.* **2007**, *107*, 1296–1323.

31. Meijer, E. J.; Tanase, C.; Blom, P. W. M.; Veenendaal, E. Van; Huisman, B.; Leeuw, D. M.; Klapwijk, T. M. *Appl. Phys. Lett.* **2007**, *3838*, 1–4.

32. Tanase, C.; Meijer, E. J. *Org. Electron.* **2003**, *4*, 33–37.

33. Movaghar, B.; Grunewald, M.; Pohlmann, B.; Wurtz, D.; Schirmacher, W. *J. Stat. Phys.* **1983**, *30* (2), 315–334.

34. Beaujuge, P. M.; Fr, J. M. J. *J. Am. Chem. Soc.* **2011**, *133*, 20009–20029.

35. Mei, J.; Diao, Y.; Appleton, A. L.; Fang, L.; Bao, Z. *J. Am. Chem. Soc.* **2013**, *135*, 6724–6746.

36. Lei, T.; Wang, J.; Pei, J. *Acc. Chem. Res.* **2014**, *47*, 1117–1126.

37. Holliday, S.; Donaghey, J. E.; Mcculloch, I. *Chem. Mater.* **2014**, *26*, 647–663.

38. Heeger, A. J. *Chem. Soc Rev* **2010**, *39*, 2354–2371.

39. Yuen, J. D.; Wudl, F. *Energy Environ. Sci.* **2013**, *6*, 392–406.

40. Ebisawa, F.; Kurokawa, T.; Nara, S.; Ebisawa, F.; Kurokawa, T.; Nara, S. *J. Appl.Phys* **2012**, *54*, 3255–3259.

41. Sariciftci, N. S.; Smilowitz, L. *Synth. Met.* **1993**, *59*, 333–352.

42. Hoppe, H.; Sariciftci, N. S. *J. Mater. Chem* **2006**, *16*, 45–61.

43. Shaheen, S. E.; Brabec, C. J.; Sariciftci, N. S. *J. Appl.Phys* **2001**, *841*, 2–5

44. Zheng, L.; Zhou, Q.; Deng, X.; Yuan, M.; Yu, G.; Cao, Y. *J. Phys. Chem. B* **2004**, *108*, 11921–11926.

45. Mccullough, R. D.; Tristram-nagle, S.; Williams, S. P.; Lowevt, R. D. *J. Am.*

Chem. Soc. **1993**, *115*, 4910–4911.

46. Yuan, Y.; Zhang, J.; Sun, J.; Hu, J.; Zhang, T.; Duan, Y. *Macromolecules* **2011**, *44*, 9341–9350.

47. Chang, B. S.; Liu, J.; Bharathan, J.; Yang, Y.; Onohara, J.; Kido, J. *Adv. Mater.* **1999**, *2*, 734–737.

48. Pschenitzka, F.; and Sturm, J. C. *Appl. Phys. Lett.* **2001**, *74*, 11–14.

49. Rogers, J. A.; Bao, Z.; Raju, V. R.; Rogers, J. A.; Bao, Z.; Raju, V. R. *Appl. Phys. Lett.* **2008**, *72*, 2716–2718.

50. Shaheen, S. E.; Radspinner, R.; Peyghambarian, N.; Jabbour, G. E. *Appl. Phys. Lett.* **2001**, *18*, 2996-2998.

51. Wang, M.; Hu, X.; Liu, P.; Li, W.; Gong, X.; Huang, F.; Cao, Y. *J. Am. Chem. Soc.* **2011**, *133*, 9638–9641.

52. Osaka, I.; Shimawaki, M.; Mori, H.; Doi, I.; Miyazaki, E.; Koganezawa, T.; Takimiya, K. *J. Am. Chem. Soc.* **2012**, *134*, 3498–3507.

53. Li, Y.; Sonar, P.; Murphy, L.; Hong, W. *Energy Environ. Sci* **2013**, *6*, 1684–1710.

54. Turbiez, M.; Pfeiffer, R.; Bienewald, F. *Adv. Mater.* **2008**, *20*, 2217–2224.

55. Nielsen, C. B.; Turbiez, M.; Mcculloch, I. *Adv. Mater.* **2012**, *25*, 1859–1880.

56. Guo, X.; Puniredd, S. R.; He, B.; Marszalek, T.; Baumgarten, M.; Pisula, W.; Mu, K. *Chem. Mater.* **2014**, *26*, 3595–3598.

57. Lu, S.; Drees, M.; Yao, Y.; Boudinet, D.; Yan, H.; Pan, H.; Wang, J.; Li, Y.; Usta, H.; Facchetti, A. *Macromolecules* **2013**, *46*, 3895–3906.

58. Wang, E.; Mammo, W.; Andersson, M. R. *Adv. Mater.* **2014**, *26*, 1801–1826.

59. Zhang, G.; Fu, Y.; Xie, Z.; Zhang, Q. *Macromolecules* **2011**, *44*, 1414–1420.

60. Park, S.; Jeong, J.; Hyun, G.; Kim, M.; Lee, H. *Sci. Rep.* **2016**, 6, 35262–35273.

61. Ye, L.; Zhang, S.; Huo, L.; Zhang, M.; Hou, J. *Acc. Chem. Res.* **2014**, *47*, 1595–1603.

62. Chochos, A. C. L.; Spanos, M.; Tatsi, E.; Drakopoulou, S.; Vasilis, G. *Prog. Polym. Sci.* **2019**, *91*, 51–79.

63. Ye, L.; Zhang, S.; Zhao, W.; Yao, H.; Hou, J. *Chem. Mater.* **2014**, *26*, 18–20.

64. Zhang, S.; Uddin, M. A.; Zhao, W.; Ye, L.; Woo, H. Y.; Liu, D.; Yang, B.; Yao, H.; Cui, Y.; Hou,J *Poly. Chem.* **2015**, *6*, 2752–2760.

65. Cai, W.; Gong, X.; Cao, Y. *Sol. Energy Mater. Sol. Cells* **2010**, *94*, 114–127.

66. Mehmood, U.; Al-ahmed, A.; Hussein, I. A. *Renew. Sustain. Energy Rev.* **2016**, *57*, 550–561.

67. Mühlbacher, B. D.; Scharber, M.; Morana, M.; Zhu, Z.; Waller, D.; Gaudiana, R.; Brabec, C. *Adv. Mater.* **2006**, *18*, 2884–2889.

68. Zhong, H.; Li, Z.; Deledalle, F.; Fregoso, E. C.; Shahid, M.; Fei, Z.; Nielsen, C. B.; Yaacobi-gross, N.; Rossbauer, S.; Anthopoulos, T. D. *J. Am. Chem. Soc.* **2013**, *135*, 2040–2043.

69. Zhu, D.; Bao, X.; Zhu, Q.; Gu, C.; Qiu, M.; Wen, S.; Wang, J.; Shahid, B; Yang, R. *Energy Environ. Sci* **2017**, *10*, 614–620.

70. Cui, Y.; Yao, H.; Hong, L.; Zhang, T.; Xu, Y.; Xian, K.; Gao, B. *Adv. Mater.* **2019**, *31*, 1–7.

71. Lin, Y.; Li, Y.; Zhan, X. *Chem. Soc. Rev.* **2012**, *41*, 4245–4272.

72. Blanchard, P.; Malacrida, C.; Cabanetos, C. *Polym. Int.* **2019**, *68*, 589–606.

73. Anthony, J. E. *Angew. Chem. Int. Ed .* **2008**, *47*, 452–483.

74. Koumura, N.; Wang, Z.; Mori, S.; Miyashita, M.; Suzuki, E. *J. Am. Chem. Soc.* **2006**, *128*, 14256–14257.

75. Sakai, J.; Taima, T.; Saito, K. *Org. Electron.* **2008**, *9*, 582–590.

76. Schulze, B. K.; Uhrich, C.; Schüppel, R.; Leo, K.; Pfeiffer, M.; Brier, E.; Reinold, E.; Bäuerle, P. *Adv. Funct. Mater.* **2006**, *18*, 2872–2875.

77. Haid, S.; Mishra, A.; Weil, M.; Uhrich, C.; Pfeiffer, M.; Bäuerle, P. *Adv. Funct. Mater.* **2012**, *22*, 4322–4333.

78. Planells, M.; Abate, A.; Snaith, H. J.; Robertson, N. *ACS Appl. Mater. Interfaces* **2014**, *6*, 17226–17235.

79. Wang, Z.; Koumura, N.; Cui, Y.; Takahashi, M.; Sekiguchi, H.; Mori, A.; Kubo, T.; Furube, A.; Hara, K. *Chem. Mater.* **2008**, *20*, 3993–4003.

80.   Sun, X.; Zhou, Y.; Wu, W.; Liu, Y.; Tian, W.; Yu, G.; Qiu, W.; Chen, S.; Zhu, D. *J. Phys. Chem. B* **2006**, *61*, 7702–7707.

81.   Kopidakis, N.; Mitchell, W. J.; Lagemaat, J. Van D.; Ginley, D. S.; Rumbles, G.; Sean, E.; Rance, W. L.; Rance, W. L. *Appl. Phys. Lett.* **2006**, *89*, 8–11.

82.   Cinar, M. E.; Ozturk, T. *Chem. Rev.* **2015**, *115*, 3036–3140.

83.   Wang, B. M.; Xu, M.; Shi, D.; Li, R.; Gao, F.; Zhang, G.; Yi, Z.; Humphry-baker, R.; Wang, P.; Zakeeruddin, S. M. *Adv. Mater.* **2008**, *20*, 4460–4463.

84.   Qin, H.; Wenger, S.; Xu, M.; Gao, F.; Jing, X.; Wang, P. *J. Am. Chem. Soc.* **2008**, *130*, 9202–9203.

85.   Zhang, G.; Bala, H.; Cheng, Y.; Shi, D.; Lv, X.; Yu, Q.; Wang, P. *Chem.Commun.* **2009**, *16*, 2198–2200.

86.   Zhou, N.; Prabakaran, K.; Lee, B.; Chang, S. H.; Harutyunyan, B.; Guo, P.; Butler, M. R.; Timalsina, A.; Bedzyk, M. J.; Ratner, M. A. *J. Am. Chem. Soc.* **2015**, *137*, 4414–4423.

87.   Chen, M.; Ho, K.; Marks, T. J. *J. Mater. Chem. A* **2017**, *5*, 12310–12321.

88.   Wang, J.; Liu, K.; Ma, L.; Zhan, X. *Chem. Rev.* **2016**, *116*, 14675–14725.

89.   Cravino, A.; Roquet, S.; Leriche, P.; Ale, O.; Fre, P.; Roncali, J. *Chem. Commun.* **2006**, *13*, 1416–1418.

90.   Cravino, A.; Roquet, S.; Ale, O.; Leriche, P.; Fre, P.; Roncali, J. *Chem. Mater.* **2006**, *18*, 2584–2590.

91.   Agarwala, P.; Kabra, D. *J. Mater. Chem. A* **2017**, *5*, 1348–1373.

92.   Kim, H.; Lee, C.; Im, J.; Lee, K.; Moehl, T.; Marchioro, A.; Moon, S.; Humphry-baker, R.; Yum, J.; Moser, J. E. *Sci. Rep.* **2012**, *2*, 591–598.

93.   Polander, L. E.; Pahner, P.; Schwarze, M.; Saalfrank, M.; Koerner, C.; Leo, K. *APL Mater.* **2014**, *2*, 1–6.

94.   Liu, K.; Yao, Y.; Wang, J.; Zhu, L.; Sun, M.; Ren, B. *Mater. Chem. Front.* **2017**, *1*, 100–110.

95.   Kitamura, T.; Ikeda, M.; Shigaki, K.; Inoue, T.; Anderson, N. A.; Ai, X.; Lian, T.; Yanagida, S. *Chem. Mater.* **2004**, *16,* 1806–1812.

96. Narbey, S.; Oswald, F.; Meyer, T.; Kervella, Y. *Energy Environ. Sci* **2015**, *8*, 2010–2018.

97. Hua, Y.; Tien, L.; Lee, L.; Zhang, C.; Zhao, J.; Chen, T.; Wong, W.; Wong, W.; Zhu, X. *J. Mater. Chem. A* **2015**, *3*, 13848–13855.

98. Yoo, S.; Domercq, B.; Kippelen, B. *Appl. Phys. Lett.* **2004**, *5427*, 6–9.

99. Payne, M. M.; Parkin, S. R.; Anthony, J. E.; Kuo, C.; Jackson, T. N. *J. Am. Chem. Soc.* **2005**, *127*, 4986–4987.

100. Okamoto, T.; Nakahara, K.; Saeki, A.; Seki, S.; Oh, J. H.; Akkerman, H. B.; Bao, Z; Matsuo, Y. *Chem. Mater.* **2011**, *23*, 1646–1649.

101. Kazim, S.; Ramos, J. F.; Gao, P.; Nazeeruddin, M. K.; Gratzel, M.; Ahmad, S. *Energy Environ. Sci.* **2015**, *8*, 1816–1823.

102. Pham, H. D.; Hu, H.; Wong, F.; Lee, C.; Chen, W.; Feron, K.; Manzhos, D. S.; Wang, H. *J. Mater. Chem. C* **2018**, *6*, 9017–9029.

103. Lin, C.; Wang, Y.; Hsu, S.; Lo, C.; Diau, E. W. *J. Phys. Chem. C* **2010**, *114*, 687–693.

104. Walker, B.; Kim, C.; Nguyen, T. *Chem. Mater. **2011**, 23*, 470–482.

105. Suraru, S.; Zschieschang, U.; Klauk, H.; Wu, F. *Chem. Commun.* **2011**, *47*, 1767–1769.

106. Tamayo, A. B.; Tantiwiwat, M.; Walker, B.; Nguyen, T. *J. Phys. Chem. C* **2008**, *112*, 15543–15552.

107. Qu, S.; Wu, W.; Hua, J.; Kong, C.; Long, Y.; Tian, H. *J. Phys. Chem. C* **2010**, *114*, 1343–1349.

108. Farr, Y.; Raissi, M.; Fihey, A.; Pellegrin, Y.; Blart, E. *Chem Sus Chem.* **2017**, *10*, 2618–2625.

109. Mahmood, A.; Hu, J.-Y.; Xiao, B.; Taang, A.; Wang, X.; Zhou, E. *J. Mater. Chem. A* **2018**, *6*, 16769–16797.

110. Sun, Q.; Dai, L.; Zhou, X.; Li, L.; Li, Q. *Appl. Phys. Lett.* **2013**, *91*, 10–13.

111. Mishra, R.; Regar, R.; Singhal, R.; Panini, P.; Sharma, G. D.; Sankar J. *J. Mater. Chem. A* **2017**, *5*, 15529–15533.

112. Urbani, M.; Gratzel, M.; Nazeeruddin, M. K.; Torres, T. *Chem. Rev.* **2014**, *114*, 12330–12396.

113. Yella, A.; Lee, H.-W.; Tsao, H. N.; Yi, C.; Chandriyan, A. K.; Nazeeruddin, M.; Diau, E. W.; Yeh, C.-Y.; Zakeeruddin, S. M.; Gratzel, M. *Science.* **2011***, 334*, 629–633.

114. Mathew, S.; Yella, A.; Gao, P.; Humphry-baker, R.; Curchod, B. F. E.; Ashari-astani, N.; Tavernelli, I.; Rothlisberger, U.; Nazeeruddin, K.; Gratzel, M. *Nat. Chem.* **2014,** *6*, 242–247.

115. Chen, G.; Sasabe, H.; Igarashi, T.; Hong, Z.; Kido, J. *J. Mater. Chem. A* **2015**, *3*, 14517–14534.

116. Kamat, P.; Hotchandani, S.; Lind, M. D; Thomas, G.; Das, S.; George, M. V. *J. Chem. Soc. Faraday Trans.* **1993**, *89*, 2397–2402.

117. Paek, S.; Choi, H.; Kim, C.; Cho, N.; So, S.; Song, K. *Chem. Commun.* **2011***, 47*, 2874–2876.

118. Merritt, V. Y.; Hovel, H. J. *Appl. Phys. Lett.* **1976**, *414*, 27–29.

119. Wu, A. J.; Si, C.; Chen, Y.; Yang, L.; Hu, B.; Lu, Z.; Huang, Y. *Chem. Eur.J.* **2018**, *24*, 3234–3240.

120. Smits, B. E. C. P.; Setayesh, S.; Anthopoulos, T. D.; Buechel, M.; Nijssen, W.; Coehoorn, R.; Blom, P. W. M.; Boer, B. D.; Leeuw, D. M. *Adv. Mater.* **2007**, *19*, 734–738.

Synthesis and optoelectronic properties of thiophene-based semiconducting oligomers

2.1. Abstract

*Three new semiconducting oligomers (**BT**, **TT** and **TT2**) made of thiophene (donor), bithiazole (weak acceptor) and rhodanine (strong acceptor) derivatives were designed and synthesized using Suzuki and Stille coupling. They exhibited excellent absorption in the visible region because of the π-π* transition as well as intramolecular charge transfer between the donor and acceptor moieties. The packing of oligomers in the film state was studied using 2D grazing incidence X-ray diffraction analysis, and the percentage of edge-on orientation was found to be greater compared to face-on in all three oligomers. HOMO and LUMO energy levels of the oligomers in the film state were calculated from ultraviolet photoelectron yield spectroscopy analysis and from the onset of the absorption spectrum, respectively. Detailed time resolved microwave conductivity experiments proved that the oligomers can act as n-type materials making them promising for optoelectronic device applications.*

2.2. Introduction

The field of OSC research mainly dominated by the studies of small molecules, oligomers and polymers having p-type characteristics (electron donating and hole transporting abilities).[1-7] The electrical conductivity, being an extrinsic macroscopic property of the materials, arises due to the oxidation of neutral molecules to cations and reduction of neutral molecules to anions in p- and n-type materials, respectively. The unbalanced development of n-type OSCs could be attributed to the instability of organic anions in the presence of air and water. The molecules possessing higher electron affinity are more prone to reduction and are not stable in the presence of air and water. Incorporation of electron deficient moieties in the molecular frame work reduces the LUMO energy levels which in turn enhance electron affinity of the system. For n-type materials to have environmentally stable electron-transporting properties, it should have suitable HOMO-LUMO levels.[8,9] Developing air-stable, electron-transporting materials through molecular designing with desirable physical and chemical properties is the main focus of research in this area.

Many n-type semiconductors were realized by functionalization through rational molecular design and synthesis.[1] An effective approach of developing n-type organic semiconductors is to convert known p-type with suitable electron-

withdrawing substituents. Functionalizing molecules with electron-withdrawing groups such as perfluoroalkyl, Cyano (CN), Fluoro (F), perfluoroaryl, carbonyl (C=O) and imide groups deepens the LUMO energy levels for electron injection and transport.
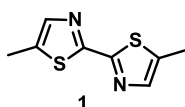
Figure 2.1 Molecular structure of Bithiazole.

Bithiazole (**1:** structure shown in **Figure 2.1**) is a moiety with nitrogen and sulphur as the heteroatoms; presence of these atoms make them electron-deficient. Rigid, coplanar and extended conjugation properties of bithiazole unit make them suitable candidate as electron deficient building block in π-conjugated materials. The structural resemblance of these moieties to thiophene, allows tuning of the optoelectronic properties of the molecules without perturbing its molecular structure.
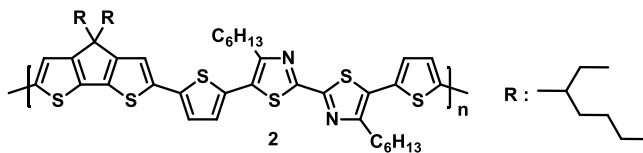
Figure 2.2 Molecular structure of **2**.

Li *et al.* reported a series of copolymers incorporated by electron-withdrawing bithiazole moiety using a donor-accepter strategy.[10] All of them

exhibit broad absorption ranging from UV to near-infrared with narrow optical bandgap of 1.70-1.94 eV, which are suitable for solar cells. They also showed better charge transfer properties and good processability. Th*e* π- conjugated copolymers possess well organized π-π stacking through fused hetero aromatic molecular frameworks. The PSC device with blend of PCBM and copolymer (**2**) shown in **Figure 2.2** achieved a PCE of 3.04%.
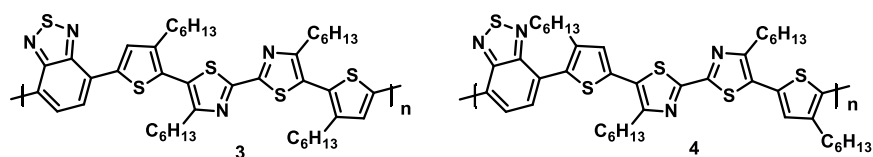
Figure 2.3 Molecular structure of copolymers; **3** and **4**.

Seki and coworkers have reported n-type copolymers (**3** and **4**; **Figure 2.3**) based on bithiazole.[11] They have incorporated benzathiadiazole and *n*-hexyl thiophene in the polymer backbone to get D-A type copolymers. The polymers exhibited different optical, electronic, and photovoltaic properties due to structural difference in the side chains of the conjugated polymers. In BHJ devices, role of additives is to control the aggregation and phase separation properties of fullerene derivatives. By incorporating solvent additive (1,8-octanedithiol), structural ordering of polymer backbone was controlled. Out of the two copolymers, **3** showed ambipolar (both p-type and n-type) characteristics in the presence of the solvent additive.
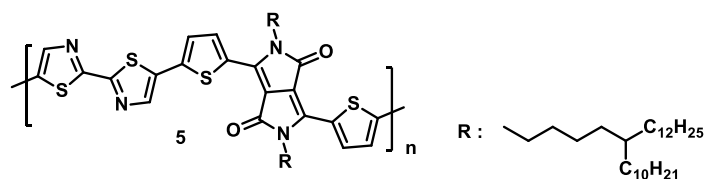
Figure 2.4 Molecular structure of the polymer **5**.

Fu *et al*. reported an electron-transporting copolymer (**5**) based on electron deficient units such as 2,2'-bithiazole and dithienyl diketopyrrolopyrrole as shown in **Figure 2.4**.[12] DFT calculations have shown that introducing bithiazole into the polymer backbone can induce planarity as well as lower the LUMO and HOMO energy levels when compared to that of bithiophene, which is a typical electron transporting moiety. Polymer **5** exhibits low bandgap (1.33 eV) and high electron affinity (-3.90 eV) values. OFET devices fabricated with **5** showed electron mobility values up to 0.3 cm^{2}V^{-1}s^{-1}. **5** was incorporated with branched 5-decylheptacyl side chains to enhance the solubility, particularly in non-halogenated, more environmentally compatible solvents. The polymer cast from a range of non-halogenated solvents showed similar film morphologies and field-effect electron mobility to those cast from halogenated solvents. The film morphologies and electron transport of **5** processed form non-halogenated solvents showed almost similar characteristics to halogenated solvents.
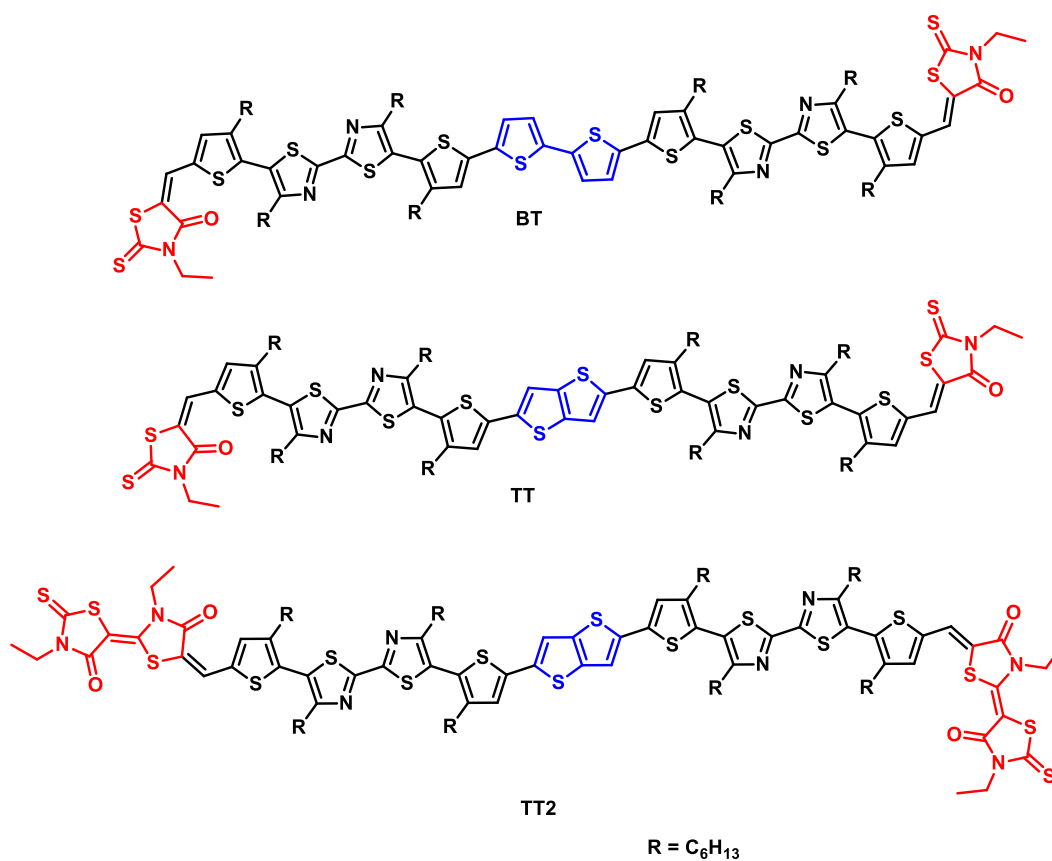
Chart 2.1 Structure of oligomers (**BT, TT, TT2**) used in the study.

In the present work, we have designed and synthesized three oligomers consisting of thiophene (strong donor), bithiazole (weak acceptor) and rhodanine (strong acceptor) derivatives (as shown in **Chart 2.1**). The middle part of the oligomers consists of two thiophenes either connected through a single bond (bithiophene) or fused together (thienothiophene). Both ends of the thiophenes are connected to bithiazoles, which are considered to be attractive materials for photovoltaic applications (both

BHJ and DSSC).[13-21] The oligomers are end-functionalized with rhodanine derivatives, which are recently emerged as one of the best acceptor moiety for semiconducting oligomers for efficient photovoltaic devices.[22-27] Introduction of functional moieties such as bithiazole and rhodanine are expected to enhance the acceptor strength of the oligomers resulting in sufficiently high electron affinity to oxidize donor (p-type) materials and hence make them act as n-type materials.

2.3. Results and Discussions

2.3.1. Synthesis

Synthetic steps leading to the formation of oligomers were shown in **Scheme 2.1**. Compounds **6**-**9** were already reported in literature.[28] Compound **9** was formylated using Vilsmeier reaction to give **10**, which was then brominated using N-bromosuccinimide (NBS) to yield **11**. Standard Stille coupling between **11** and 5,5'-bis(tributylstannyl)-2,2'-bithiophene gave **12**, whereas, the coupling between **11** and 2,5-bis(trimethylstannyl)thieno[3,2-*b*]thiophene gave **13**. **12** and **13** were reacted with acceptor *N*-ethyl rhodanine to give **BT** and **TT**, respectively. **13** was reacted with 3,3'-diethyl-2'-thioxo-[2,5'-bithiazolidine]-4',5-dione to give **TT2**. Chemical structures of the key intermediates and final

compounds were identified using ^{1}HNMR, ^{13}CNMR, IR and HRMS spectroscopy.
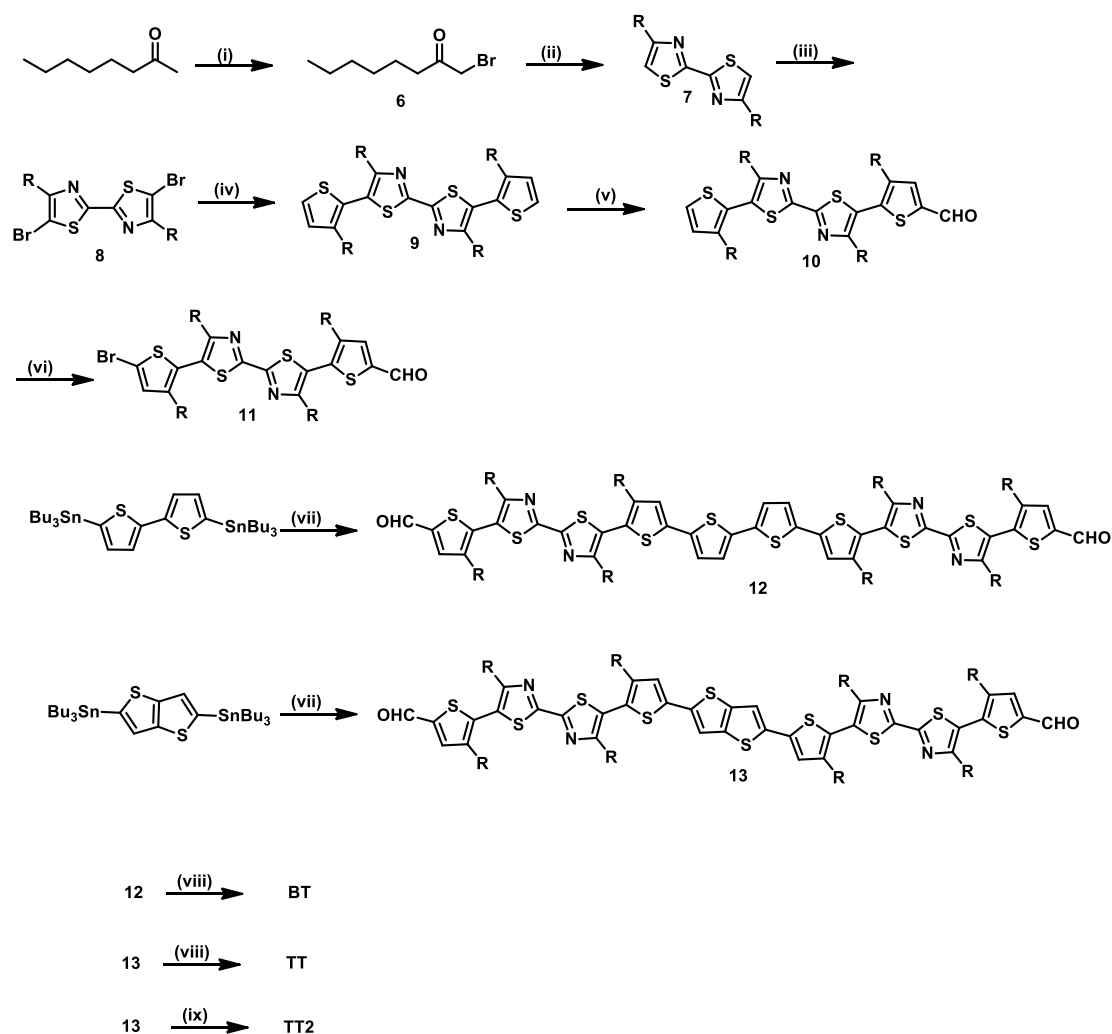
Scheme 2.1 *Synthetic route for the preparation of molecules; Reagents and conditions: (i) Br$_2$, Urea, Glacial acetic acid,12 h; (ii) Dithioxamide, Absolute ethanol, 4 h, reflux; (iii) NBS, Glacial acetic acid, 3 h; (iv) 2-(3-hexylthiophen-2-yl)-4,4,5,5-tetramethyl-1,3,2-dioxaborolane, Pd(PPh$_3$)$_4$, K$_2$CO$_3$,Toluene, 24 h, reflux; (v) POCl$_3$, DMF, Dichloroethane, 0-60 °C, 12 h; (vi) NBS, CHCl$_3$, Glacial acetic acid, 4 h; (vii) Pd(PPh$_3$)$_4$,toluene,16 h, reflux; (viii)3-ethyl-2-thioxothiazolidin-4-one, CHCl$_3$, triethylamine, 60 °C, 30 h; (ix) 3,3'-diethyl-2'-thioxo-[2,5'-bithiazolidine]-4',5-dione, CHCl$_3$, triethylamine, 60 °C, 30 h.*

2.3.2. Photophysical properties
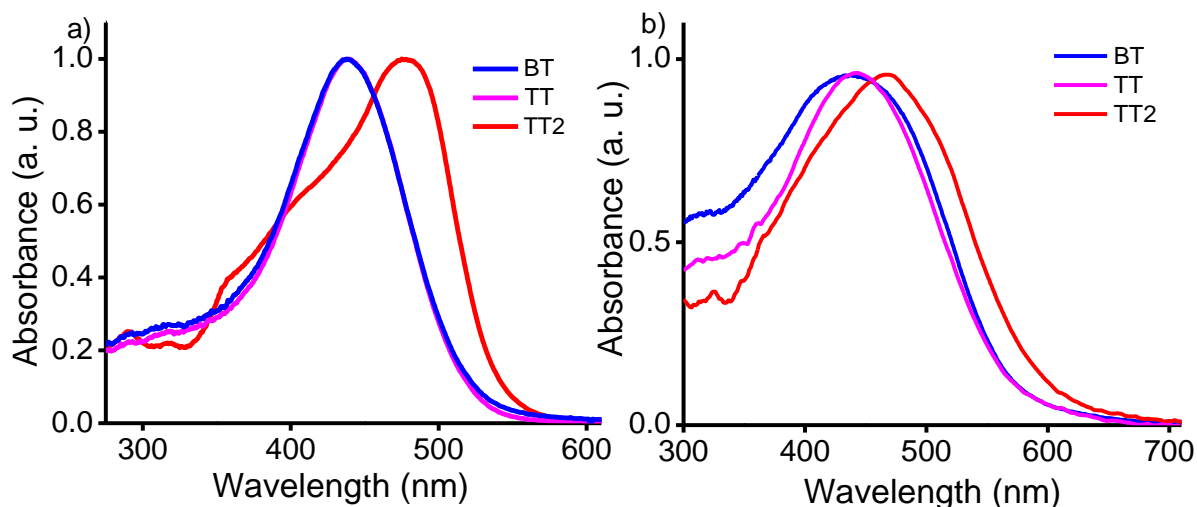
Figure 2.5 Normalised UV-vis absorption spectra (a) in chloroform (10^{-5} M) and (b) in film state of **BT**, **TT** and **TT2**.

The UV-visible absorption spectra of the oligomers in solution state (chloroform, 10^{-5} M) and film state (spin coated from chloroform on a quartz plate) are shown in **Figure 2.5a** and **2.5b**, respectively. The oligomers exhibited intense absorption ranging between 300-600 nm in the solution state which was attributed to the π-π* transition and also contribution from the intramolecular charge transfer between the donor and acceptor moieties.

The absorption maxima (λ_{max}) for **BT**, **TT** and **TT2** measured in chloroform were found to be 438, 438 and 476 nm, respectively. The extinction coefficients (ε) were found to be 5.2x10^5, 6.3x10^5, 7.6x10^5 M^{-1}

cm^{-1} for **BT**, **TT** and **TT2**, respectively. It should be noted that when the bithiophene donor (**BT**) was replaced with fused thienothiophene unit (**TT**), the λ_{max} value remained the same, whereas, extinction coefficient was increased. This observation indicates that the absorptivity of the oligomer increased by replacing bithiophene with thienothiphene, whereas the effective conjugation of the molecule remained same. When the acceptor unit was changed from rhodanine (**TT**) to bisrhodanine (**TT2**), the λ_{max} value exhibited a red shift of 38 nm and the ε value showed further increase. This could be attributed to the higher acceptor strength of the bisrhodanine compared to that of rhodanine. The wavelength corresponding to the onset of the absorption for the oligomers were found to be 524, 524 and 541 nm for **BT**, **TT** and **TT2**, respectively. The resulting optical band-gaps were calculated to be 2.37, 2.37 and 2.29 eV, respectively. In the film state, the absorption became broad and the onset of the absorption shifted towards 600 nm probably due to the contribution from aggregates. The onset of absorption red-shifted (**BT**: 573 nm; **TT**: 574 nm; **TT2**: 600 nm) and the corresponding optical band-gaps were decreased (**BT**: 2.16 eV; **TT**: 2.16 eV; **TT2**: 2.07 eV). As expected, the band-gap was lower in the presence of strong acceptor (bisrhodanine) both in solution and film state.
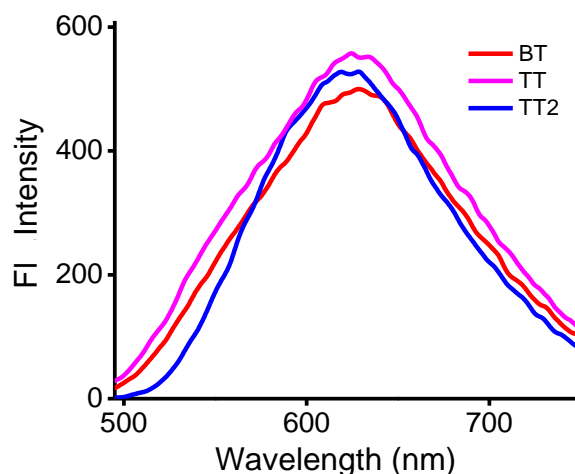
Figure 2.6 Emission spectra of the oligomers in chloroform (conc. =10^{-5} M, $\lambda_{ex} = 440$ nm).

The emission spectra of all three derivatives were found to be very weak due to the presence of donor and acceptor moieties in conjugation, which results in charge transfer states, particularly in the excited state, facilitating non-radiative decay of excitation energy. The emission maxima of the fluorescence spectra were found to be at 628, 626 and 628 nm for **BT**, **TT** and **TT2**, respectively (**Figure 2.6**). The oligomers were non-emissive in the film state due to aggregation resulting in further increase in non-radiative decay of the excited state.

2.3.3 XRD analysis

To probe the packing of oligomers in the film state, 2D grazing incidence X-ray diffraction (GIXRD) analysis were performed. The results of these

experiments in pristine films are shown in **Figure 2.7**. GIXRD patterns of the

three oligomers were performed using out-of-plane and in-plane directions.
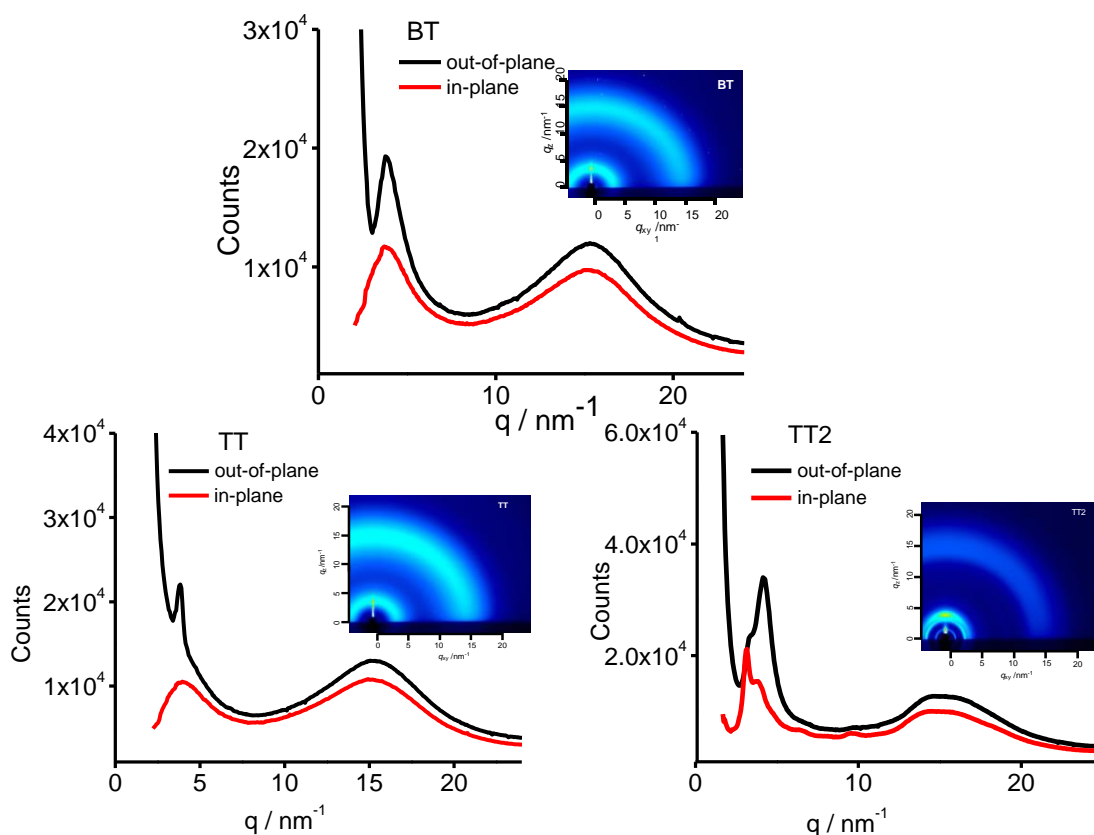
Figure 2.7 2D-GIXRD patterns of **BT, TT** and **TT2** pristine films casted from chlorobenzene on glass/ITO substrate. The extracted spectra in the out-of-plane (black) and in-plane (red) directions with the 2D images in the inset are shown

All oligomers gives a weak interlamellar first diffraction in the out-of-plane

direction as well as in-plane directions. The films also exhibited reflections

corresponding to the π-π stacking at higher angles in both directions.

Interlamellar *'d'* spacing values were obtained to be 1.61, 1.64 and 1.52 nm for

BT, **TT** and **TT2**, respectively and the corresponding π-π stacking distances were obtained to be 0.40, 0.41 and 0.41 nm, respectively.

GIXRD study indicates that edge-on orientation is predominant in the oligomers since the peaks assigned to the lamellar *d*-spacing as well as π-π stacking appear mainly in the out-of-plane pattern. Fraction of edge-on orientation were obtained to be 63, 68 and 62% respectively for **BT**, **TT** and **TT2**, whereas, face-on orientation were obtained to be 37, 32 and 38% respectively. The higher percentage of edge-on orientation in all the three oligomers must be attributed to the presence of many alkyl chains which inhibits the face-on orientation.The sharpest out-of-plane peak was obtained for **TT2** among the oligomers, which is attributed to the planar central thienothiophene and bisrhodanine which facilitates crystallization.

2.3.4. Ultraviolet photoelectron yield spectroscopy of oligomers

Ultraviolet photoelectron yield spectroscopy (UV-PYS) in the film state was employed to determine the HOMO energy levels of the oligomers, which were obtained from the ionization threshold energies. The results of these experiments in film state are shown in **Figure 2.8**.

The HOMO energy levels of **BT**, **TT** and **TT2** were obtained at -5.75, -5.89 and -6.17 eV, respectively. The band gaps obtained from the film state

absorption were added to the HOMO to obtain the LUMO levels, which were obtained as -3.59, -3.73 and -4.10 eV, respectively, for **BT**, **TT** and **TT2**. Comparing the HOMO and LUMO of these oligomers with that of **P3HT** (HOMO: -4.90 eV and LUMO -2.70 eV) showed that these compounds may function as acceptors when blended with **P3HT** donor.
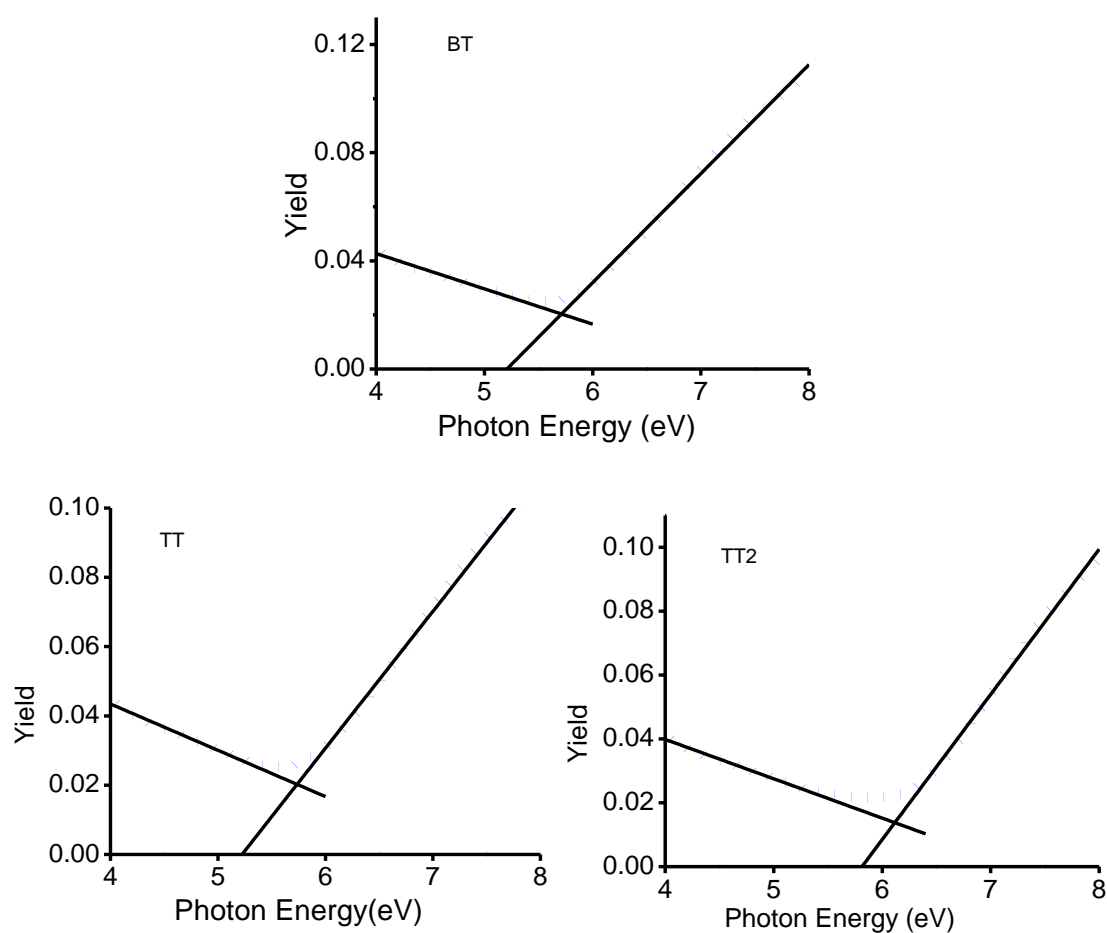
Figure 2.8 UV photoelectron yield spectroscopy of **BT**, **TT** and **TT2**.
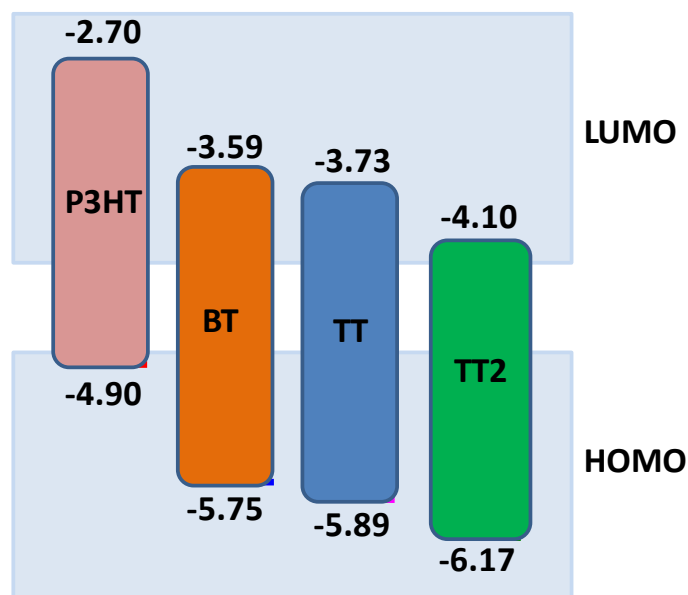
Scheme 2.2 Schematic energy diagram of the HOMO and LUMO levels of the oligomers and **P3HT**.

Table 2.1 Absorption, emission parameters and energy level values obtained from PYS spectroscopy.

Oligomer	λ_{abs} (nm)	λ_{em} (nm)	ε (M^{-1}cm^{-1})	E_{opt}[a] (eV)	HOMO[b] (eV)	LUMO[c] (eV)
BT	438	628	5,23,600	2.13	-5.75	-3.62
TT	438	626	6,32,200	2.13	-5.89	-3.76
TT2	476	628	7,65,700	2.03	-6.17	-4.14

[a]obtained from the onset of the thin film absorption spectra, [b]obtained from the binding energy of PYS experiments, [c]obtained from adding the bandgap to the HOMO values.

The energy offset between the LUMO levels of the oligomers with that of **P3HT** were good enough for efficient photoinduced electron transfer from

P3HT to the oligomers, and subsequent charge separation at the donor-acceptor interface. The schematic diagram showing the energetics of all the three oligomers with **P3HT** is shown in **Scheme 2.2**. All the photophysical and optical parameters are summarized in **Table 2.1**.

2.3.5. Photoconductivity measurements

Photoconductivities of the oligomers were measured using flash-photolysis time-resolved microwave conductivity technique (FP-TRMC), which is a electrode-less, non-contact technique giving information about the short range intrinsic charge carrier transport property using laser as the excitation source.[22-24] This technique could be used to quantify the $\phi\Sigma\mu$ values, where ϕ is the charge carrier generation quantum yield on excitation with laser light and $\Sigma\mu$ is the sum of charge carrier mobilities, i.e., the sum of electron and hole mobilities (μ_e and μ_h, respectively).

Photoconductivity of the oligomers and the corresponding blends with **P3HT** are shown in **Figure 2.9** The dependence of $\phi_{max}\Sigma\mu$ values as a function of wt% of **P3HT** is shown in **Figure 2.9d** and the dependence of the corresponding half-lifetime of the charge carriers ($\tau_{1/2}$) as a function of wt% of **P3HT** is shown in **Figure 2.9e**. Photoconductivity of the oligomers and the corresponding blends with **P3HT** are shown in **Figure 2.9** The

dependence of $\phi_{max}\Sigma\mu$ values as a function of wt% of **P3HT** is shown in **Figure 2.9d** and the dependence of the corresponding half-lifetime of the charge carriers ($\tau_{1/2}$) as a function of wt% of **P3HT** is shown in **Figure 2.9e**.

In the pristine state, the oligomers exhibited a comparable $\phi_{max}\Sigma\mu$ values (**BT**: 2×10^{-5} cm^{-2}V^{-1}s^{-1}, **TT**: 2.4×10^{-5} cm^{-2}V^{-1}s^{-1}, **TT2**: 1.7×10^{-5} cm^{-2}V^{-1}s^{-1}). Photoconductivity of all oligomers increases with increase in the wt% of **P3HT** until it reaches a maximum and then decreases with further increase in the latter. A small difference could be observed in the case of **TT2** where the trend is not maintained and it shows a random nature. The increase in $\phi_{max}\Sigma\mu$ of the oligomers in thepresence of **P3HT** could be attributed to the enhanced generation of charge carriers (electron and hole) due to the oxidation of the excited state of the former in the presence of latter. In other words, the electron affinity of the oligomers are sufficiently high to oxidize the excited state of **P3HT** and hence to separate the excitons formed upon photoexcitation into charges just like an n-type material in a photovoltaic cell.Half-lifetime of the charge carriers ($\tau_{1/2}$) shows an increase with increase in the wt% of **P3HT** reaching a maximum (5.4 μs for **BT**, 3.9 μs for **TT** and 1.6 μs for **TT2**, respectively) followed by decrease as in the case of $\phi\Sigma\mu$. This indicates that the oligomers not

only separate the charge carriers but also preventing recombination probably by allowing them to travel enough distance along the donor/acceptor network. The $\phi_{max}\Sigma\mu$ values and $\tau_{1/2}$ values were given in **Table 2.2**. The above studies proved that these oligomers are promising semiconducting materials with n-type characteristics.

Table 2.2 Summary of the Laser flash photolysis-TRMC experiments obtained in presence of different weight% of **P3HT** upon 355 nm laser excitation.

	BT			TT			TT2	
P3HT (wt%)	$\phi\Sigma\mu_{max}$ (m^2/Vs) ($\times10^{-3}$)	$\tau_{1/2}$ (s) ($\times10^6$)	**P3HT** (wt%)	$\phi\Sigma\mu_{max}$ (m^2/Vs) ($\times10^{-3}$)	$\tau_{1/2}$ (s) ($\times10^{-6}$)	**P3HT** (wt%)	$\phi\Sigma\mu_{max}$ (m^2/Vs) ($\times10^{-3}$)	$\tau_{1/2}$ (s) ($\times10^{-6}$)
0	0.02	0.91	0	0.02	0.59	0	0.02	0.22
33	1.6	3.9	33	1.3	3.8	33	0.41	1.5
50	5.1	5.4	50	1.9	3.1	50	1.5	1.11
60	4.7	4.0	60	2.7	3.1	60	0.7	1.0
66	4.8	1.7	66	3.7	1.7	75	1.4	0.54
75	4.0	1.5	75	2.3	0.86	81	0.6	0.37
83	3.5	1.0	83	2.4	0.46	90	2.8	0.49
100	0.7	0.65	100	0.7	0.62	100	0.7	0.62
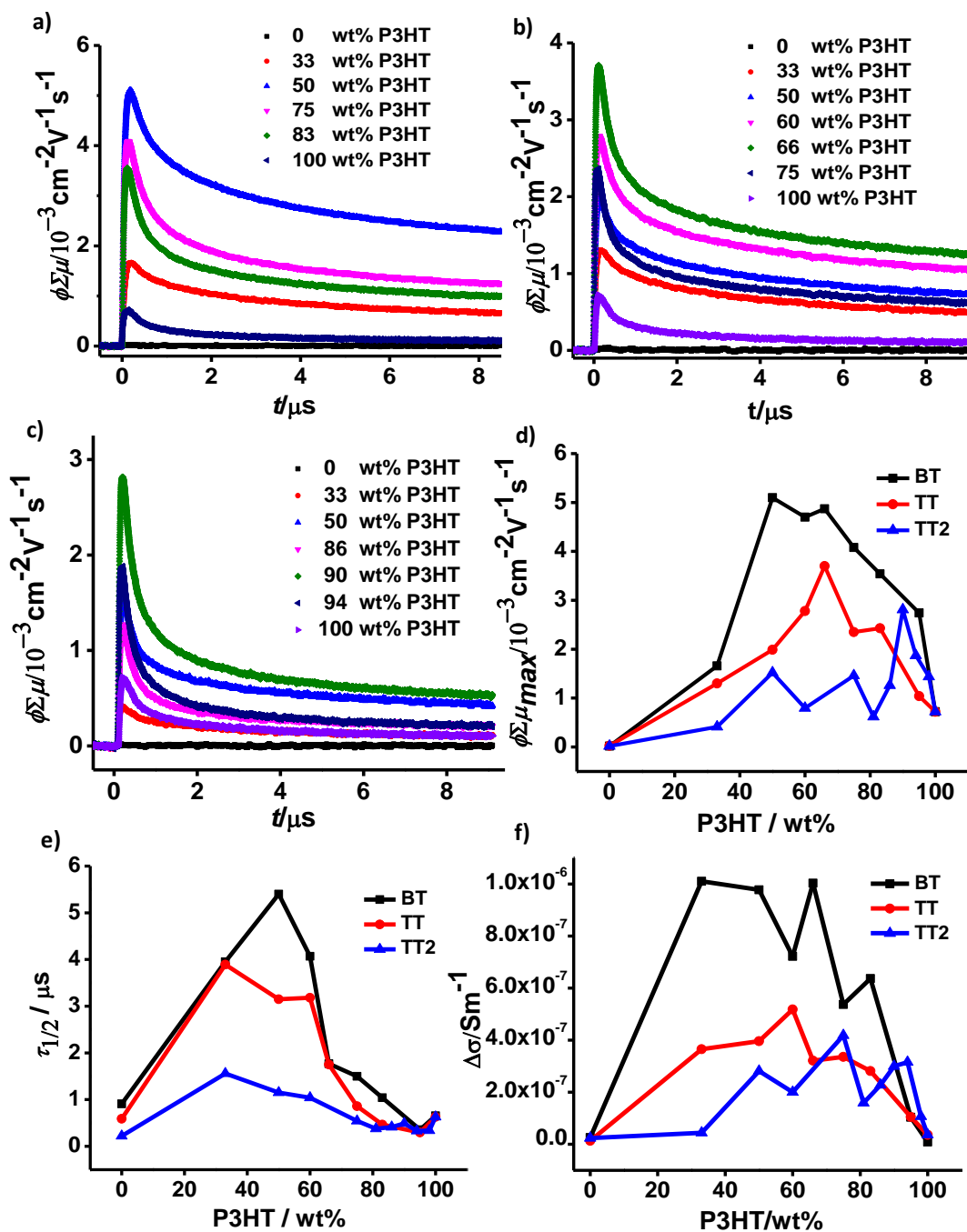
Figure 2.9 FP-TRMC transients of (a) **BT** (b) **TT** (c) **TT2** in presence of increasing weight percentage of **P3HT**, (d) ϕ_{max} values as a function of wt% of **P3HT** (e) $\tau_{1/2}$ values as a function of wt% of **P3HT** under 355 nm laser irradiation (f) $\Delta\sigma$ values as a function of wt% of **P3HT** under white light illumination.

2.3.6. Photovoltaic measurements

Majority of the conjugated polymers/oligomers reported so far have been hole transporting in nature, and the development of efficient electron-transporting materials (n-type) has been very challenging. But electron transport materials are absolutely necessary for certain kind of applications such as solar cells. Though lot of research is done for the development of n-type materials, the molecular diversity of n-type materials is still lower and are mainly based on electron efficient polycyclic rings such as naphthalene and perylenediimides apart from fullerene derivatives.[25-27,29-34] n-Type materials based on oligomers employing donor-accepter approach are less.[35-40] The oligomers reported in this work may give light to the development of oligomers based on n-type materials for organic electronics. Particularly considering the edge-on orientation of the oligomers in the film state, they might be potential candidate for n-type transistors.

In order to check the suitability of the oligomers as n-type materials in photovoltaic devices, bulk-heterojunction photovoltaic devices were fabricated in combination with **P3HT** (acts as the donor).The best blend ratio obtained from the TRMC experiment was selected for the fabrication of PV devices. o-Dichlorobenzene was used as the solvent and a device structure of

glass/ITO/ZnO/BHJ/MoO$_3$/Ag used as the solvent and a device structure of was employed. The *J-V* characteristics of the devices are shown in **Figure 2.10** and photovoltaic parameters are summarized in **Table 2.3**.
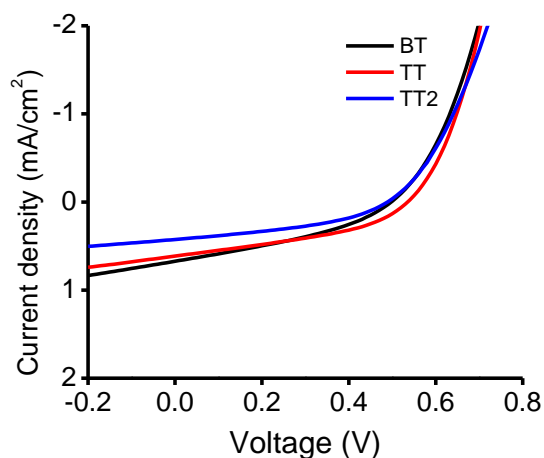
Figure 2.**10** *J–V* characteristics of the photovoltaic devices fabricated from a blend solutions of **BT, TT** and **TT2** with **P3HT** casted from o-dichlorobenzene solution (device structure: glass/ITO/ZnO/BHJ/MoO$_3$/Ag.

All the three oligomers exhibited lower photovoltaic efficiency values due to low charge carrier mobility. Slight improvements in the efficiencies could be expected on further optimization. The power conversion efficiency of **TT** was slightly higher compared to the other two oligomers which was found to be 0.13% with an open circuit voltage (*V*$_{OC}$ of 0.535), short circuit current density (*J*$_{SC}$ of 0.614) and fill factor (*FF* of 0.394). **BT** (*V*$_{OC}$:0.49, *J*$_{SC}$:0.673, *FF*:0.355) and **TT2** (*V*$_{OC}$:0.489, *J*$_{SC}$:0.426, *FF*:0.398) exhibited η values of 0.119% and 0.083%, respectively (**Table 2.3**). All the three

oligomers exhibited lower photovoltaic efficiency values which were comparable to each other.

Table 2.3 Photovoltaic performance parameters of the oligomers.

Oligomer	P3HT: Oligomer ratio	J_{SC} (mAcm^{-2})	V_{OC} (V)	FF	η (%)
BT	1:1	0.673	0.497	0.355	0.119
TT	1.5:1	0.614	0.535	0.394	0.130
TT2	3:1	0.426	0.489	0.398	0.083

The X-ray diffraction (XRD) studies of the three oligomers in the film state blended with **P3HT** was measured and compared with the pristine films of the respective oligomers. The blend ratios which showed highest transient intensity in TRMC experiments for each oligomers were selected for the XRD analysis. The resulting XRD profiles are shown in **Figure 2.11**. All oligomers showed sharp peaks corresponding to the lamellar stacking. The diffraction corresponding to π-stacking was found to be sharp in **TT**, whereas, that in **BT** and **TT2**was broad and merged with the alkyl chain crystallization peaks. On blending with **P3HT**, the diffractions corresponding to the oligomer stacking become invisible due to the strong diffractions from **P3HT**. In the blend film, the lattice spacing at about 16.4 Å corresponds to the inter-chain spacing of

P3HT, whereas, the π-π stacking was observed in the 3.7 Å region. Since the peaks of the oligomers are mostly in the same region as that of **P3HT**, it was difficult to predict how the stacking isaffected in the oligomers after blending with **P3HT**.However, the stacking of **P3HT** was not affected by blending with oligomers also may not be affected by **P3HT**.
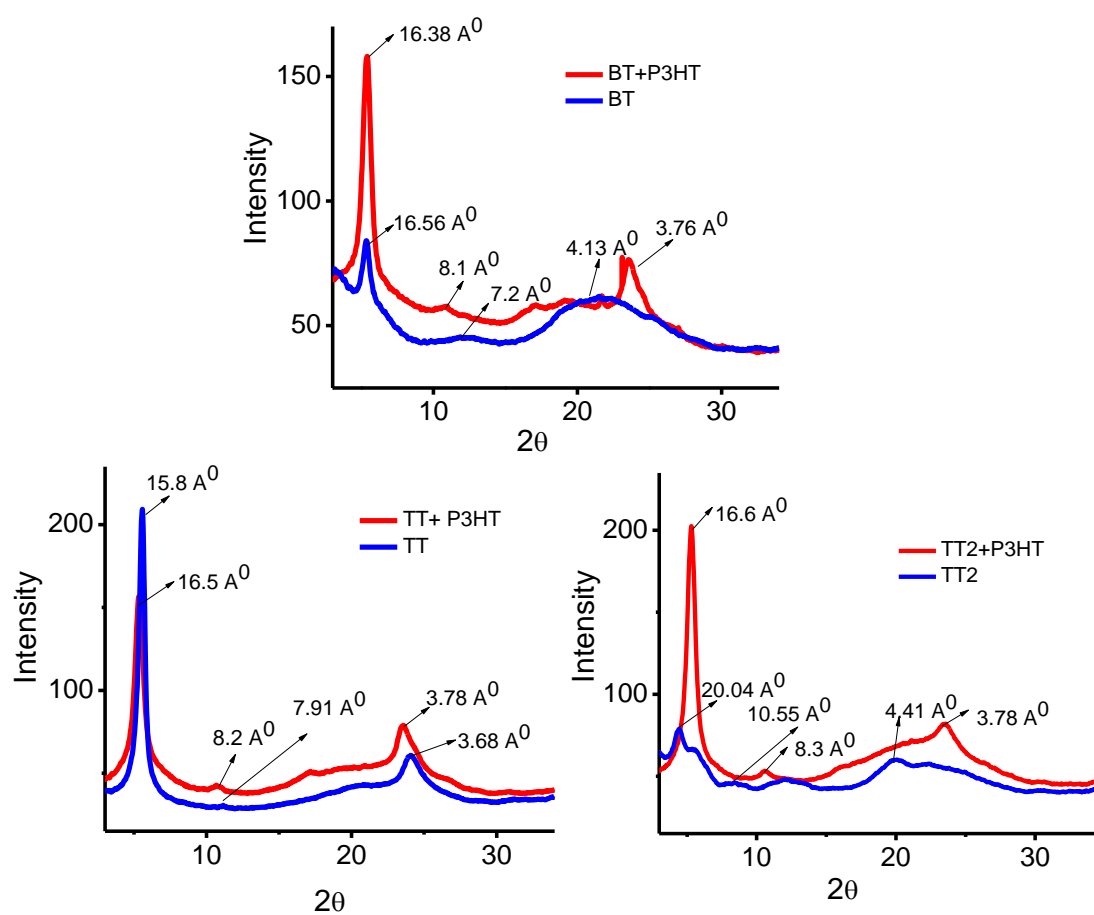
Figure 2.11 XRD diffraction patterns of **BT**, **TT** and **TT2** alone and blend films with **P3HT** (**BT**: **P3HT** 1:1, **TT:P3HT** 1:1.5, **TT2:P3HT** 1:3).

The lower photovoltaic efficiencies of the oligomers could be mainly attributed to the predominant edge-on orientation of the molecules as evident from the X-ray analysis. Rational choice of alkyl chains (for instance, the use of branched chains[41]) may improve the face-on orientation of the molecules thereby increasing the PCE. Lower FF value of these devices was another reason, which may arise due to the lower and imbalanced charge carrier mobility. Though the photovoltaic efficiencies of devices made from the oligomers are very much low, they seem to be promising n-type materials.

2.4. Conclusions

Three new oligomers based on bithiophenes or thienothiophenes as donor, bithiazoles as spacers and rhodanine and bisrhodanine units as acceptor were synthesized. The absorption maximum and the extinction coefficient were improved in the presence of thienothiophene as donor and dirhodanine unit as acceptor. XRD studies indicated that the percentage of edge-on orientation was more compared to that of the face-on orientation. Ultraviolet photoelectron spectroscopy and film state absorption were employed to understand the HOMO-LUMO energy levels. The energy offset between the LUMO levels of the oligomers with that of **P3HT** were good enough for efficient photoinduced intermolecular electron transfer from **P3HT** to the oligomers indicating that the

oligomers can act as n-type materials. This was confirmed by FP-TRMC analysis which showed that the oligomers are excellent n-type materials in presence of **P3HT** as evident from the increase in photoconductivity transient signals in the presence of latter. Our studies revealed that the oligomers are promising for organic electronic applications.

2.5. Experimental section

2.5.1. Materials and characterization techniques

The reagents and materials for synthesis were purchased from Sigma-Aldrich, Merck, TCI and Spectrochem chemical suppliers, and are used as received. Air and water sensitive synthetic steps were performed in an argon atmosphere using standard Schlenk techniques. ^{1}H and ^{13}C-NMR spectra were recorded using Bruker-500 MHz spectrometer. The compounds were thoroughly purified using the recycling preparative HPLC system of Japan Analytical Industry Co. Ltd, LC-9220 II NEXT SERIES (eluent CHCl$_3$). Absorption spectra were recorded using Shimadzu UV-Visible 2401PC spectrophotometer. Fluorescence spectra were recorded on a PerkinElmer LS55 fluorescence spectrometer.UV photoelectron yield spectroscopy (PYS) measurements were performed on a Sumitomo Heavy Industry Co. PCR-202. GIXRDexperiments were

conducted at the Spring-8 on the beam line BL19B2 using 12.39 keV (λ =
1 Å) X-ray. The GIXRD patterns were recorded with a 2-D image detector
(Pilatus 100K).

Flash-photolysis time-resolved microwave conductivity (FP-TRMC):
Transient conductivity was measured by the FP-TRMC technique. A
resonant cavity was used to obtain a high degree of sensitivity in the
measurement. The resonant frequency and the microwave power were set
at B9.1 GHz and 3 mW, respectively, so that the electric field of the
microwave was sufficiently small not to disturb the motion of charge
carriers. The value of conductivity is converted to the product of the
quantum yield (ϕ) and the sum of charge carrier mobilities ($\Sigma\mu$), by the
following equation.

$$\phi \sum \mu = \frac{I}{e.A.I_0.\mathrm{F_{light}}} \cdot \frac{\Delta Pr}{Pr} \qquad (1)$$

where e, A, I_0, $\mathrm{F_{light}}$, ΔP_r, and P_r are the unit charge of a single electron, a
sensitivity factor [$(S\ m^{-1})^{-1}$], incident photon density of the excitation laser
(photons per m^2), a correction (or filling) factor (m^{-1}), a change in reflected
microwave power, and a power of reflected microwave, respectively. The
change in conductivity is equivalent to $\Delta P_r/(AP_r)$. 500 nm laser light with a
photon density of 6.4×10^{15} photons per cm^2 was used as the excitation source.

The sample was set at the highest electric field in a resonant cavity. The experiments were carried out at room temperature.

Synthesis of 10:
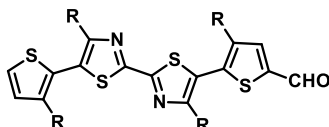
A Vilsmeier reagent was prepared in cold condition using $POCl_3$ (0.33 mL, 3.5 mmol) and DMF (1.2 mL, 16.1 mmol) in a RB flask under nitrogen(N_2) atmosphere. Then it was transferred to compound **9** (1.2 g, 1.7 mmol) in anhydrous dichloroethane (12 mL) kept at 0^0C under Nitrogen atmosphere. After being stirred for 2 hours(hrs) at $0\ ^oC$, it was refluxed at 60^0C for 12 hours. The reaction mixture was poured into ice cold water (200 mL), neutralized with Na_2CO_3, and extracted with chloroform. The combined organic layer was washed with water and dried over magnesium sulphate. After removal of solvent, it was purified by column chromatography (silica gel, 50% CH_2Cl_2-hexane) to afford a greenish yellow viscous liquid (Yield: 63%). ^1H NMR (500 MHz, $CDCl_3$) δ_H: 9.89 (s, 1H), 7.67 (s, 1H), 7.37 (d, 1H), 7.00 (d, 1H), 2.67-2.72 (m, 4H), 2.59 (t, 2H, $J_1 = 8$ Hz, $J_2 = 7.5$ Hz), 2.54 (t, 2H, $J_1 = 7.5$ Hz, $J_2 = 8$ Hz), 1.66-1.72 (m, 4H), 1.22-1.30 (m, 28H), 0.85 (m, 12H). ^{13}C NMR (125 MHz, $CDCl_3$) δ180.99, 159.54, 157.82, 156.30, 155.81, 142.83, 141.77, 141.40,

135.69, 134.40, 127.15, 124.58, 124.21, 123.26, 121.68, 29.83, 29.79, 29.77, 28.80, 28.58, 28.14, 27.91, 27.88, 27.79, 27.30, 27.24, 27.18, 20.77, 20.74, 12.33, 12.26, 12.23. HRMS: m/z = 697.33 (M$^+$ + H).

Synthesis of 11:
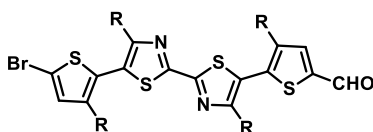
Compound **10** (240 mg, 0.344 mmol)was dissolved in a mixture of chloroform (14 mL) and glacial acetic acid (3.84 mL). *N*-Bromosuccinimide (122.54 mg, 0.688 mmol) was added in small portions, and the reaction mixture was stirred in the dark for 4 hrs at room temperature. The reaction mixture was then added to water and extracted with chloroform. The crude product was purified by column chromatography (silica gel, 50% CH_2Cl_2-hexane) to afford the product **11** as a yellow solid which was recrystallized from hot methanol. (Yield: 82%). ^{1}H NMR (500 MHz, CDCl$_3$) δ_H: 9.89 (s, 1H), 7.67 (s, 1H), 6.96 (s, 1H), 2.66-2.72 (m, 4H), 2.59 (t, 2H, J_1 = 7.5 Hz, J_2= 8 Hz), 2.48 (t, 2H, J_1 = 7.5 Hz, J_2 = 8 Hz), 1.22-1.72 (m, 32H), 0.84-0.87 (m, 12H). ^{13}C NMR (125 MHz, CDCl$_3$) δ182.78, 161.06, 160.08, 158.16, 158.10, 144.65, 144.38, 143.23, 137.48, 136.03, 131.73, 126.50, 124.49, 123.73, 113.10, 31.58, 31.55, 31.53,

30.42, 30.36, 29.91, 29.71, 29.57, 29.02, 28.99, 28.96, 28.91, 22.56, 22.55, 22.53, 14.06, 14.03, 14.02. HRMS: *m/z* = 777.24 (M$^+$ + H).

Synthesis of 12:
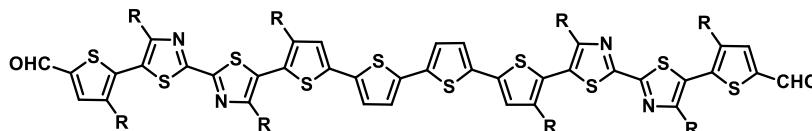
Compound **11** (0.208 g, 0.268 mmol) and 5,5'-bis(tributylstannyl)-2,2'-bithiophene (0.100 g, 0.13 mmol) were weighed into a two-necked RB flask and dissolved in dry toluene (5 mL). Air was removed from the flask and filled with nitrogen by applying freeze−pump−thaw method for three times. Pd(PPh$_3$)$_4$(16 mg, 0.013 mmol) was added under N$_2$ counter flow and the reaction mixture was refluxed at 110 °C for 16 hrs. The reaction mixture was then poured into water and extracted with chloroform. The combined organic fraction was dried over Na$_2$SO$_4$ and evaporated to dryness under reduced pressure. The resulting crude product was purified by column chromatography (silica gel, 50% CH$_2$Cl$_2$-hexane) to afford product as a red solid.Yield: 80%.^{1}H NMR (500 MHz, CDCl$_3$)δ_H: 9.90 (s, 2H), 7.677 (s, 2H), 7.08-7.11 (m, 6H), 2.70-2.76 (m, 8H), 2.58-2.61 (m, 4H), 2.52-2.55 (m, 4H), 1.68-1.76 (m, 8H), 1.25-1.33 (m, 56H), 0.86 (t, 24H).^{13}C NMR δ_C (150 MHz, CDCl$_3$,): 181.77, 160.16, 158.75, 157.13, 156.77, 143.62, 143.51, 142.20, 136.46, 135.15, 135.10, 134.88, 124.40, 123.60,

123.43, 123.19, 122.61, 30.59, 30.53, 30.52, 29.49, 29.35, 28.92, 28.82, 28.57, 28.08,28.03,28.01, 27.95, 27.91, 21.56, 21.54, 21.51, 13.06, 13.03, 13.00. MALDI-TOF: m/z calcd. for $C_{86}H_{114}N_4O_2S_{10}$ [M]$^+$: 1554.614, found 1554.434.

Synthesis of 13:
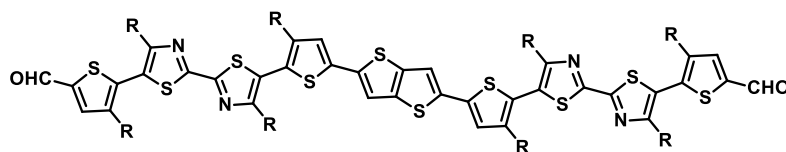
Compound **13** was synthesized employing a similar procedure for **12** using compound **11** (120 mg, 0.154 mmol) and 2,5-bis(trimethylstannyl)thieno[3,2-b] thiophene (32 mg, 0.062 mmol). The resulting crude product was purified by column chromatography (silica gel, 50% CH_2Cl_2−hexane) to afford product as a red orange solid. Yield: 84%. ^{1}H NMR (500 MHz, CDCl$_3$)δ_H:9.90 (s, 2H), 7.677 (s, 2H), 7.33 (s, 1H), 7.08-7.18 (m, 3H), 2.70-2.75 (m, 8H), 2.52-2.61 (m, 8H), 1.72-1.73 (m,8H), 1.25-1.27 (m, 56H), 0.86 (t, 24H).^{13}C NMRδ_C (150 MHz, CDCl$_3$): 182.72, 161.12, 159.79, 158.13, 157.78, 144.63, 144.54, 143.22, 139.18, 138.73, 138.62, 138.04, 137.50, 136.05, 125.60, 125.35, 124.46, 123.69, 115.91, 31.93, 31.62, 31.57, 31.55, 30.52, 30.37, 29.94, 29.87, 29.71, 29.61, 29.59, 29.37, 29.13, 29.08, 29.04, 28.98, 28.94, 22.71, 22.66, 13.00. MALDI-TOF: m/z calcd for $C_{84}H_{112}N_4O_2S_{10}$ [M+H]$^+$: 1529.599, found 1529.434.

Synthesis of BT:
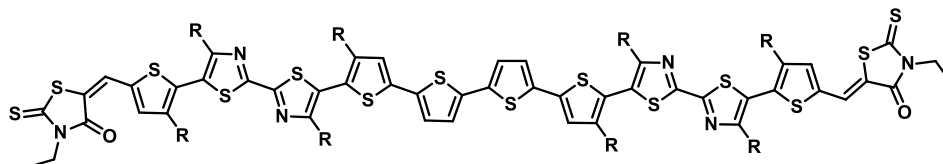
Compound **12** (40 mg, 0.02 mmol), 3-ethyl-2-thioxothiazolidin-4-one (33.1 mg, 0.2 mmol), triethylamine (3 drops) in chloroform (3 mL) were heated at 120 °C for 30 h. The reaction mixture was then poured into water and extracted with chloroform. The combined organic fraction was dried over Na_2SO_4 and evaporated to dryness under reduced pressure. The resulting crude product was purified by column chromatography (silica gel, 50% CH_2Cl_2−hexane) to afford product as blackish red solid. Yield: 95%. M. P. 105 °C.^{1}H NMR (500 MHz, $CDCl_3$)δ_H:7.82 (s,2H), 7.26-7.34 (m, 6H), 7.09-7.11 (m, 2H), 4.17-4.21 (m, 4H), 2.61-2.76 (m, 8H), 2.53-2.61 (m, 8H), 1.72-1.75 (m, 8H), 1.63 (m, 6H),1.28-1.31 (m, 56H) 0.86 (t, 24H).^{13}C NMR δ_C (150 MHz, $CDCl_3$): 192.07, 167.33, 162.60, 161.07, 158.12, 154.96, 145.25, 144.53, 139.58, 138.08, 137.53, 136.18, 134.05, 100.00, 127.81, 125.38, 124.67, 123.78, 122.40, 121.74, 39.97, 31.61, 31.58, 31.55, 30.51, 30.43, 30.03, 29.86, 29.71, 29.62, 29.07, 29.01, 28.89, 22.60, 22.55, 14.08, 14.04, 12.29; IR ($\bar{\upsilon}$): 3082, 2933, 2852, 1693, 1541, 1329, 1216, 1123 cm^{-1};MALDI-TOF: m/z calcd for $C_{96}H_{124}N_5O_2S_{14}$ $[M]^+$: 1840.587, found 1840.365.

Synthesis of TT:
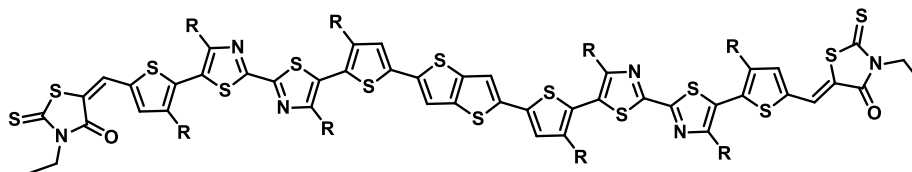
TT was synthesized employing similar procedure as **BT** using compound **13** (40 mg, 0.02 mmol), 3-ethyl-2-thioxothiazolidin-4-one (32.8 mg, 0.2 mmol), triethylamine (3 drops) and chloroform (3 mL). The resulting crude product was purified by column chromatography (silica gel, 50% CH_2Cl_2−hexane) to afford product as blackish red solid. Yield: 88%. M. P. 120 °C.^{1}H NMR (500 MHz, CDCl$_3$) δ_H :7.81 (s, 2H), 7.28-7.08 (m, 6H), 4.16-4.21 (m, 4H), 2.61-2.77 (m, 8H), 2.53-2.61 (m, 8H), 1.71-1.77 (m, 8H), 1.61 (m, 6H),1.28-1.31 (m, 56H) 0.86 (t, 24H). ^{13}C NMR (150 MHz, CDCl$_3$) δ_C: 192.06, 167.32, 161.17, 159.83, 158.12, 157.80, 145.24, 144.52, 138.07, 137.53, 136.18, 135.44, 134.02, 125.48, 124.65, 124.46, 124.26, 123.78, 121.74, 100.00, 39.97, 31.61, 31.58, 31.55, 30.51, 30.43, 30.03, 29.87, 29.62, 29.11, 29.06, 29.01, 28.89, 22.60, 22.55, 14.08, 14.04, 12.29; IR ($\bar{v}$): 2931, 2850, 2359, 1706, 1702, 1588, 1330, 1234, 1130 cm^{-1}; MALDI-TOF: m/z calcd. for $C_{94}H_{122}N_5O_2S_{14}$ [M]$^+$: 1814.571, found 1814.371.

Synthesis of TT2:
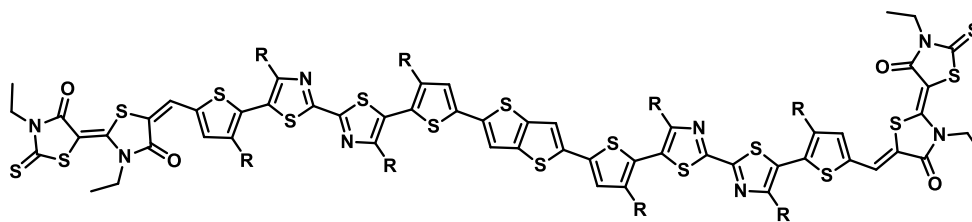
 TT2 was synthesized employing similar procedure used for **TT** employing compound **13** (75 mg, 0.004 mmol), 3,3'-diethyl-2'-thioxo-[2,5'bithiazolidine]-4',5-dione (128 mg, 0.04 mmol), triethylamine (3 drops) and chloroform (6 mL). The resulting crude product was purified by column chromatography (silica gel, CH_2Cl_2) to afford product as blackish red solid. Yield:76%. M. P. 118.5 ^{0}C. ^{1}H NMR (500 MHz, $CDCl_3$)δ_H: 7.89 (s, 2H), 7.12-7.36 (m, 6H), 4.19-4.20 (m, 4H), 2.73-2.78 (m, 8H), 2.54-2.61 (m, 8H), 1.29-1.75 (m, 20H),1.29-1.32 (m, 56H) 0.85 (t, 24H).).^{13}C NMRδ_C (150 MHz, $CDCl_3$,): 189.72, 167.10, 166.50, 161.04, 159.97, 158.13, 157.83, 145.32, 144.71, 144.54, 138.76, 138.67, 138.34, 138.05, 134.93, 133.28, 125.57, 123.92, 119.24, 115.98, 100.01, 94.22, 40.39, 40.02, 31.63, 31.60, 30.52, 30.06, 29.91, 29.71, 29.61, 29.55, 29.09, 28.92, 22.57, 14.81, 14.09, 14.04, 12.19; IR ($\bar{v}$): 2927, 2850, 1691, 1597, 1542, 1456, 1216 cm^{-1}; MALDI-TOF: m/z calcd. for $C_{104}H_{132}N_8O_4S_{16}$ [M]$^+$: 2068.590, found 2068.911.

Solar cell fabrication**:** The OPV device configuration was ITO/Al (110 nm)/ZnO (30nm) / BHJ active layer/ MoO_3(10 nm)/Ag (100 nm) with an active area of 7.1

mm^2. The thickness of the active layer was measured using a surface profiler (ULVAC model Dektak 150). Current-voltage (*J-V*) curves were measured using a source-measure unit (ADCMT Corp., 621A) under AM 1.5 G solar illumination at 100 mW cm^{-2} (monitored by a calibrated standard cell, Bunko Keiki SM-250KD) from a 300 W solar simulator (SAN-EI Corp., XES-301S).

2.5. References

1. Marks, T. J. *Acc. Chem. Res.* **2011**, *44*, 501–510.
2. Zaumseil, J.; Sirringhaus, H. *Chem. Rev.* **2007**, *107*, 1296–1323.
3. Facchetti, A. *Chem. Mater.* **2011**, *23*, 733–758.
4. Zhao, X.; Zhan, X. *Chem. Soc. Rev* **2011**, *40*, 3369–4260.
5. Grimsdale, A. C.; Chan, K. L.; Martin, R. E.; Jokisz, P. G.; Holmes, A. B. *Chem. Rev* **2009**, *109*, 897–1091.
6. Dodabalapur, A. Organic and Polymer Transistor for Electronics. **2006**, *9*, 24–30.
7. Facchetti, A. *Mater. today* **2007**, *10*, 28–37.
8. Chang, Y.; Kuo, M.; Chen, C.; Lu, H.; Chao, I. *J. Phys. Chem. C* **2010**, *114*, 11595–11601.
9. Dong, H.; Wang, C.; Hu, W. *Chem. Commun.* **2010**, *46*, 5211–5222.
10. Li, K.; Huang, J.; Hsu, Y.; Huang, P.; Lin, J.; Ho, K.; Wei, K.; Lin, H.; Chu, C. *Macromolecules* **2009**, *42*, 3681–3693.
11. Balan, B.; Vijayakumar, C.; Saeki, A.; Koizumi, Y.; Seki, S. *Macromolecules* **2012**, *45*, 2709–2719.
12. Fu, B.; Wang, C.; Rose, B. D; Jiang, Y; Chang, M; Chu, P.; Yuan, Z.; Fuentes-hernandez, C.; Kippelen, B.; Brédas; J. L, Collard; D. M., Reichmanis; E. *J. Chem. Mater. 2015*, 27, 2928-2937
13. Chen, Y.; Yan, Y.; Du, Z.; Bao, X.; Liu, Q.; Roy, V. A. L.; Sun, M.; Yang, R.; Lee, C. S. *J. Mater. Chem. C* **2014**, *2*, 3921–3927.

14. Du, Z.; Chen, W.; Qiu, M.; Chen, Y.; Wang, N.; Wang, T.; Sun, M.; Yu, D.; Yang, R. *Phys. Chem. Chem. Phys.* **2015**, *17*, 17391–17398.

15. Du, Z.; Chen, Y.; Chen, W.; Qiao, S.; Wen, S.; Liu, Q.; Zhu, D.; Sun, M.; Yang, R. *Chem. - An Asian J.* **2014**, *9*, 2621–2627.

16. Chen, Y.; Du, Z.; Chen, W.; Liu, Q.; Sun, L.; Sun, M.; Yang, R. *Org. Electron.* **2014**, *15*, 405–413.

17. Chen, Y.; Du, Z.; Chen, W.; Wen, S.; Sun, L.; Liu, Q.; Sun, M.; Yang, R. *New J. Chem.* **2014**, *38*, 1559–1564.

18. Wang, K.; Liang, R. Z.; Wolf, J.; Saleem, Q.; Babics, M.; Wucher, P.; Abdelsamie, M.; Amassian, A.; Hansen, M. R.; Beaujuge, P. M. *Adv. Funct. Mater.* **2016**, *26*, 7103–7114.

19. Zhang, M.; Guo, X.; Li, Y. *Adv. Energy Mater.* **2011**, *1*, 557–560.

20. Yang, M.; Peng, B.; Liu, B.; Zou, Y.; Zhou, K.; He, Y.; Pan, C.; Li, Y.; Zou, Y. *J. Phys. Chem. C* **2010**, *114*, 17989–17994.

21. Shi, Q.; Fan, H.; Liu, Y.; Chen, J.; Ma, L.; Hu, W.; Shuai, Z.; Li, Y.; Zhan, X. *Macromolecules* **2011**, *44*, 4230–4240.

22. Saeki, A.; Fukumatsu, T.; Seki, S. *Macromolecules* **2011**, *0*, 3416–3424.

23. Saeki, A.; Tsuji, M.; Seki, S. *Adv. Energy Mater.* **2011**, *1*, 661–669.

24. Yoshikawa, S.; Saeki, A.; Saito, M.; Osaka, I.; Seki, S. *Phys. Chem. Chem. Phys.* **2015**, *17*, 17778–17784.

25. Zhou, E.; Cong, J.; Wei, Q.; Tajima, K.; Yang, C.; Hashimoto, K. *Angew. Chem. Int. Ed* .**2011**, *50*, 2799–2803.

26. Park, G. E.; Kim, H. J.; Choi, S.; Lee, D. H.; Uddin, M. A.; Woo, H. Y.; Cho, M. J.; Choi, D. H. *Chem. Commun.* **2016**, *52*, 8873–8876.

27. Zhang, H.; Xue, L.; Han, J.; Fu, Y. Q.; Shen, Y.; Zhang, Z.; Li, Y.; Wang, M. *J. Mater. Chem. A* **2016**, *4*, 8724–8733.

28. Lee, J.; Jung, B.; Lee, S. K. Y. U.; Lee, J.; Cho, H. *J. Polym. Sci., Part A Polym. Chem.* **2005**, *43*, 1845–1857.

29. Liu, X.; Lee, E. K.; Kim, D. Y.; Yu, H.; Oh, J. H. *ACS Appl. Mater. Interfaces*

2016, *8*, 7291–7299.

30. Li, H.; Hwang, Y. J.; Earmme, T.; Huber, R. C.; Courtright, B. A. E.; Obrien, C.; Tolbert, S. H.; Jenekhe, S. A., *Macromolecules* **2015**, *48*, 1759–1766.

31. Wang, Z.; Zhao, J.; Dong, H.; Qiu, G.; Zhang, Q.; Hu, W., *Phys. Chem. Chem. Phys.* **2015**, *17*, 26519–26524.

32. Palai, A. K.; Kim, S.; Shim, H.; Cho, S.; Kumar, A.; Kwon, J.; Park, S. U.; Pyo, S. *RSC Adv.* **2014**, *40*, 41476–41482.

33. Srivani, D.; Gupta, A.; Raynor, A. M.; Bilic, A.; Li, J. L.; Bhosale, S. V.; Bhosale, S. V. *RSC Adv.* **2016**, *6*, 38703–38708.

34. Meng, D.; Sun, D.; Zhong, C.; Liu, T.; Fan, B.; Huo, L.; Li, Y.; Jiang, W.; Choi, H.; Kim, T. *J. Am. Chem. Soc.* **2016**, *138*, 375–380.

35. Shi, H.; Fu, W.; Shi, M.; Ling, J.; Chen, H. *J. Mater. Chem* **2015**, *3*, 1902–1905.

36. Schwenn, P. E.; Gui, K.; Nardes, A. M.; Krueger, K. B.; Lee, K. H.; Mutkins, K.; Rubinstein-Dunlop, H.; Shaw, P. E.; Kopidakis, N.; Burn, P. L. *Adv. Energy Mater.* **2011**, *1*, 73–81.

37. Woo, C. H.; Holcombe, T. W.; Unruh, D. A.; Sellinger, A.; Frechet, J. M. *Chem. Mater.* **2010**, *22*, 1673–1679.

38. Sharma, G. D.; Anil Reddy, M.; Ramana, D. V.; Chandrasekharam, M. *RSC Adv.* **2014**, *4*, 33279–33285.

39. Li, Y.; Zhong, L.; Wu, F. P.; Yuan, Y.; Bin, H. J.; Jiang, Z. Q.; Zhang, Z.; Zhang, Z. G.; Li, Y.; Liao, L. S. *Energy Environ. Sci.* **2016**, *9*, 3429–3435.

40. Liu, X.; Xie, Y.; Cai, X.; Li, Y.; Wu, H.; Su, S. J.; Cao, Y. *RSC Adv.* **2015**, *5*, 107566–107574.

41. Chen, M. S.; Niskala, J. R.; Unruh, D. A.; Chu, C. K.; Lee, O. P.; Frechet, J. M. *Chem. Mater.* **2013**, *25*, 4088–4096.

Thiophene-bithiazole based metal-free dye: Effect of co-adsorbents on photovoltaic efficiency

3.1. Abstract

*A novel molecule (**BT1**) consisting of a bithiazole chromophore sandwiched between two thiophenes, functionalized with benzothiophene unit at one end and cyanoacrylic acid acceptor at the other end was synthesized, photophysical properties were studied, and employed as a photosensitizer in dye-sensitized solar cells. The molecule exhibited an intense absorption in the UV-visible region with absorption extending up to 500 nm. The ground and excited state potentials of **BT1** were calculated to be 1.29 and 1.21 V, respectively vs NHE using cyclic voltammetry. The solar cells fabricated from **BT1** exhibited an efficiency of 1.14%. The effect of various co-adsorbents (**CDCA**, **TP1** and **TP2**) on the DSSC performance were investigated in detail.*

3.2. Introduction

Harvesting solar energy and converting it into electricity using photovoltaic technology is one of the most promising ways of clean and abundant alternative energy resources. Among the various photovoltaic technologies, dye sensitized solar cells have the potential to become a commercial success because of their low fabrication cost and respectable efficiency.[1-6] The photosensitizer is the essential component in DSSC, which governs the photon harvesting, charge generation and charge transfer processes. The ultimate photovoltaic conversion efficiency of DSSC depends on large number of factors such as absorption of the dye, photoelectrodes, the nature of electrolyte etc.

The photosensitizer is the essential component in DSSC, which governs the photon harvesting, charge generation and charge transfer processes.[7,8] Sensitizers comprise of two major categories such as metal-based dyes and metal-free dyes. Among the metal-based sensitizers, Ruthenium polypyridyl complexes and zinc porphyrin systems are the most studied metal based sensitizers. Anchoring ligands and ancillary ligands are the two types of ligands mainly attached to the metal in the metal-based sensitizer. The anchoring of dyes on to the semiconductor surface is achieved with the help of the anchoring ligands. The overall properties of sensitizers can be tuned through the ancillary ligands.[9] Intense metal to ligand charge transfer (MLCT) bands in the visible

region exhibited by polypyridyl complexes of metal ions having d^6 configuration make them as potential candidates for photovoltaic applications. Through modification of anchoring ligands and ancillary ligands, the energy states of the MLCT can be altered.

In recent times, a wide range of metal-based photosensitizers for DSSC applications has been studied. Among the metal-based sensitizers, ruthenium polypyridyl complexes and zinc porphyrin systems are the most studied metal-based sensitizers. Ruthenium dyes based sensitizers in DSSCs exhibited good power conversion efficiencies reaching up to 11.5%. Structures of some of the efficient ruthenium dyes are depicted in **Figure 3.1**.[10-13] Ruthenium complexes are capable of directing excitation energy from the metal core to the carboxylate group [i.e., metal to ligand charge transfer (MLCT)]. This property attributed to the high efficiency of the DSSC based on ruthenium sensitizers. High material cost due to rarity, lack of absorption in the red region of the visible spectrum, and complicated purification processes are the major drawbacks of ruthenium based systems.[14] Zinc porphyrin dyes, another class of metal-based sensitizers, also exhibit good photovoltaic properties. Presence of Soret band (400-500 nm) and Q-band (550-750 nm) in the absorption spectrum is one of the peculiar properties of porphyrins, which make them a panchromatic photosensitizer. Structures of a few efficient Zinc porphyrin dyes are depicted in **Figure 3.1.**[15-18]
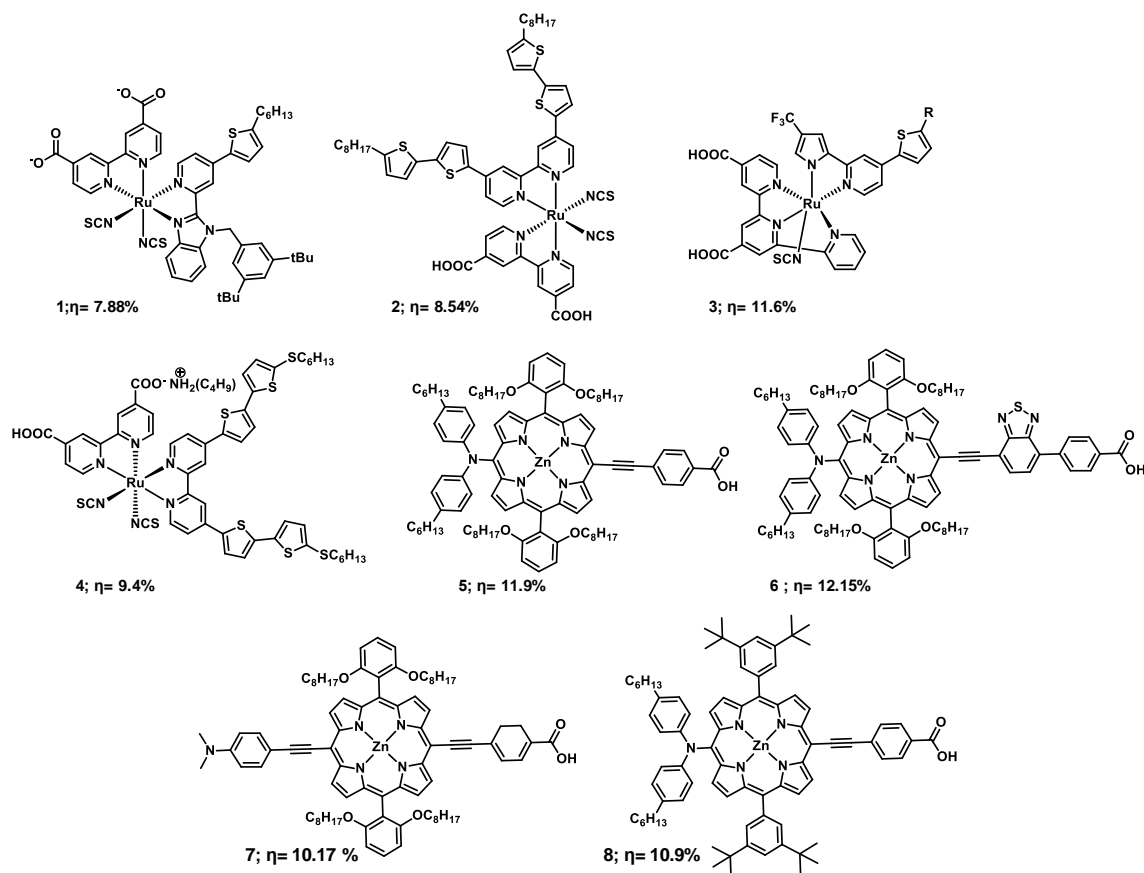
Figure 3.1. Structures of some metal-based sensitizers (**1-8**) for DSSC application.

In recent years, there is a widespread interest for the development of metal-free dyes for DSSC applications.[19-23] The important advantage of metal-free sensitizers compared to Ru sensitizers includes lower cost and structural design flexibility. In addition to that molar extinction coefficient of the charge transfer band in metal-free dyes are normally much higher than that of MLCT band in Ru dyes. Thus it can improve the light harvesting ability considerably enabling thinner TiO$_2$ films to be used as photoanode. Metal-free sensitizers usually

consist of donor and acceptor moieties connected in a conjugated fashion. In some cases, conjugated spacers are used to maintain the electronic communication between the donor and acceptor moieties. Although the efficiency is lower compared to the metal based dyes, the metal-free dyes have attracted considerable attention in recent years due to the above mentioned advantages.[24-26] Triphenylamine derivatives are the most commonly used donors in organic based metal-free dyes. Interestingly, thiophene based conjugated systems are less explored in DSSCs, although many reports of molecules consisting of thiophene attached to triphenylamines are there.[27-32]
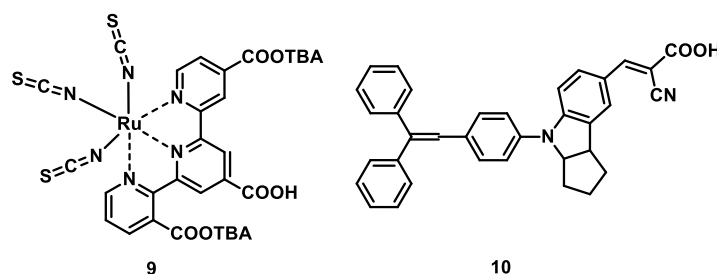
Figure 3.2 Molecular structure of **9** and **10**.

Co-sensitization is one of the strategies to improve the PCE of DSSCs, in which two or more dyes sensitized on a semiconductor film.[33] In such cases, a co-sensitizer absorbs the complimentary region to the dye absorption and helps to cover the whole visible spectrum. One of the important structural requirements of co-sensitizer is the capability to prevent aggregation of the sensitizer dye. In 2003, Noda and coworkers fabricated DSSCs based on two dyes, **9** and **10**, the

structures of which are shown in **Figure 3.2**.[34] Ruthenium complex, **9** was having absorption extending to 900 nm. On the other hand, **10**, an indoline dye, having a strong absorption in 400-600 nm range. The current-voltage characteristics show that multiple dye systems suppressed the dark current in the device to a greater extent than the single dye based device. The multiple dye system showed a good performance of 11%.

The dark current generation in DSSCs is a major factor limiting the energy-conversion efficiency, which arises due to the transfer of excited electrons from the conduction band of semiconductor to the oxidized form of the dyes and redox electrolyte.[35] Usage of co-adsorbent on TiO_2 along with photosensitizer in DSSCs is one of the approaches to reduce the rate of back electron transfer. Substances competitively adsorbed along with photosensitizers onto the TiO_2 surface of DSSCs are called co-adsorbents.[36] Organic amphiphilic molecules with carboxylic or phosphonic acid functional groups are used as co-adsorbents.
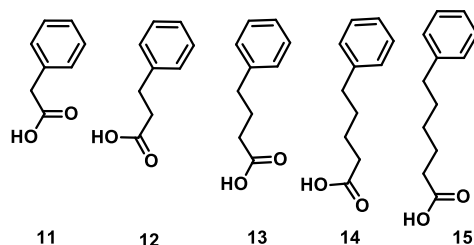
Figure 3.3 Molecular structures of compounds;**11 –15**.

Nath *et al.*, reported a series of phenylalkanoic acids (**11-15**; chemical structures are shown in **Figure 3.3**) as co-adsorbents for N719 dye based DSSCs.[37] Results showed that the presence of alkyl chains having comparable lengths with that of the dye molecules and a compatible structure facilitated an efficient regeneration of the oxidized dyes. On increasing the chain length, J_{SC} values exhibits an enhancement from 13.31 to 14.29 mA/cm^2. The increasing hydrophobic chain length of co-adsorbents have effectively reduced the dye aggregation. The rate of back electron transfers and increased recombination lifetime also follows the same trend as the J_{SC} values.
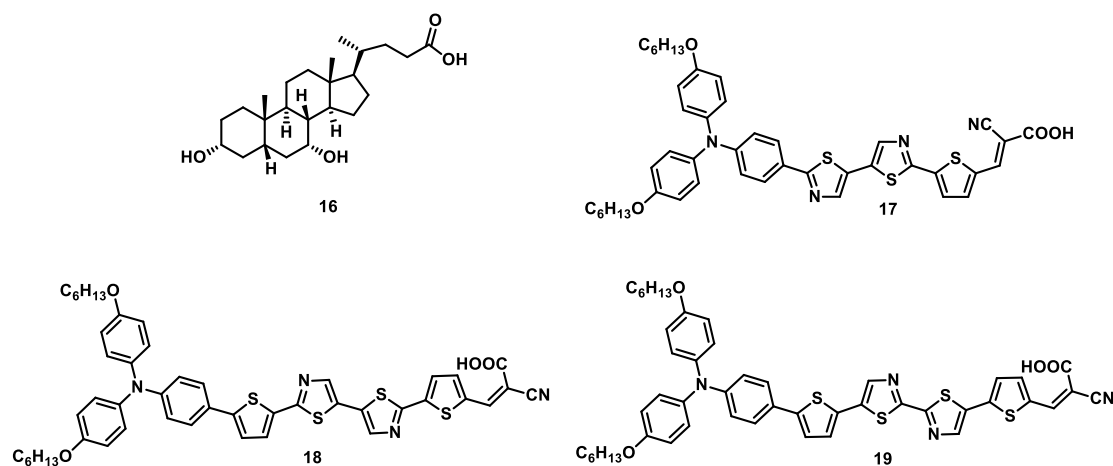
Figure 3.4 Molecular structures of compounds; **16 –19**.

Lin and coworkers studied the effect of chenodeoxycholic acid (**CDCA**, **16**) on the photovoltaic properties of bithiazole containing organic dyes (**16-19**; chemical structures are shown in **Figure 3.4**).[38] The photoconversion efficiencies of these dyes were considerably increased upon the addition of **16** because of the

prevention of dye aggregation. The improved photocurrent was probably due to the suppression of self-quenching of the excited electrons in the dyes by co-adsorption which has increased the electron injection yields from the dye to the TiO_2.

In this chapter, we have designed and synthesized a thiophene based donor-acceptor system (**BT1**), which consists of benzothiophene unit at one end, a bithiazole unit sandwiched between two thiophene units as the linker and cyanoacrylic acid acting both as the acceptor and anchoring group. Bithiazoles are relatively weak acceptors and widely used as a constituent in oligomers and polymers for organic bulk heterojunction solar cell devices.[39,40] However, only a few number of bithiazole based systems are designed for DSSC application.[41-43] It is known that improvement of open circuit voltage (V_{OC}) and short circuit current (J_{SC}) could be achieved by preventing π-π stacking of organic dye molecules.[42] Co-adsorbents are commonly used for this purpose. To study the effect of co-adsorbents on the performance of **BT1**, we have selected a commercially available molecule, **CDCA**. In addition to that, two new co-adsorbents having similar thiophene-cyanoacrylic acid anchoring group as that of **BT1** were synthesized (**TP1** and **TP2**). Chemical structure of the sensitizer and co-adsorbents are depicted in **Chart 3.2**. Herein, our aim is to use **TP1** and **TP2** as co-adsorbents for reducing recombination rate through preventing π-π

stacking interactions of **BT1**. The effect of different co-adsorbents on the

photovoltaic performance of **BT1** was analyzed.
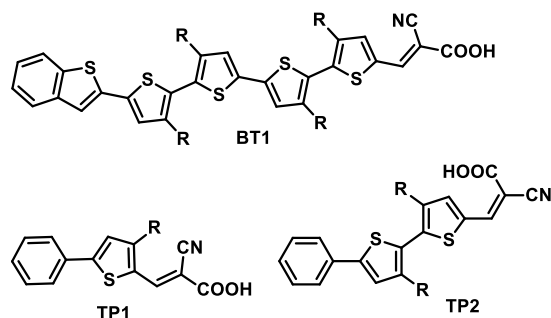
Chart 3.2 Structure of the molecules used in the study.

3.3. Results and Discussion

3.3.1. Synthesis
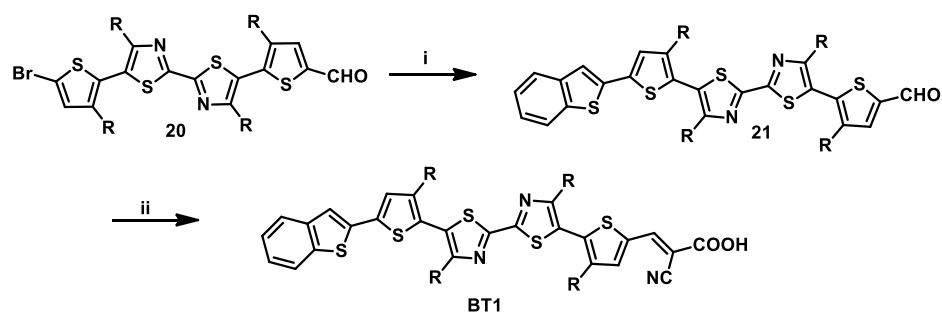
Scheme 3.1 *Synthetic route for the preparation of **BT1**; Reagents and conditions: (i) benzo[b]thiophen-2-yltributylstannane, Pd(PPh₃)₄, Toluene, 16 h, reflux; (ii) Cyanoacetic acid, Piperidine, CHCl₃, reflux, 30 h.*

   BT1 was synthesized as shown in **Scheme 3.1**. Synthesis of compound **20** was already discussed in Chapter 2. Stille coupling of **20** with benzo[b]thiophen-2-yltributylstannane gives **21**, which was then reacted with cyanoacetic acid to give **BT1**. The molecule was characterized using ¹H NMR and ¹³C NMR.
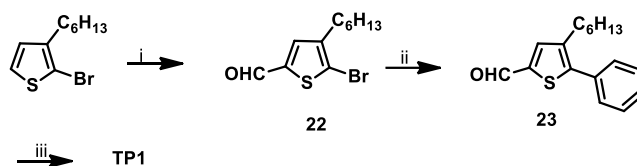
Scheme 3.2 *Synthetic Scheme of **TP1**: Reagents and conditions: (i) DMF, POCl₃ DCE, 0 – 60 °C, 12 h; (ii) 4,4,5,5-tetramethyl-2-phenyl-1,3,2-dioxaborolane, THF-H₂O, K₂CO₃, Pd(PPh₃)₄, 48 h, reflux ; (iii) Cyanoacetic acid, Piperidine, CHCl₃, reflux, 30 h.*
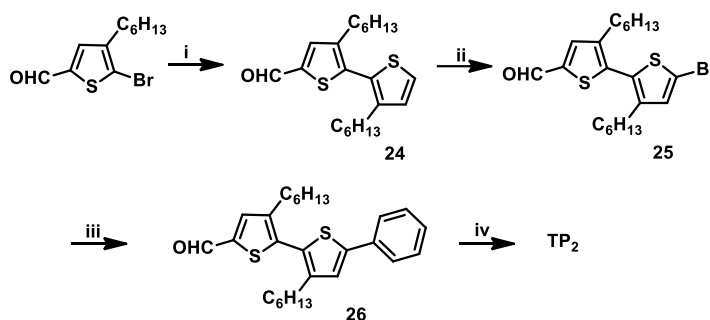
Scheme 3.3 *Synthetic Scheme of **TP2**: Reagents and conditions: (i) 3-hexylthiophene-2-boronic acid pinacolester, THF-H₂O, K₂CO₃, Pd(PPh₃)₄, 48 h, Reflux (ii) NBS, CHCl₃, Glacial acetic acid, 4 h;(iii) 4,4,5,5-tetramethyl-2-phenyl-1,3,2-dioxaborolane, THF-H₂O, K₂CO₃, Pd(PPh₃)₄, 48 h, reflux; (iv) Cyanoacetic acid, Piperidine, CHCl₃, reflux, 30 h.*

The co-adsorbents **TP1** and **TP2** synthesized as per the **Scheme 3.2** and **Scheme 3.3**. Various reactions like Vilsmeier-Haack formylation, Suzuki coupling and Knoevenagel condensation are involved in the synthesis strategy.

3.3.2. Absorption and emission properties

The normalized absorption spectra of **BT1** in THF and spin coated film on a quartz plate are shown in **Figure 3.4a**. It exhibits an absorption band in the UV-visible region extending up to 500 nm with an absorption maximum at 388 nm.

The molar extinction coefficient was found to be 31,400 M^{-1}cm^{-1}, indicating reasonable light harvesting ability of the dye molecule. The absorption in the
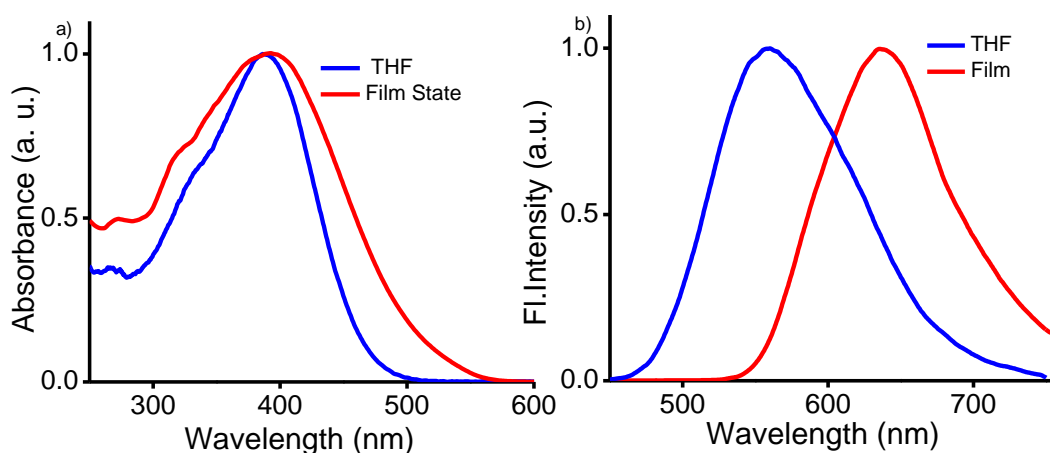
Figure 3.4 (a) Absorption spectra and (b) emission spectra of **BT1** in THF (Conc. = 10^{-5} M, λ_{ex} = 390 nm) and film state (on quartz plate).

UV-visible region is mainly attributed to the aromatic π-π* transition with some contribution from the intramolecular charge transfer between the donor and acceptor unit. Considerable broadening was observed in the film state on the quartz plate with the absorption extending up to 570 nm, and the λ_{max} slightly red-shifted to 392 nm. Optical bandgap ($E_{0,0}$) was obtained from the intersection of absorption and emission spectrum which was obtained as 2.5 eV.[44]

Absorption spectrum of **BT1** on TiO$_2$ is shown in **Figure 3.5a**, which is similar to the absorption on a quartz substrate. In order to check the role of

aggregation, absorption spectra of **BT1** were measured in different percentage
of THF-water mixture (**Figure 3.5a**). With 10% THF and 90% water mixture,
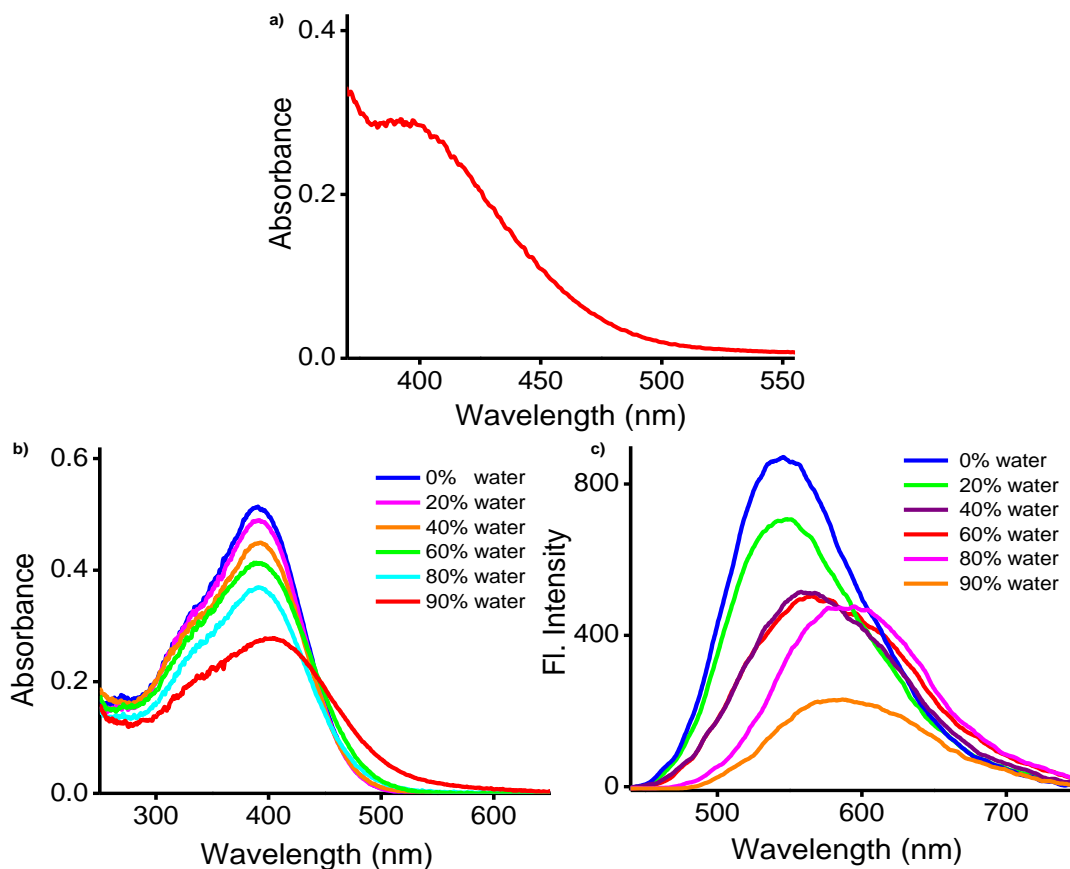
Figure 3.5 (a) Film state absorption of **BT1** on TiO$_2$, (b) absorption and (c) emission spectra of
BT1 with increasing percentage of water ($\lambda_{\text{ex}} = 400\text{nm}$).

the absorption shifted to the red with a broadening as obtained in the film state
which indicates that the molecule undergoes slight aggregation. **BT1** exhibited
fluorescence emission maximum at 558 nm in the solution state and 636 nm in
the film state (**Figure 3.4b**). A red shift of about 78 nm was observed in the film
state compared to the solution state. Emission spectra were also measured in

different percentages of THF-water mixture. With increasing percentage of water, fluorescence of **BT1** was quenched and underwent a red shift of about 30 nm. The significant red-shift of the emission maximum in the film state could not be attributed to the aggregation of the molecules alone. In the solution state there is a greater possibility for twisted conformation of the molecules to minimize the steric effects, whereas, in the film state, planarization of the chromophore backbone may happen. Such planarization results in increase in the effective conjugation length thereby shifting the emission maximum towards red. Hence both aggregation and planarization of the backbone must be the reason for the significant red shift obtained in the film state in the case of **BT1**.

3.3.3 Electrochemical properties
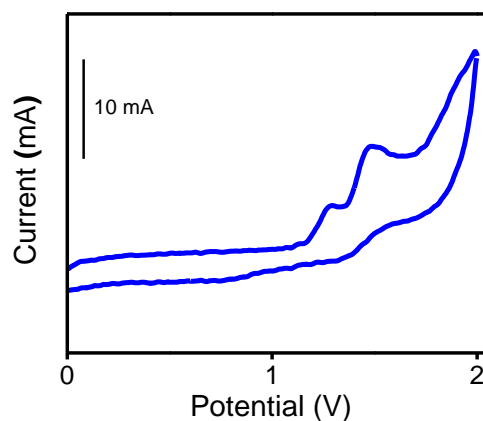
Figure 3. 6 Cyclic Voltammogram of **BT1** in DCM.

In order to examine the energy levels to ensure electron transfer at the TiO_2/dye/redox electrolyte interface, cyclic voltammetric studies were performed in DCM solution using 0.1 M tetrabutylammonium hexafluorophosphate as the supporting electrolyte, Pt as the counter electrode and Ag/AgCl as the reference electrode. The reference electrode was calibrated using ferrocene/ferrocenium (Fc/Fc$^+$) redox couple as an external standard.

The first half wave potential of **BT1** was obtained at 1.07 V versus Ag/AgCl and 0.53 V versus Fc/Fc$^+$. All the potentials measured were converted to NHE considering Fc/Fc$^+$ as +0.765 V vs NHE in DCM.[45] Therefore the ground state oxidation potential of **BT1** is 1.29 V vs NHE, which corresponds to the ground state energy level. The excited state energy was calculated from the reduction potential and the value obtained was -0.65 V vs NHE, which corresponds to the excited state energy level. This ground and excited energy levels were exactly placed within the energy requirements for electron transfer at electrolyte/TiO_2 interfaces.

Table 3.1 Absorption, emission and electrochemical parameters of the dye, **BT1**

Dye	λ_{abs} (nm)	ε ($M^{-1}cm^{-1)}$	λ_{em} (nm)	E_{0-0} (eV)	E_{HOMO} (V vs NHE)	E_{LUMO} (V vs NHE)
BT1	388	31,400	558	2.50	1.29	-0.65
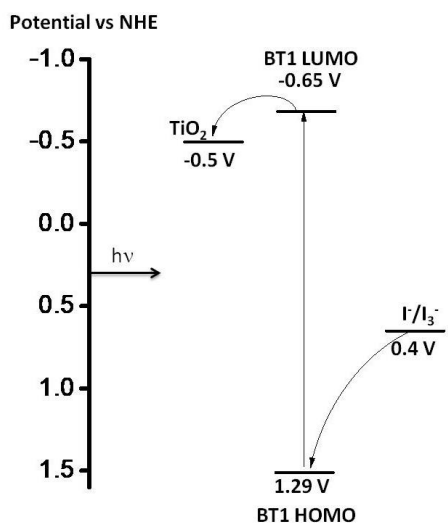
Scheme 3. 4. Scheme showing the energetics of TiO_2/dye/redox electrolyte interface.

As shown in **Scheme 3.4**, the HOMO level of **BT1** is more positive than the electrolyte, indicating that the oxidized dye can be efficiently regenerated by the redox species in the electrolyte. The excited state energy level is considerably more negative than the TiO_2 implying electron injection from the excited dye into the conduction band of TiO_2 is energetically favorable. All the absorption, emission and electrochemical parameters are shown in **Table 3.1**.

3.3.4 Characterization of Co-adsorbents

The photophysical characterization of the newly prepared co-adsorbents, **TP1** and **TP2** were carried out. **TP1** exhibits absorption in the range of 250-450 nm with λ_{max} at 374 nm. **TP2** absorbs in the range of 250-500 nm with λ_{max} at 384 nm. **TP1** and **TP2** exhibits emission maximum at 461 and 624 nm respectively (**Figure 3.7**). HOMO and

LUMO values were obtained from the DFT calculations. All the above parameters of

the co-adsorbents are shown in **Table 3.2**.
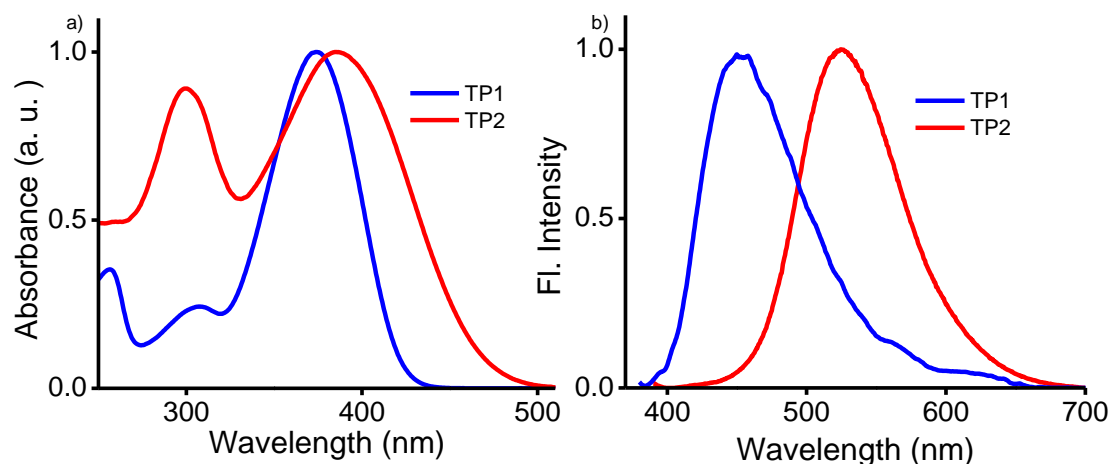
Figure 3.7 (a) Absorption and (b) emission spectra of **TP1** and **TP2.**

Table 3. 2 Absorption, emission and energy levels of the co-adsorbents.

Dye	λ_{abs} (nm)	ε ($M^{-1}cm^{-1)}$	λ_{em} (nm)	E_{0-0} (eV)	E_{HOMO} (V vs NHE)	E_{LUMO} (V vsNHE)
TP1	374	22,000	461	3.37	-5.99	-2.618
TP2	384	9000	624	3.18	-5.85	-2.655

3.3.5. DFT calculations

To further understand the electronic properties of **BT1**, DFT calculations

were performed at the B3LYP/6-31G* level and the optimized HOMO and

LUMO of the neutral state of **BT1** in vacuum.
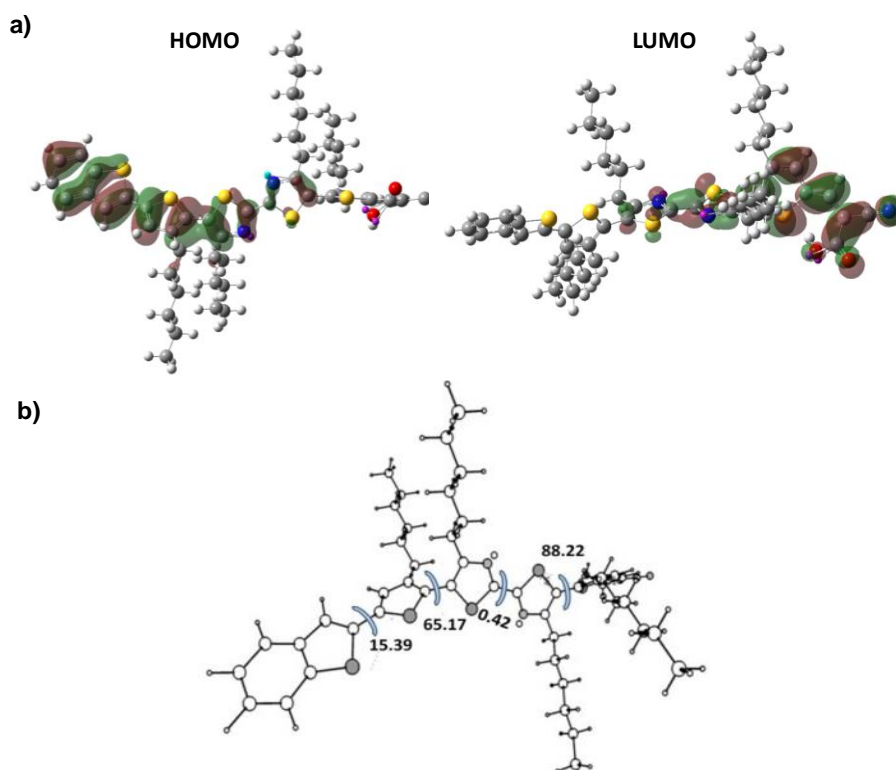
Figure 3.8 (a) HOMO and LUMO levels of the energy minimized structure and (b) optimized structure of **BT1** obtained from DFT calculations.

The molecule is designed in such a way that it creates an energy level gradient from benzothiophene (donor) to bithiazole (weak acceptor) to cyanoacrylic acid (strong acceptor). As a result, it was expected that the electron distribution of the HOMO should be mainly located on the benzothiophene unit, whereas that of LUMO mainly located along the acceptor cyanoacetic acid unit. The optimized HOMO and LUMO of **BT1** obtained by DFT calculation proved this assumption (**Figure 3.8**). Interestingly, both HOMO and LUMO are slightly extended to the bithiazole unit. Energies of the HOMO and LUMO levels of the energy

optimized structures were calculated which was obtained as -5.64 and -2.84 eV, respectively. The optimized structure of the molecule with dihedral angles of various bonds is shown in **Figure 3.6b**. The dihedral angles between the bithiazole and two bridging thiophene units are 65.17° and 88.22°.

3. 3. 6. Photovoltaic properties

Photovoltaic performances of **BT1** as DSSC sensitizer was evaluated in the absence and presence of co-adsorbents. The **BT1**-coated TiO$_2$ film was used as the working electrode, platinized fluorine-doped tin oxide (FTO) glass as the counter electrode. The electrolyte composition consists of mixed solution of 0.6 M BMII, 0.1 M LiI, 0.05 M I$_2$, 0.5 M TBP.
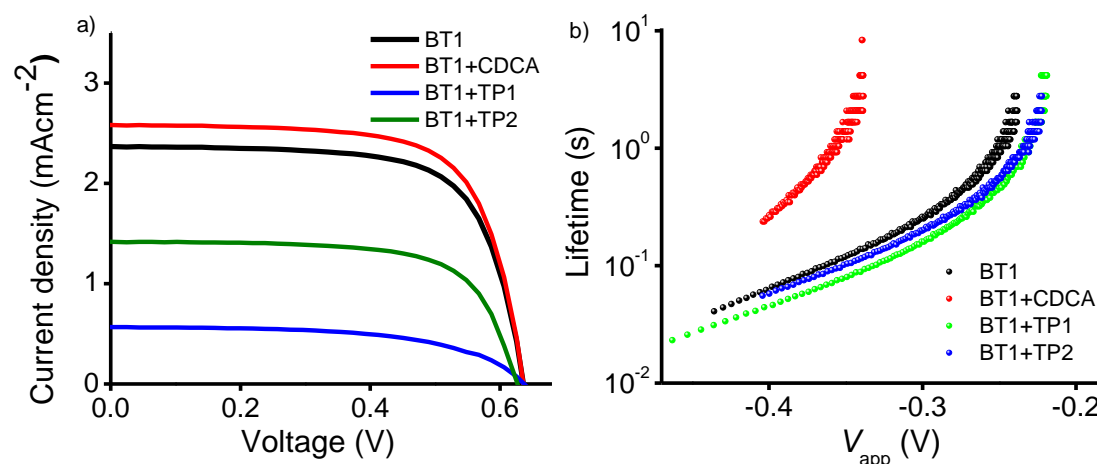
Figure 3.9 (a) Current-voltage characteristics (b) electron lifetimes of DSSCs sensitized by **BT1** in the absence and presence of different co-adsorbents, under irradiation of AM 1.5G simulated solar light.

Photocurrent-voltage (*J-V*) plots of the cells based on **BT1** with different co-adsorbents are shown in **Figure 3.9a** and electron lifetimes for the corresponding data are shown in **Figure 3.9b**. The detailed parameters such as short circuit current density (J_{SC}), open-circuit voltage (V_{OC}), fill factor (*FF*) and photovoltaic conversion efficiency (η) are summarized in **Table 3.3**. The cell consisting of **BT1** in the presence of **CDCA** as co-adsorbent exhibited the highest efficiency of 1.27% (J_{SC} = 2.57 mAcm^{-2}, V_{OC} = 0.64, *FF* = 0.77). The efficiency was slightly higher compared to the cell based on **BT1** alone, which was about 1.14%. The cell of **BT1** with other co-adsorbents such as **TP1** and **TP2** exhibited lower efficiency compared to **BT1** alone.

The incident photon-to-current conversion efficiency (IPCE) spectra is shown in **Figure 3.10**. The solar cells based on **BT1** alone exhibited action
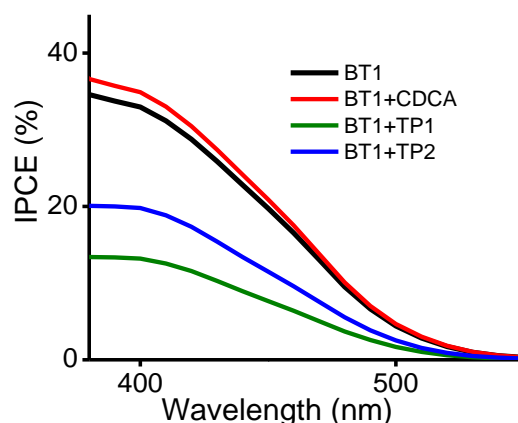
Figure 3.10 IPCE plot of the DSSCs using **BT1** in the absence and presence of different co-adsorbents.

spectra in the range of 380-500 nm with the highest IPCE value of 33% at 400 nm. The IPCE value reduced significantly to 13% and 20%, respectively in the presence of co-adsorbent **TP1** and **TP2**, whereas, IPCE value slightly improved in the case of **BT1** in the presence of **CDCA** as co-adsorbent to 35%. **BT1** showed better performance with **CDCA**, whereas the performances were lowered in the presence of co-adsorbents **TP1** and **TP2**. The results of IPCE measurements were in accordance with the photovoltaic performances.

Table 3.3 Photovoltaic performance parameters of **BT1** in the presence of different co-adsorbents.

Soaking condition	J_{SC} $(mAcm^{-2})$	V_{OC} (V)	FF	η (%)
BT1 alone [a]	2.36	0.64	0.75	1.13
BT1+ TP1 [a]	0.53	0.64	0.56	0.20
BT1+ TP2 [a]	1.43	0.63	0.66	0.59
BT1+ CDCA [a]	2.56	0.64	0.76	1.25
BT1+ CDCA [b]	1.57	0.63	0.70	0.70

Illumination: 100 mWcm^{-2} simulated AM 1.5G solar light; composition of electrolyte: [a] 0.6 M BMII, 0.1 M LiI, 0.05 M I$_2$, 0.5 M TBP. [b]Commercial electrolyte from dyesol.

There are two plausible explanations for the drop in the photovoltaic performance in the presence of co-adsorbents **TP1** and **TP2**, which are as follows, a) the competition between the dye and co-adsorbents for the TiO$_2$ surface resulting in less dye intake and more of the intake of co-adsorbents

having lesser absorption in the visible region, and b) less effective in preventing the aggregation of the dye particularly in the case of the short adsorbent, **TP1** (Schematic representation shown in **Scheme 3.5**).
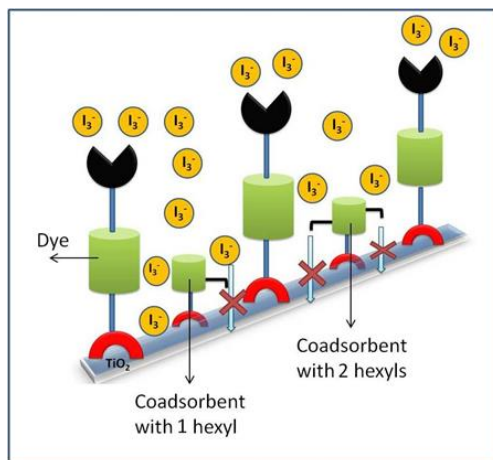
Scheme 3.5 Scheme showing the co-adsorbents preventing recombination.

The electron lifetime plots in **Figure 3.9b** shows that **BT1** in the presence of **CDCA** exhibited a higher lifetime than with other co-adsorbents since the former was expected to prevent recombination to a better extent than the latter. The enhancement in efficiency of **BT1** co-adsorbed with **CDCA** could be attributed to the reduction in back electron transfer which is evident from the electron lifetime measurements as well as from the electrochemical impedance spectra.

Electrochemical impedance spectroscopy (EIS) was employed to study the interfacial charge recombination in DSSC under dark condition.[46-48] EIS Nyquist
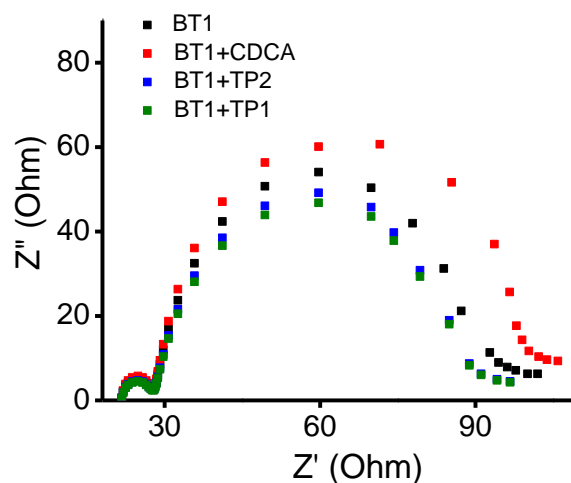
Figure 3.11 EIS Nyquist plot for DSSCs based on **BT1** with various co-adsorbents measured at -0.65 V forward bias in the dark.

plot for DSSCs based on **BT1** with different co-adsorbents are shown in **Figure 3.11**. The first semicircle indicates charge transfer resistance at the Pt/electrolyte interface. The major semicircle shown in the Nyquist plot corresponds to the electron transport resistance at the TiO_2/dye/electrolyte interface which implies the resistance to recombination between electrons in TiO_2 conduction band and oxidized I_3^- species in electrolyte. The larger the semicircle, slower is the recombination kinetics. It is evident from **Figure 3.11** that **BT1** co-adsorbed with **CDCA** exhibits higher recombination resistance which is consistent with the electron lifetime plots given in **Figure 3.9 b**. Increase in charge recombination resistance resulted in increased electron lifetime by suppressing back electron transfer thereby enhancing photovoltaic performance for **BT1**coadsorbed with **CDCA** in comparison with other two co-adsorbents.

Metal-free thiophene based systems exhibited enhancement in efficiency by employing co-adsorbents like CDCA, DCA, etc.[20,25,49-52] A Triphenylamine based sensitizer containing thiophene as a π-bridge exhibited an increase in efficiency of 45% in the presence of CDCA as co-adsorbent as compared to that of devices without CDCA.[28] Multifunctional co-adsorbents with naphthalene and anthracene as π-conjugated aryl unit exhibited significant enhancement in photovoltaic parameters by suppressing charge recombination and increasing electron lifetime.[52] 43-86% enhancement in efficiency was obtained with a bithiazole based DSSC in presence of CDCA coadsorbent.[53] From the DSSC analysis, it could be seen that the photoconversion efficiency of the **BT1** dye is low when compared to several systems reported in the literature. This might be attributed to the low J_{SC} value which arises from the lower absorption efficiency of **BT1** in the visible region. As evident from the energy minimized structure, the significant twist in the chromophores backbone, which reduces the effective conjugation length, might be one contributing factor to this. Problem associated with absorptivity could be partially solved by selecting a stronger donor instead of benzothiophene. Stronger donor units may improve the extinction coefficient and increase ICT character yielding a broad coverage of the visible spectrum. It is also anticipated that a change in the electrolyte system may enhance the photovoltaic efficiency.

3.4. Conclusions

A new metal-free organic dye based on bithiazole and thiophene units containing cyanoacrylic acid as the anchoring group was synthesized. Detailed photophysical and DSSC device characterization has been carried out. The effect of different co-adsorbents on DSSC performance for **BT1** was examined. The solar cell performance of **BT1** was enhanced in the presence of **CDCA**, whereas it declined in the presence of other thiophene based co-adsorbents, **TP1** and **TP2**.

3.5. Experimental section

3.5.1. Materials and characterization techniques

The reagents and materials for synthesis were purchased from Sigma-Aldrich, Merck, TCI and Spectrochem chemical suppliers, and used as received. Air and water sensitive synthetic steps were performed in an argon atmosphere using standard Schlenk techniques. ^{1}H and ^{13}C-NMR spectra were recorded using Bruker-500 MHz spectrometer. Absorption spectra were recorded using Shimadzu UV-Visible-2401PC spectrophotometer. Steady-state fluorescence experiments were performed using a SPEX Fluorolog F112X spectrofluorimeter.CV experiments were performed using a BAS 50W voltammetric analyser. Density functional theory (DFT) calculations were performed at the B3LYP/6-31G* level using Gaussian 09 program.

3.5.2. Fabrication and Characterization of DSSC

The FTO plates used for TiO_2 deposition were cleaned stepwise by using detergent, distilled water, acetone, isopropanol and kept for UV-ozone treatment for 30 min. Deposition of $TiCl_4$ was done by immersing electrodes into a 40 mM $TiCl_4$ aqueous solution at 70 °C for 30 min and then washed with distilled water and ethanol. The photoanodes were then annealed at 500 °C for 30 min. After cooling, transparent TiO_2 paste of particle size 20 nm was deposited followed by annealing at 125 °C for 10 min. Above this layer, TiO_2 paste consisting of TiO_2 particles of about 400 nm particle size was coated and annealed at 125 °C for 10 min. This was followed again by $TiCl_4$ treatment and annealing. The electrodes were then put into programmed heating at 325°C for 15 min, 450ºC for 15 min, and 500˚C for 30 min and slowly cooled down to room temperature. Electrodes were immersed into **BT1** dye solution in THF (0.3 mM) with or without co-adsorbents (10 mM) and kept at room temperature for 15 h. Counter electrodes were prepared by coating with a drop of H_2PtCl_6 solution (2 mg of Pt in 1 mL ethanol) on FTO plates having pre-drilled holes, and cleaned using the same procedure as for photoanodes. The electrodes were assembled with hot press using 25 μmsurlyn spacer. The space in between both the electrodes were filled with liquid I^-/I_3^- electrolyte which was composed of various compositions of 1-butyl-3-methylimidazolium iodide (BMII), lithium iodide (LiI), iodine (I_2),

guanidinium thiocyanate (GuSCN) and 4-*tert*-butyl pyridine (TBP) in acetonitrile. The drilled holes were sealed with microscopic cover slide and surlyn to avoid electrolyte leakage. Three cells were fabricated for each condition and the cells were measured after keeping it for 12 h in dark.

The photovoltaic performance of the fabricated DSSC were measured using an AM 1.5 solar simulator (Newport Instruments, USA) equipped with a source meter (Keithley 2400) at 25 °C. The IPCE measurement of the devices was performed under DC mode using a 250 W xenon lamp coupled with Newport monochromator. A monochromatic beam was continuously irradiating on the sample and the current was measured using Keithley 6430 source meter. NIST calibrated Si photodiode was used to find the incident power spectral response of the light. The *J-V* properties of cells were measured using square shade mask with active area 0.25 cm^2 (without mask active area is 0.36 cm^2). The power of the simulated sunlight was calibrated by using a reference Si photodiode supplied by Newport instruments. Open circuit voltage (V_{oc}) decay measurements are done at open circuit. The cell was in the dark at the beginning of the measurement, and then the lights were turned on until the voltage got stabilized, followed by switching the light off and recording the decay of photovoltage. Lifetime data was transformed from the voltage decay part of the measurement through previously reported methods.[20] The EIS measurements of DSSC were

carried out using a micro Autolab (μ3AUT70904) equipped with FRA mode under forward bias in the dark. The measurements were performed in a frequency range of 0.1 to 10^5 Hz with ac amplitude of 10 mV.

3.5.3. Synthesis

BT1 was synthesized as shown in **Scheme 3.1**. The coadsorbents**TP1** and **TP**2 synthesized based on **Scheme 3.2** and **3.3** (**23**[54],**24**[55] **25**[56] and **26**[56] reported in the literature).

Synthesis of 21:
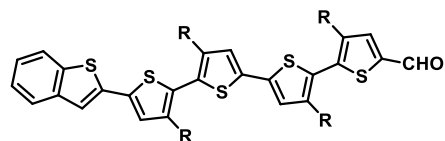
Compound **20** (220 mg, 0.28 mmol) and benzo[b]thiophen-2-yltributylstannane (120.1 mg, 0.28 mmol) were weighed into a two-necked RB flask and dissolved in dry toluene (6 mL). Air was removed from the flask and filled with nitrogen by applying freeze-pump-thaw method for three times. $Pd(PPh_3)_4$ (38 mg, 0.02 mmol) was added under N_2 counter flow and the reaction mixture was refluxed at 110 °C for 16 h. The reaction mixture was then poured into water and extracted with chloroform. The combined organic fraction was dried over Na_2SO_4 and evaporated to dryness under reduced pressure. The resulting crude product was purified by column chromatography (silica gel, 50% CH_2Cl_2-hexane) to afford product as a yellow oil. (Yield: 84%). ^1H NMR (500 MHz, $CDCl_3$) δ_H : 9.89 (s, 1H), 7.79 (d, 1H, *J=8*), 7.74 (d, 1H, *J=7.5*), 7.67

(s, 1H), 7.30-7.36 (m, 2H), 7.18 (s, 1H), 2.70-2.77 (m, 4H), 2.54-2.61 (m, 4H), 1.20-1.80 (m, 32H), 0.86 (t, 12 H).^{13}C NMR (125 MHz, CDCl$_3$) δ_C:181.79, 160.14, 158.82, 157.13, 156.81, 143.62, 143.49, 142.17, 139.27, 138.11, 136.89, 135.66, 135.08, 125.73, 124.31, 124.09, 123.76, 123.66, 122.62, 122.51, 121.15, 118.96, 30.58, 30.52, 30.41, 29.49, 29.35, 29.15, 28.91, 28.82, 28.58, 28.09, 28.01, 27.95, 27.90, 21.56, 21.52, 13.06, 13.04, 13.01. HRMS: m/z = 829.33.33 (M$^+$).

Synthesis of BT1:
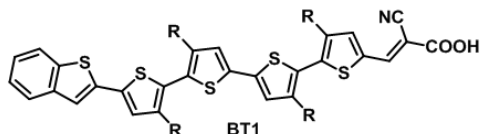
Compound **21** (40 mg, 0.048 mmol) and 2-cyanoacetic acid (27.6 mg, 0.32 mmol) in chloroform (3 mL) were heated at 60 °C for 30 h. After cooling to room temperature, the mixture was added to water. The precipitate was isolated by filtration and washed with water. The residue was then purified by column chromatography (silica gel 80% CH$_2$Cl$_2$-EtOH) to give a blackish red solid. It was again purified by precipitating from cold methanol. (Yield: 88%). ^{1}H NMR (500 MHz, CDCl$_3$) δ_H: 8.29 (s, 1H), 7.79 (d, 1H, J=7.5), 7.73 (s, 2H), 7.41 (s, 1H), 7.31-7.35 (m, 2H), 7.18 (s, 1H), 2.54-2.76 (m, 8H), 1.20-1.80 (m, 32H), 0.86 (t, 12 H). ^{13}C NMR (125 MHz, CDCl$_3$)δ_C : 161.36, 159.71, 158.43, 157.87, 145.18, 144.59, 140.30, 139.29, 139.17, 138.01, 137.55, 136.67, 135.66, 126.77, 125.61, 125.01, 124.79, 124.71, 123.55, 123.30, 122.18, 120.03, 31.62, 31.61, 31.56, 31.53, 30.53, 30.38, 30.06, 29.82, 29.64, 29.62, 29.14,

29.12, 29.07, 29.00, 28.80, 22.59, 22.55, 14.08, 14.04.Anal. Calcd. for $C_{50}H_{61}N_3O_2S_5$:

C, 67.00; H, 6.86; N, 4.69; S, 17.89. Found :C, 66.34; H, 6.901; N, 4.65; S, 16.97.

Synthesis of 22:
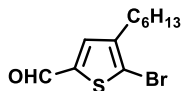
A vilsmeier reagent was prepared using $POCl_3$ (2.22 mL, 24.27 mmol, 2 eq.) and

dimethylformamide (8.45 mL, 109.21 mmol, 9 eq.) and it was added to solution of 2-

bromo-3-hexylthiophene (3 g, 12.13 mmol, 1 eq.) in dichloroethane at 0 °C under

argon. After being stirred for 12 h at 60 °C, the mixture was poured into ice water,

neutralised with Na_2CO_3 and then extracted with CH_2Cl_2 and dried over Na_2SO_4. It was

purified by column chromatography (15% Ethyl acetate-hexane). Pure product was

obtained as a light yellow liquid (Yield - 85%). ^1H NMR (500 MHz, $CDCl_3$)δ_H9.74 (s,

1H), 7.46 (s, 1H), 2.57 (t, 2H), 1.63-1.57 (m, 2H), 1.36-1.30 (m, 6H), 0.90-0.87 (t, 3H);

HRMS: $m/z = 274$ (M^+).

Synthesis of 23:
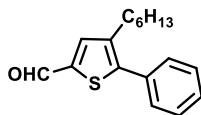
2-bromo-3-hexyl-5-formyl-thiophene (547 mg, 1.99 mmol, 1 eq.), 4,4,5,5-

tetramethyl-2-phenyl-1,3,2-dioxaborolane (486 mg, 2.39 mmol, 1.2 eq.) and K_2CO_3

(2.74 g, 19.87 mmol, 10 eq.) were dissolved in THF - H_2O mixture (9:1). Air was

removed out of the set up and replaced by nitrogen, three times by using a freeze-thaw-

pump method, then $Pd(PPh_3)_4$ was added under nitrogen-counter flow. The reaction

mixture was heated and stirred under nitrogen for two days, then poured into water and extracted with CH_2Cl_2. After washing the combined organic layer with brine and water, it was dried over Na_2SO_4 and the solvent evaporated purified by column chromatography (1:1 $CHCl_3$-hexane). Yield: 89%. ^{1}H NMR (500 MHz, $CDCl_3$)δ_H: 9.86 (s, 1H), 7.66 (s, 1H), 7.46-7.40 (m, 5H), 2.66 (t, J=7.75, 2H), 1.64-1.60 (m, 2H), 1.32-1.22 (m, 6H), 0.85 (t, J 6.75, 3H). HRMS: m/z = 295.11 (M^+ + Na).

Synthesis of TP1:
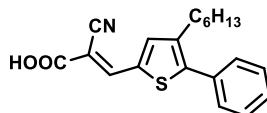
To a mixture of 4-hexyl-5-phenylthiophene-2-carbaldehyde (100 mg, 0.367 mmol, 1 eq.) and cyanoacetic acid (62.43 mg, 0.367 mmol, 2 eq.) were added acetonitrile (10 mL) and piperidine (0.04 mL, 0.44 mmol, 1.2 eq.) at room temperature. The solution was refluxed overnight. After cooling to room temperature, the organic phase was separated and the aqueous layer extracted with CH_2Cl_2. The combined organic phases were washed with brine, dried with $MgSO_4$, and concentrated *in vacuo*. The crude residue was purified by column chromatography (DCM: MeOH = 9: 1) to give adduct as a yellow liquid. Yield: 70%. ^{1}H NMR (500 MHz, $CDCl_3$)δ_H: 8.30 (s, 1H), 7.70 (s, 1H), 7.46-7.43 (m, 5H), 2.69-2.63 (m, 2H), 1.63-1.57 (m, 2H), 1.29-1.25 (m, 6H), 0.85 (t, 3H). ^{13}C NMR (125 MHz, $CDCl_3$) δ_C: 148.90, 146.61, 139.86, 139.67, 132.72, 132.00, 128.11, 127.87, 127.76, 115.02, 30.44, 29.61, 28.67, 28.00, 27.35, 21.51, 13.00. HRMS: m/z = 362.11 (M^+ + Na).

Synthesis of 24:
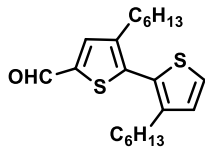
2-bromo-3-hexyl-5-formylthiophene (3.45 g, 12.54 mmol, 1 eq.) and 3-hexylthiophene-2-boronic acid pinacolester (4 g, 13.78 mmol, 1.1 eq.) were weighed in a two necked RB flask and dissolved in anaerobic THF- H_2O mixture (2:1). K_2CO_3 (17 g, 125 mmol, 10 eq.) was added to the mixture and the flask was connected to a reflux condenser equipped with a septum. Air was pumped out of the set up and replaced by nitrogen using freeze-thaw-pump method, then $Pd(PPh_3)_4$ was added under Ar-counter flow. The reaction mixture was refluxed for two days under nitrogen atmosphere then poured in to water and extracted with CH_2Cl_2. After washing the combined organic layer with brine and water, it was dried over Na_2SO_4 and the solvent evaporated under reduced pressure and purified by column chromatography (1:1 $CHCl_3$-hexane). Yield: 85%. ^{1}H NMR (500 MHz, $CDCl_3$)δ_H9.87 (s, 1H),7.66 (s, 1H), 7.36 (d, *J*=5, 1H), 6.99 (d, *J*=5, 1H), 2.57-2.52 (m, 4H), 1.60-1.52 (m, 4H), 1.27-1.25 (m, 12H), 0.85 (t, 6H); HRMS: *m/z* = 362.17 (M$^+$).

Synthesis of 25:
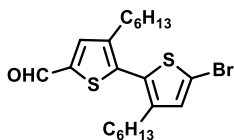
N-bromosuccinnimide (71 mg, 0.4 mmol, 1.1 eq.) was added in small portions to solution of 3,3'-dihexyl-2,2'-bithiophene-5-carbaldehyde, **24** (132 mg, 0.36 mmol, 1

eq.) in chloroform and acetic acid (1:1) at 0 °C. After being stirred for 6h at room temperature, the reaction mixture was poured into water and extracted with dichloromethane. The organic layer was thoroughly washed with water, aqueous Na_2CO_3, brine and again with water and dried over Na_2SO_4 and the solvent evaporated and purified by column chromatography (1:1 $CHCl_3$-hexane). Pure product was obtained as a light yellow liquid. Yield: 95%. ^1H NMR (500 MHz, $CDCl_3$)δ_H : 9.87 (s, 1H), 7.64 (s, 1H), 6.97 (s,1H), 2.55 (t,2H), 2.47 (t, 2H), 1.58 - 1.50 (m, 4H), 1.30 - 1.21 (m, 12H), 0.87 (t, 3H), 0 .85 (t, 3H); HRMS: m/z = 442.08 (M^+).

Synthesis of 26:
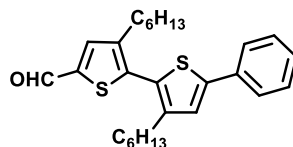
5-bromo-3,3'-dihexyl-2,2'-bithiophene-5-carbaldehyde (1 g, 2.26 mmol, 1 eq.) and phenyl-2-boronic acid pinacol ester (508 mg, 2.49 mmol, 1.1 eq.) were weighed in a two necked RB flask and dissolved in anaerobic THF - H_2O mixture (2:1). K_2CO_3 (3.08 g, 22.65 mmol, 10 eq.) was added to the mixture and the flask was connected to a reflux condenser equipped with a septum. Air was pumped out of the set up and replaced by Ar, three times by using a freeze-thaw-pump method, then $Pd(PPh_3)_4$ (130 mg, 0.11 mmol, 0.05 eq.) was added under Ar-counter flow. The reaction mixture was refluxed for two days, then poured in to water and extracted with CH_2Cl_2. After washing the combined organic layer with brine and water, it was dried over Na_2SO_4 and the solvent evaporated and purified by column chromatography (1:1 $CHCl_3$-hexane). ^1H NMR (500

MHz, CDCl$_3$)δ_H: 9.87 (s, 1H), 7.65 (s, 1H), 7.60 (d, *J* =7.5, 2H), 7.39 (t, *J*= 7.5, 2H), 7.29 (t, *J*= 7.25, 1H), 7.21 (s, 1H), 2.61 (t, 2H), 2.55 (t, 2H), 1.59 - 1.58 (m, 4H), 1.26 (t,12H), 0.86 (t, 6H). ^{13}C NMR (125 MHz, CDCl$_3$) δ_C:182.86, 144.95, 144.22, 143.65, 142.39, 139.89, 137.73, 133.80, 128.96, 127.93, 127.90, 127.85, 126.54, 125.68, 125.03, 31.62, 31.58, 30.70, 30.51, 29.20, 29.10, 28.99, 28.87, 22.58, 22.56, 14.08, 14.06. HRMS: *m/z* = 461.19 (M$^+$ + Na).

Synthesis of TP2:
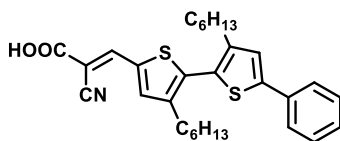
To a mixture of 5-phenyl -3, 3', -dihexyl-2, 2'-bithiophene -5-carbaldehyde (180 mg, 0.410 mmol, 1 eq.) and cyanoacetic acid (69.80 mg, 2.50 mmol, 2 eq.) were added acetonitrile (10 mL) and few drops of piperidine added at room temperature. The solution was refluxed overnight. After cooling to room temperature, the organic phase was separated and the aqueous layer extracted with CH$_2$Cl$_2$. The combined organic phases were washed with brine, dried with MgSO$_4$, and concentrated *in vacuo*. The crude residue was purified by column chromatography (DCM: MeOH = 9: 1) to give adduct as a yellow orange liquid. ^{1}H NMR (500 MHz, CDCl$_3$)δ_H: 8.28 (s, 1H), 7.73 (s, 1H), 7.60 (d, *J*=8, 2H), 7.39 (t, 2H), 7.31 (t, 1H), 7.21 (s, 1H), 2.62 (t, 2H), 2.57 (t, 2H), 1.59-1.58 (m, 4H), 1.28-1.26 (m, 12H), 0.85 (t, 6H). ^{13}C NMR (125 MHz, CDCl$_3$) δ_C: 146.18,144.24, 143.45, 142.99, 140.18, 138.34, 133.94, 132.71, 128.23, 127.93,

127.52, 126.90, 125.17, 124.66, 124.09, 115.01, 30.57, 30.50, 29.64, 29.45, 28.67, 28.30, 28.06, 27.99, 27.70, 21.53, 13.05, 13.01. HRMS: $m/z = 528.20$ (M$^+$ + Na).

3.6. References

1. Gong, J.; Liang, J.; Sumathy, K. *Renew. Sustain. Energy Rev.* **2012**, *16*, 5848–5860.

2. Hagfeldt, A.; Boschloo, G.; Sun, L.; Kloo, L.; Pettersson, H. *Chem. Rev.* **2010**, *110*, 6595–6663.

3. Gratzel, M. *Acc. Chem. Res.* **2000**, *33*, 269–277.

4. Wang, H.; Liu, Y. A.; Li, M.; Huang, H.; Xu, H.; Hong, R.; Shen, H. *Optoelectron. Adv. Mat.* **2010**, *4*, 1166–1169.

5. Ye, M.; Wen, X.; Wang, M.; Iocozzia, J.; Zhang, N.; Lin, C.; Lin, Z. *Mater. Today* **2014**, *18*, 155–162.

6. Zhang, L.; Cole, J. M. *ACS Appl. Mater. Interfaces* **2015**, *7*, 3427–3455.

7. Lee, C.P; Lin, R.Y.; Li, C. T.; Chu, T. C.; Sun, S.; Lin, J.T.; Ho, K. C. *RSc Adv.* **2015**, 5, 23810-825.

8. Kanaparthi, R. K.; Kandhadi, J; Giribabu, L. *Tetrahedron* **2012**. *68*, 8383-8393.

9. Polo, A. S.; Itokazu, M. K.; Yukie, N.; Iha, M. *Coord. Chem. Rev.* **2004**, *248*, 1343–1361.

10. Chen, C.; Wu, S.; Wu, C.; Chen, J.; Ho, K. *Angew. Chemie - Int. Ed.* **2006**, *45*, 5822–5825.

11. Mathew, S.; Yella, A.; Gao, P.; Humphry-baker, R.; Curchod, B. F. E.; Ashari-astani, N.; Tavernelli, I.; Rothlisberger, U.; Nazeeruddin, K.; Gratzel, M. *Nat. Chem.* **2014**, *6*, 242–247.

12. Yella, A.; Lee, H.-W.; Tsao, H. N.; Yi, C.; Chandiran, A. K.; Nazeeruddin, M.; Diau, E. W.-G.; Yeh, C.-Y.; Zakeeruddin, S. M.; Gratzel, M. *Science* **2011**, *334*, 629–633.

13. Duvva, N.; Kanaparthi, R. K.; Kandhadi, J.; Marotta, G.; Salvatori, P.; Angelis, F. D. E.; Giribabu, L. *J. Chem. Sci.* **2015**, *127*, 383–394.

14. Giribabu, L.; Kanaparthi, R. K. *Curr. Sci.* **2013**, *7*, 847–855.

15. Yella, A.; Mai, C.; Zakeeruddin, S. M.; Chang, S.; Hsieh, C.; Yeh, Y.; Grätzel, M. *Angew. Chem. Int. Ed* . **2014**, *53*, 2973–2977.

16. Bessho, T.; Zakeeruddin, S. M.; Yeh, C.; Diau, E. W.; Grätzel, M. *Angew. Chem. Int. Ed* . **2010**, *49*, 6646–6649.

17. Chang, Y.; Wang, C.; Pan, T.; Hong, S.; Lan, C. *Chem. Commun.* **2011**, *47*, 8910–8912.

18. Yella, A.; Lee, H.-W.; Tsao, H. N.; Yi, C.; Chandiran, A. K.; Nazeeruddin, M.; Diau, E. W.-G.; Yeh, C.-Y.; Zakeeruddin, S. M.; Gratzel, M. *Science* **2011**, *334*, 629–633.

19. Lai, H.; Hong, J.; Liu, P.; Yuan, C.; Li, Y.; Fang, Q. *RSC Adv.* **2012**, *2*, 2427–2432.

20. Soman, S.; Rahim, M. A.; Lingamoorthy, S.; Suresh, C. H.; Das, S. *Phys. Chem. Chem. Phys.* **2015**, *17*, 23095–23103.

21. Tamilavan, V.; Kim, A.; Kim, H.; Kang, M.; Ho, M. *Tetrahedron* **2014**, *70*, 371–379.

22. He, J.; Hua, J.; Hu, G.; Jiang, X.; Gong, H.; Li, C. *Dyes. Pigment.* **2014**, *104*, 75–82.

23. Wang, J.; Liu, K.; Ma, L.; Zhan, X. *Chem. Rev.* **2016**, *116*, 14675–14725.

24. Wu, Y.; Zhu, W. *Chem. Soc. Rev* **2013**, *42*, 2039–2058.

25. Preat, J.; Jacquemin, D.; Perp, E. A. *Energy Environ. Sci.* **2010**, *22*, 891–904.

26. Hagfeldt, A.; Boschloo, G.; Sun, L.; Kloo, L.; Pettersson, H. *Chem. Rev.* **2010**, *110*, 6595–6663.

27. Zhu, L.; Bin, H.; Zhong, C.; Ming, C. *Dyes. Pigment.* **2014**, *105*, 97–104.

28. Narayanaswamy, K.; Swetha, T.; Kapil, G.; Pandey, S. S.; Hayase, S.; Singh, S. P. *Electrochem. Acta* **2015**, *189*, 256–263.

29. Zhou, P.; Dang, D.; Wang, Q.; Duan, X.; Xiao, M.; Tao, Q.; Tan, H.; Yang, R.; Zhu, W. *J. Mater. Chem. A* **2015**, *3*, 13568–13576.

30. Krishna, N. V.; Suman, V.; Mrinalini, M; Prasanthkumar, S; Giribabau,L. *Chem. Sus. Chem* **2017**, *10*, 4668–4689.

31. Zhang, W.; Feng, Q.; Wang, Z.-S.; Zhou, G. *Chem. Asian J.***2013***, 8*, 939–946.

32. Cheol, B.; Seok, M.; Ju, M.; Hoon, D.; Ahn, K.; Hong, J. E. *Synth. Met.***2014**, *188*, 130–135

33. Krishna, N. V.; Suman, V.; Mrinalini, M.; Prasanthakumar, S.; Giribabu, L. *Chem. Sus. Chem* **2017**, *10*, 4668–4689.

34. Ogura, R. Y.; Nakene, S.; Morooka, M.; Orihashi, M.; Suzuki, Y.; Noda, K. *Appl. Phys. Lett.* **2015**, *94*, 73308–73310.

35. Marinado, T.; Hahlin, M.; Jiang, X.; Quintana, M.; Johansson, E. M. J.; Gabrielsson, E.; Plogmaker, S.; Hagberg, D. P.; Boschloo, G.; Zakeeruddin, S. M *J. Phys. Chem.* **2010**, 11903–11910

36. Tuyet, P.; Son, V.; Anh, T.; Phan, P.; Nhut, T.; Le, V.; My, D.; Dang, D.; Anh, V.; Huynh, T. V. *Appl. Surf. Sci.* **2017**, *392*, 441–447

37. Nath, N. C. D.; Lee, H. J.; Choi, W.; Lee, J. *J. Nanosci. Nanotechnol.***2013**, *13*, 7880–7885

38. Lai, L.; Ho, C.; Chen, Y.; Wu, W.; Dai, F.; Chui, C.; Huang, S.; Guo, K.; Lin, J.; Tian, Yang, S; Wong, W. *Dye. Pigment.***2013**, *96*, 516–524.

39. Lin, Y.; Fan, H.; Li, Y.; Zhan, X. *Adv. Mater.* **2012**, *24*, 3087–3106.

40. Lin, Y.; Cheng, P.; Liu, Y.; Shi, Q.; Hu, W.; Li, Y.; Zhan, X. *Org. Electron.* **2012**, *13*, 673–680.

41. Maragani, R.; Ansari, M. S.; Banik, A.; Misra, R.; Qureshi, M. *ACS Omega* **2017**, *2*, 5981–5991.

42. Chem, J. M.; He, J.; Wu, W.; Hua, J.; Jiang, Y.; Qu, S.; Li, J.; Long, Y.; Tian, H. *J. Mater. Chem* **2011**, *21*, 6054–6062.

43. Chen, B.; Chen, Y.; Chou, P. *J. Mater. Chem* **2011**, *21*, 4090–4094.

44. Wu, G; Kong, F; Zhang, Y.; Zhang, X.; Li, J.; Chen, W.; Liu, W.; Ding, Y.; Zhang, C.; Zhang, B.; Yao,J; Dai,S. *J. Phys. Chem. C* **2014**, *118*, 8756–8765.

45. Robson, K. C. D.; Sporinova, B.; Koivisto, B. D.; Schott, E.; Brown, D. G.; Berlinguette, C. P. *Inorg. Chem.* **2011**, *50*, 6019–6028.

46. Wang, Q.; Moser, J.; Gratzel, M. *J. Phys. Chem. B* **2005**, *109*, 14945–14953.

47. Wu, G.; Kong, F.; Zhang, Y.; Zhang, X.; Li, J.; Chen, W.; Liu, W.; Ding, Y.; Zhang, C.; Zhang, B.; Yao,J; Dai,S. *J. Phys. Chem. C* **2014**, *118*, 8756–8765.

48. Cisneros, R.; Beley, M.; Fauvarque, J.; Lapicque, F. *Electrochem. Acta* **2015**, *171*, 49–58.

49. Tamilavan, V.; Cho, N.; Kim, C.; Ko, J.; Ho, M. *Synth. Met.* **2012**, *162*, 2155–2162.

50. Tamilavan, V.; Kim, A.; Lee, H.; Kim, H.; Kim, S.; Kang, M.; Ho, M. *Synth. Met.* **2014**, *191*, 141–150.

51. Guo; F. , He; J, Qu; S, Li; J, Zhang;Q, Wu: W, Hu; J. *RSC Adv.* **2013**, *3*, 15900–15908.

52. Taek, I.; Seok, B.; Kyung, Y.; Jong, M.; Seok, W.; Ho, S.; Soo, M.; Deuk, K.; Yeoun, J.; Hyun, S. *Org. Electron.* **2014**, *15*, 3316–3326.

53. Yen, Y.; Lin, T.; Hsu, C.; Chen, Y.; Chou, H.; Tsai, C.; Lin, J. T. *Org. Electron.* **2013**, *14*, 2546–2554.

54. Li, W.; Maddux, T.; Yu, L. *Macromolecules* **1996**, *91*, 7329-7334.

55. Guo, Y.; Su, J.; An, Z.; Chen, X.; Chen, P. *J. Mol. Struct.* **2015**, *1094*, 195-202.

56. Hayashi, N.; Nishihara, T.; Matsukihira, T.; Nakashima, H.; Miyabayashi, K.; Miyake, M.; Ã, H. H. *Bull. Chem. Soc. Jpn.* **2007**, *80*, 371-386.

Understanding structure-property relationships of triphenylamine - bithiazole dyes

4.1. Abstract

*Triphenylamine-bithiazole based two metal-free organic dyes were designed and synthesized employing D-π-A strategy for dye sensitized solar cells which differed in the anchoring groups attached to it. Photovoltaic characteristics of the dyes were studied in the presence of a co-adsorbent exhibiting a maximum efficiency of 4.7%. The electron lifetimes obtained from open circuit voltage decay measurement shows that the addition of co-adsorbent **CDCA** helped in reducing aggregation of both TPA-bithiazole dyes thereby improving the photovoltage for devices resulting in improvement of efficiency in comparison to the dye alone devices. electrochemical impedance spectroscopy measurements indicated that the devices sensitized by the compound having cyanoacrylic acid as anchoring group in presence of co-adsorbent exhibited the largest resistance for recombination between the electrons injected to TiO$_2$ and electrolyte leading to a better lifetime and photovoltage.*

4.2. Introduction

Among the third-generation photovoltaic technologies, dye-sensitized solar cells being the molecular level devices functioning efficiently and cost effectively. The efficiency of DSSCs can be improved by the optimization of the structure of sensitizers,[1] use of different kinds of electrolytes,[2] incorporation of co-adsorbents and co-sensitizers.[3] Use of various anchoring groups is of particular importance in the design approach of sensitizers as they influence the dye loading efficiency, electron-transport properties and charge recombination rates.[4] Conventionally, a donor-π-acceptor design strategy is being used to get organic dyes with excellent PCEs. The D-π-A model induces intramolecular electronic communication through the polarization of electron cloud towards the acceptor, which facilitates efficient electron injection to TiO_2.

Anchoring dye molecules on the surface of semiconducting metal oxides like TiO_2 is imperative for the injection of electrons from the excited states of dyes to the conduction band of TiO_2. Mainly covalent bonding between the dye and TiO_2 is responsible for the strong electronic coupling between them.[4] Cyanoacrylic acid is the commonly used acceptor and anchoring group in metal-free organic dyes for DSSC. Anchoring of dye molecules on to the TiO_2 surface can be achieved through covalent attachment, electrostatic interaction, hydrogen bonding, hydrophobic interaction, van der Waals forces, or physical entrapment, etc.[5] Mostly, DSSCs employ covalent bonding between the dyes and

semiconductor metal surface in order to ensure strong coupling. Other interactions lead to the formation of weak bonds which in turn results in lesser adsorption.[6] There are six different modes of adsorption possible for carboxylic acid group such as, monodentate ester, bidentate chelating, bidentate bridging, monodentate H-bonding, bidentate H-bonding, and coordinating mode through a C=O group (**Scheme 4.1**).
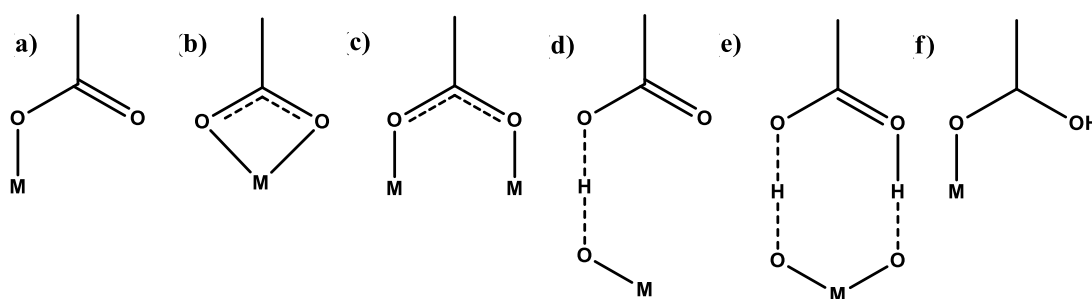
Scheme. 4.1 Different anchoring modes of carboxylic acid onto the metal oxide (TiO$_2$): (a) monodentate ester, (b) bidentate chelating, (c) bidentate bridging, (d) monodentate H-bonding, (e) bidentate H-bonding, (f) monodentate through C-O group. (adapted from ref. 6)

In recent years, many new anchoring groups were being used for developing efficient organic dyes for DSSC application. Among the new anchoring groups, rhodanine derivatives emerged as a promising candidate.[7-11] When a donor moiety is connected covalently to a rhodanine containing carboxylic acid moiety, efficient anchoring on to the mesoporous TiO$_2$ surface was observed. The rhodanine anchors improves the electronic coupling between the oxygen and nitrogen atoms of rhodanine and TiO$_2$ substrate and facilitates shorter electron transfer distances. The rhodanine derivatives can also enhance the absorption

characteristics because of their ability to function as strong electron acceptors. In case of rhodanine containing sensitizers, the IR frequencies corresponding to the N-H and C=O stretching absorptions disappeared as a result of its attachment to the TiO$_2$ substrate. This indicates the coordinate bond formation between the oxygen and nitrogen atoms of the rhodanine tautomers and the Lewis acidic sites of the TiO$_2$ substrate.[4]
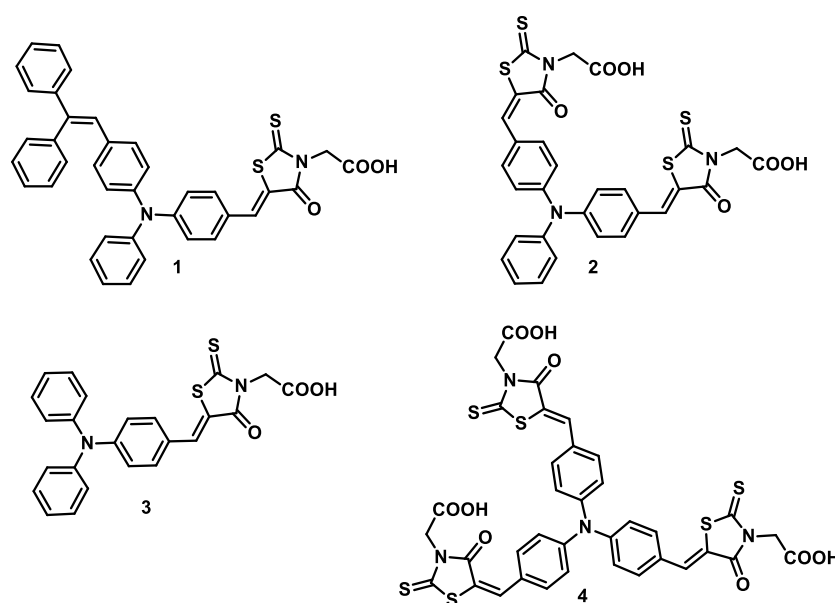
Figure 4.1 Molecular structures of **1-4**.

Chen and coworkers reported a rhodanine based dye (**1**) with triphenylamine as donor for DSSC application.[12] In **1**, the presence of diphenylvinyl to the adjacent phenyl ring of the TPA core increases the extinction coefficient and λ_{max} by the extension of conjugation. As explained in the previous chapter, this group prevents the dye aggregation by acting as a three-dimensional barrier for

electrolytes which improves the open-circuit voltage (V_{OC}). The dye showed a high light-to-electricity conversion efficiency of 6.27% with short-circuit photocurrent density (*J*sc) of 15.5 mA cm^{-2}, open circuit photovoltage (*V*oc) of 0.64 V, and *FF* of 0.63. Yang *et al*., reported a series of triphenylamine - rhodanine dyes (**2**-**4;** chemical structures are shown in **Figure 4.1**) with varying number of rhodanine-3-acetic acid as anchoring group for DSSCs.[13] They incorporated multiple electron acceptors to the adjacent phenyl ring of TPA-based dyes, which have some significant effect on the photovoltaic performance of the devices. Dye **3** exhibited better performance due to the increased bathochromic shift and broadening of absorption spectrum.
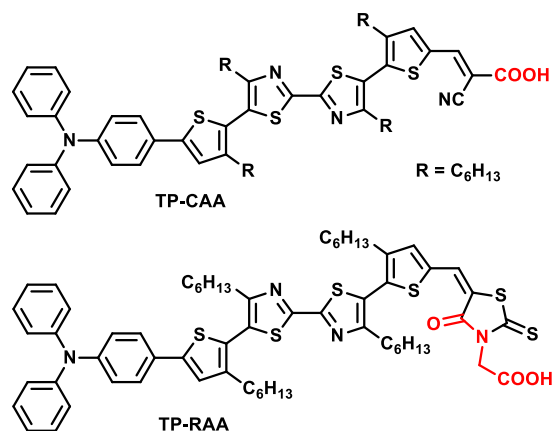
Scheme. 4.2 Structure of the molecules used in the present study.

In the present work, we have designed and synthesized two novel triphenylamine-bithiazole based dyes for applying as photosensitizers in DSSC devices (**Scheme. 4.2**). The dyes exhibited structural similarity with respect to

the donor and π bridge, but vary in terms of anchoring groups *viz.*, cyanoacrylic acid (**TP-CAA**) and rhodamine-3-acetic acid (**TP-RAA**). In these D-π-A molecules, triphenylamine act as donor, bithiazole as π-bridging unit for conjugation and cyanoacrylic acid/rhodanine derivative as acceptor. As discussed earlier, triphenylamine derivatives are one of the most promising candidates for DSSC because of their strong donor property, the easiness to introduce functional groups, and their unique propellar structure that prevents aggregation on the surface of TiO_2.[14] Introduction of bithiazole spacers with hexyl groups to the triphenylamine was to widen the absorption spectra coupled with enhanced solubility and restricted aggregation on the semiconductor surface.[15] The selected anchoring groups for this work not only play a significant role in surface adsorption but also act as excellent electron acceptors which are essential for the intramolecular electron transfer promoted from the excited donor of the dye to the TiO_2 upon light absorption.

4.3. Results and Discussion

4.3.1. Synthesis

The dyes were synthesized as shown in **Scheme 4.3**. Synthesis of compound **5** was already shown in previous chapter. Suzuki coupling of **5** with (4-(diphenylamino)phenylboronic acid gave **6** which was then reacted with acceptors such as 2-cyanoacetic acid and 2-(4-oxo-2-thioxothiazolidin-3-

yl)acetic acid, to give **TP-CAA** and **TP-RAA**, respectively. The dyes were characterized using analytical techniques such as ^{1}H NMR, ^{13}C NMR and mass spectrometry.
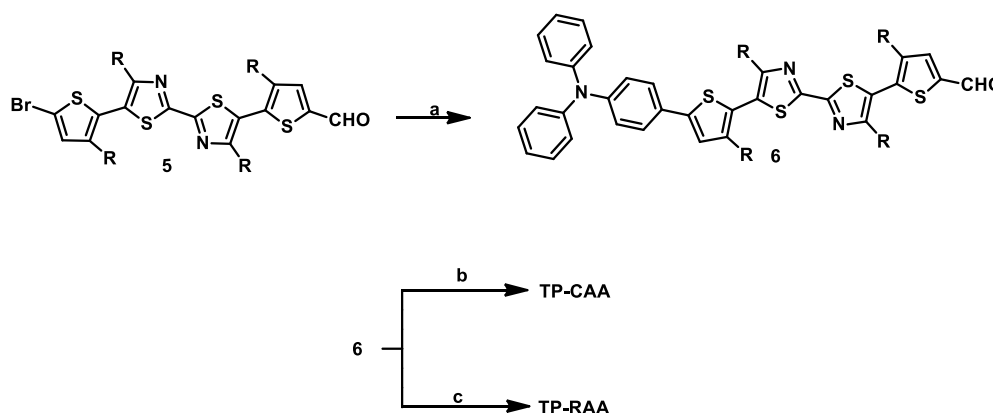
Scheme 4.3 *Reagents and conditions: (a) (4-(diphenylamino)phenylboronic acid, K$_2$CO$_3$, THF-Water, Pd(PPh$_3$)$_4$, 2 h, reflux; (b) 2-cyanoacetic acid, CHCl$_3$, piperidine, 30 h, reflux; (c) 2-(4-oxo-2-thioxothiazolidin-3-yl)acetic acid, CHCl$_3$, piperidine, 18 h, reflux.*

4.3.2. Photophysical properties of the dyes
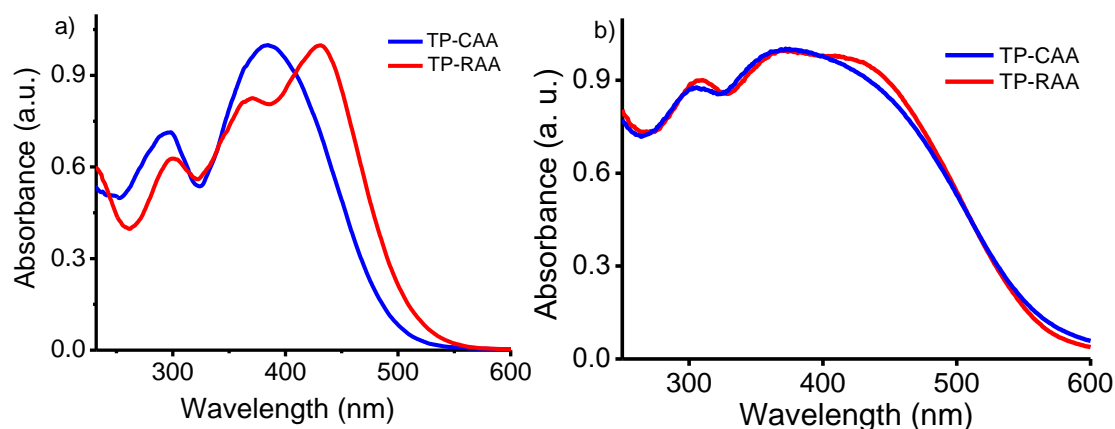
Figure 4.2 Absorption spectra of dyes (a) in solution (DCM 10^{-5} M) and (b) film state.

The compounds exhibited intense absorption band in the UV-vis region which extended up to around 550 nm (**Figure 4.2a**). The absorption in the UV region (~up to 350 nm) can be attributed to the aromatic π-π* transition involving the conjugated skeleton. On the other hand, absorption in the visible region (400-500 nm) can be attributed to the intramolecular charge transfer between the donor and acceptor unit in the molecules. The absorption maxima (λ_{max}) of **TP-CAA** and **TP-RAA** were at 384 nm and 431 nm, respectively. A considerable red-shift of 47 nm was obtained for **TP-RAA** compared to **TP-CAA**, which must be due to the higher electron accepting ability of the rhodanine derivative, resulting in higher ICT character of the dye molecules.

The film state absorption was broad compared to that in the solution state owing to the planarization of the dyes in the film state. Both dyes exhibited almost similar absorption spectra with a λ_{max} value of 380 nm (**Figure 4.2b**) in the film state. Absorption band gap was calculated from the onset of absorption spectra in the film state, and the values obtained were 2.53 eV and 2.43 eV for **TP-CAA** and **TP-RAA**, respectively. The molar extinction coefficients of **TP-CAA** and **TP-RAA** in solution state were calculated to be 40,590 and 40,400 M^{-1} L cm^{-1}, respectively, which shows that the dyes have good light harvesting ability in comparison to the conventional ruthenium complexes (13,900 $M^{-1}cm^{-1}$ for N719 dye).[16] This enhanced molar extinction coefficient augment in

fabricating devices with thinner photoelectrodes thereby reducing recombination that happens as part of the light induced charge transport process. [17]
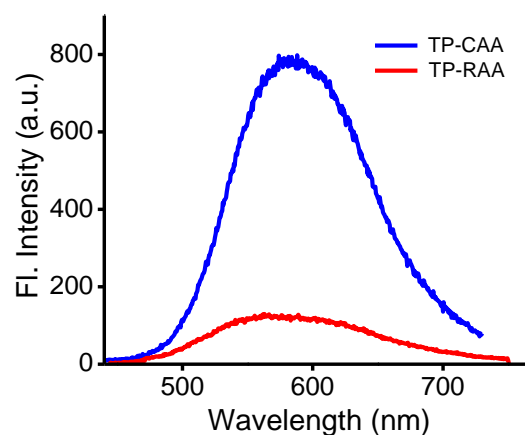
Figure 4.3 Emission spectra of dyes in solution (DCM 10^{-5} M).

In general, both dyes were poorly emissive in the solution state and non-emissive in the film-state. In DCM solution, they exhibited broad fluorescence emission with emission maxima at 584 nm (**TP-CAA**) and 576 nm (**TP-RAA**) (**Figure 4.3**). Due to the higher acceptor strength, the emission intensity was remarkably quenched for **TP-RAA** when compared to that of **TP-CAA**, which is in agreement with the absorption properties.

In order to understand the dye absorption characteristics after adsorption on TiO_2 surface, TiO_2 films of 12 μm were immersed in DCM solutions of the dyes and kept for 12 hours. The corresponding absorption profiles are shown in **Figure 4.4**. Upon dye adsorption onto TiO_2 surface, λ_{max} was bathochromically

shifted by 26 nm and 24 nm for **TP-CAA** and **TP-RAA**, respectively, when compared to the corresponding spectra in DCM. Considerable broadening with shoulder peaks in the red-region was also observed for both dyes on the TiO_2
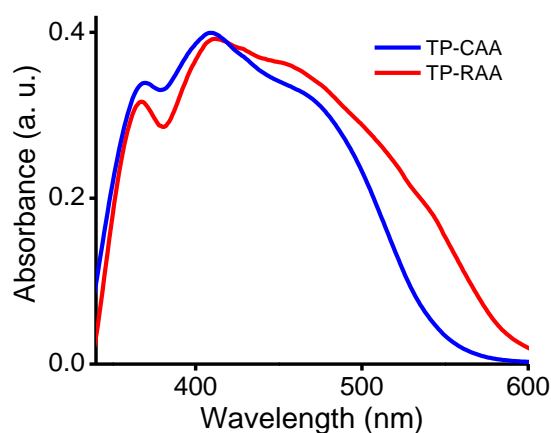
Figure 4.4 Absorption spectra of dyes adsorbed on TiO_2 thin film (thickness 12 μm).

surface. This implies that **TP-RAA** and **TP-CAA** adsorb efficiently to the semiconductor surface. The red-shift in the absorption maximum along with the formation of shoulder bands in the red-region indicates the formation of J-aggregates.

4.3.3. Electrochemical properties of the dyes

In order to estimate the energy level alignment of the dyes versus TiO_2 and redox electrolyte, cyclic voltammetric studies were performed in DCM solution using 0.1 M tetrabutylammonium hexafluorophosphate as the supporting electrolyte, Pt as the counter electrode and Ag/AgCl as the reference electrode.

The reference electrode was calibrated by using a ferrocene/ferrocenium (Fc/Fc^+) redox couple as an external standard.
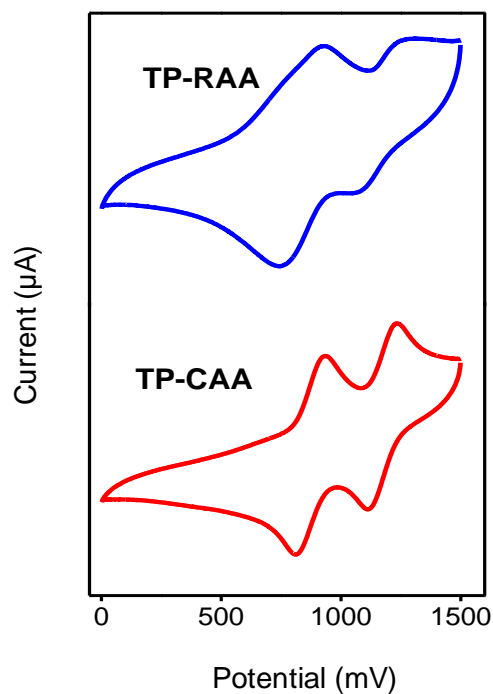
Figure 4.5 Cyclic voltammogram of **TP-CAA** and **TP-RAA.**

The first half wave potential of **TP-CAA** was obtained at 0.87 V *vs.* Ag/AgCl and 0.41 V *vs.* Fc/Fc^+(**Figure 4. 5**). All the potentials measured were converted to NHE considering Fc/Fc^+ as +0.765 V *vs.* NHE in DCM.[18] Thus the ground state oxidation potential of **TP-CAA** is 1.16 V *vs.* NHE, which corresponds to the HOMO level. Similarly, a value of 1.14 V was obtained for **TP-RAA**. HOMO values were similar in the case of both dyes which show that the ground states are not much sensitive to the acceptor groups. As mentioned in the previous section, band gap energies (E_{0-0}) were estimated to be 2.53 eV for **TP-**

CAA and 2.43 eV for **TP-RAA**. The excited state potential of **TP-CAA** was calculated from the E_{HOMO} - E_{0-0} and the value obtained was -1.37 V *vs*. NHE for **TP-CAA** which corresponds to its LUMO level. Similarly, excited state potential value obtained for **TP-RAA** was -1.29 V.
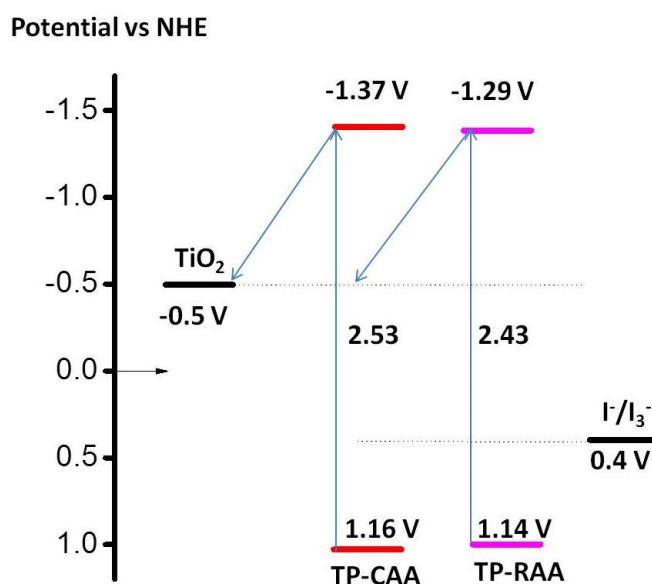
Scheme 4.4. Scheme showing the energetics of TiO_2/dye/redox electrolyte interface for **TP-CAA** and **TP-RAA**.

An ideal sensitizer should have an excited state precisely placed above the TiO_2 conduction band and a ground state accurately placed below the redox potential of the electrolyte in order to have enough driving force for both injection and regeneration. The HOMO and LUMO levels of the TPA-bithiazole dyes were found to be accurately placed within the energy requirements for electron transfer at electrolyte/TiO_2 interfaces as shown in **Scheme 4.4**. The relatively large energy gap between the excited states of the TPA-bithiazole dyes

and TiO$_2$ conduction band entails us to use additives like 4-tert-butylpyridine in electrolyte, which can alter the TiO$_2$ conduction band to more negative potentials thereby improving the open circuit voltage and net efficiency.[19] Detailed photophysical and electrochemical parameters of the dyes are shown in **Table 4.1**.

Table 4.1 Absorption, emission and electrochemical parameters of **TP-CAA** and **TP-RAA** in DCM.

Dyes	λ_{abs} (nm)	ε (M^{-1}cm^{-1})	λ_{em} (nm)	E_{0-0} (eV)	E_{HOMO} (V vs NHE)	E_{HOMO} (V vs NHE)
TPCAA	384	40,590	584	2.53	1.16	-1.37
TPRAA	431	40,400	576	2.43	1.14	-1.29

4.3.4. DFT Calculations
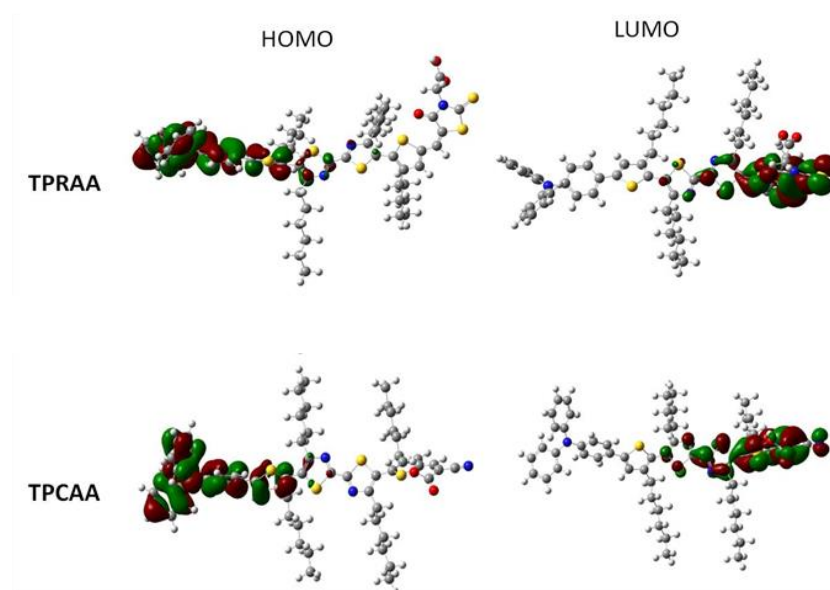
Figure 4.6 Distribution of the HOMO and LUMO in the energy minimized structures of **TP-CAA** and **TP-RAA**.

Density functional theory (DFT) calculations at the B3LYP/6-31G* level was performed to shed light on the electronic structure of the dyes using Gaussian 09 program, and the optimized HOMO and LUMO topologies for the dyes are shown in **Figure 4.6**. Calculations shows that HOMO energy level of the dye are largely populated on the triphenylamine moiety indicating the donor ability of the group while the LUMO energy levels are delocalized over the acceptor units making the electron injection to the semiconductor efficiently.

4.3.5. Photovoltaic properties

DSSCs were fabricated using the TPA-bithiazole dyes as photosensitizer in the presence and absence of **CDCA** (co-adsorbent). The electrolyte consists of 0.6 M BMII, 0.1 M LiI, 0.05 M I_2 and 0.5 M TBP.
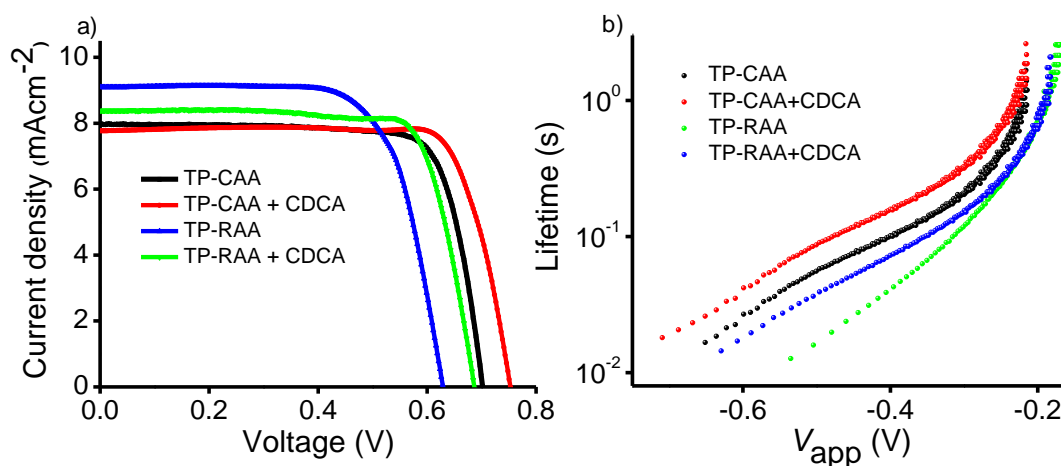
Figure 4.7 (a) Current-voltage characteristics (b) electron lifetimes of DSSCs sensitized by **TP-CAA** and **TP-RAA** in the presence and absence of **CDCA**, under AM1.5G irradiation.

Photocurrent-voltage (*J-V*) characteristic curves for the devices based on **TP-CAA** and **TP-RAA** in the presence and absence of **CDCA** are shown in **Figure 4.7 a** and corresponding electron lifetimes for the same devices measured using open circuit voltage decay (OCVD) are shown in **Figure 4.7 b**.[20,21] The detailed parameters such as short circuit current density (*J*$_{SC}$), open-circuit voltage (*V*$_{OC}$), fill factor (*FF*) and photovoltaic conversion efficiency (*η*) are summarized in **Table 4.2.**

Table 4.2 Photovoltaic performance parameters of **TP-CAA** and **TP-RAA** in the presence and absence of co-adsorbent, **CDCA**

Soaking Conditions	*J*$_{SC}$ (mAcm^{-2})	*V*$_{OC}$ (V)	*FF*	*η* (%)
TP-CAA	7.98	0.70	0.78	4.36
TP-CAA+ CDCA	7.77	0.75	0.79	4.70
TP-RAA	9.10	0.63	0.71	4.04
TP-RAA +CDCA	8.38	0.69	0.78	4.47

TP-CAA with acrylic acid anchoring group exhibited an overall light to electricity conversion of 4.36% (*J*$_{SC}$: 7.98 mAcm^{-2}, *V*$_{OC}$: 0.70 V, *FF*: 0.78) under AM1.5G irradiation in the absence of co-adsorbent. Upon addition of **CDCA** as co-adsorbent, the efficiency improved to 4.70% (*J*$_{SC}$: 7.77 mAcm^{-2}, *V*$_{OC}$: 0.75 V, *FF*: 0.79). This improvement is mainly attributed to the enhancement in voltage as a result of inhibiting aggregation on addition of **CDCA** which resulted in elevation of *V*$_{OC}$ by 50 mV. It has been well documented that organic dyes are

prone to aggregation on semiconductor surface which can be prevented by the effective use of co-adsorbents.[22,23] The absorption spectra of TPA-bithiazole dyes on TiO_2 in comparison to that in solution state clearly showed the presence of aggregation as explained in **Section 4.3.2**.

Addition of **CDCA** helped in preventing this aggregation to a certain extent as is evident from the absorption spectra of **TP-CAA**+**CDCA** on TiO_2 (**Figure 4.8a**) where the shoulder corresponding to aggregation got blue shifted. However, the presence of **CDCA** resulted in lesser dye loading which leads to lower J_{SC} values for device fabricated with **CDCA**. Similar trend was also observed for **TP-RAA** dye substituted with rhodanine acetic acid anchoring group on addition of **CDCA** (**Figure 4.8b**).
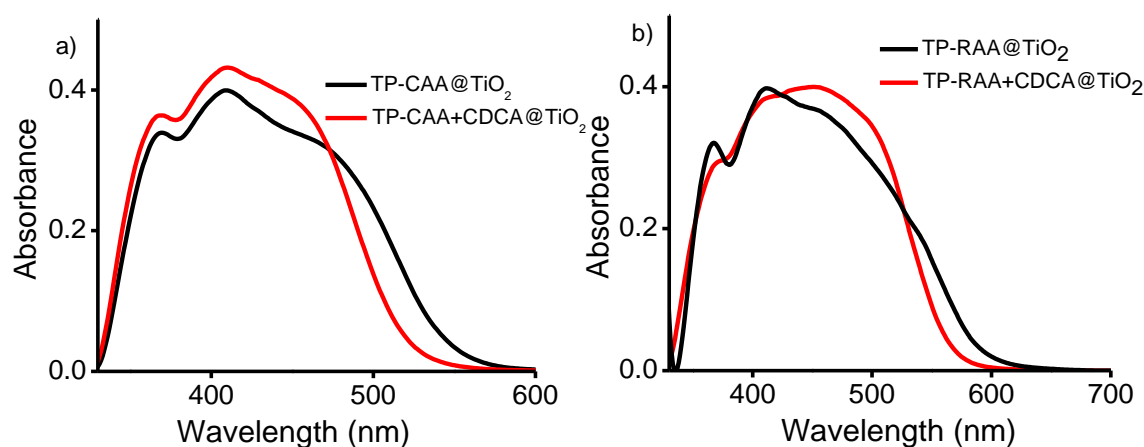
Figure 4.8 Absorption spectra of (a) **TP-CAA** and **(b) TP-RAA** co-adsorbed with and without **CDCA** adsorbed on TiO_2 thin film.

For the **TP-RAA** dye, the efficiency value obtained in the presence and absence of **CDCA** are 4.47% (J_{SC}: 8.38 mAcm^{-2}, V_{OC}: 0.69 V, *FF*: 0.78) and

4.04% (J_{SC}: 9.10 mAcm^{-2}, V_{OC}: 0.63 V, *FF*: 0.71), respectively. The short circuit current density (J_{SC}) improved to a considerable extent for **TP-RAA** in comparison to **TP-CAA** which is in agreement with the improved absorption profile for **TP-RAA** as shown in **Figure 4. 1**. The J_{SC} can be directly correlated to the molar extinction coefficient of the dye molecules, thus **TP-RAA** with a better light harvesting ability in 400-600 region yields a higher J_{SC}. Even though the **TP-RAA** dye has a better light harvesting capability the net efficiency of **TP-RAA** is lower than that of **TP-CAA** which is primarily due to the loss in photovoltage as a result of higher aggregation (as explained in **Section 4.3.2**) which adversely affect the light to current conversion efficiency. Here also addition of **CDCA** helped in alleviating aggregation thereby improving the photovoltage by about 60 mV.

The electron lifetime measurements of both dyes are shown in **Figure 4.7b** which is in good agreement with the photovoltaic data. From **Figure 4.7a**, it is quite clear that addition of co-adsorbent **CDCA** helped in reducing aggregation of both TPA-bithiazole dyes thereby improving the photovoltage for devices with co-adsorbent and a better efficiency in comparison to the dye alone devices. This suggests that a more effective suppression of back electron transfer occurs between the injected electrons and electrolyte, which leads to the enhancement in the V_{OC} value owing to a reduced charge recombination rate. Recombination rate is higher with the dye containing the rhodanine acetic acid anchoring group

TP-RAA. In presence of iodide/triiodide electrolyte, dyes containing rhodanine moieties are reported to show higher recombination rates.[24]

IPCEs of the **TP-CAA** and **TP-RAA** based cells in the presence and absence of **CDCA** are shown in **Figure 4.9**. The results of IPCE measurements were in accordance with the photovoltaic performances. Solar cells based on **TP-CAA** exhibited action spectra in the range of 400-600 nm with the highest IPCE value of 78% at 400 nm and in the presence of **CDCA**, IPCE value slightly dropped to
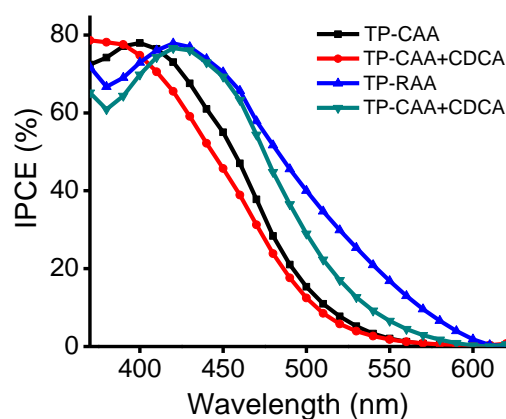
Figure 4.9 IPCE plot of the DSSCs using **TP**-**CAA** and **TP**-**RAA** based cells in the absence and presence of **CDCA**.

75%. **TP-RAA** displayed a broader photocurrent action spectrum in 450-600 nm region with highest value of 78% at 420 nm without **CDCA** and 77% at 420 nm with **CDCA**. This broader action spectrum resulted in improved photocurrent densities for rhodanine acetic acid anchoring groups in comparison to the cyanoacrylic acid anchoring group. The shift in action spectra for both dyes are in well agreement with the absorption profile of these dyes on TiO_2 surface as

explained in **Section 4.3.2**. Even though **TP-RAA** has a better absorption profile the enhanced aggregation expedite more recombinations resulting in lower lifetime (as shown in **Figure 4.6b**) leading to reduced photovoltage and efficiency as explained before.
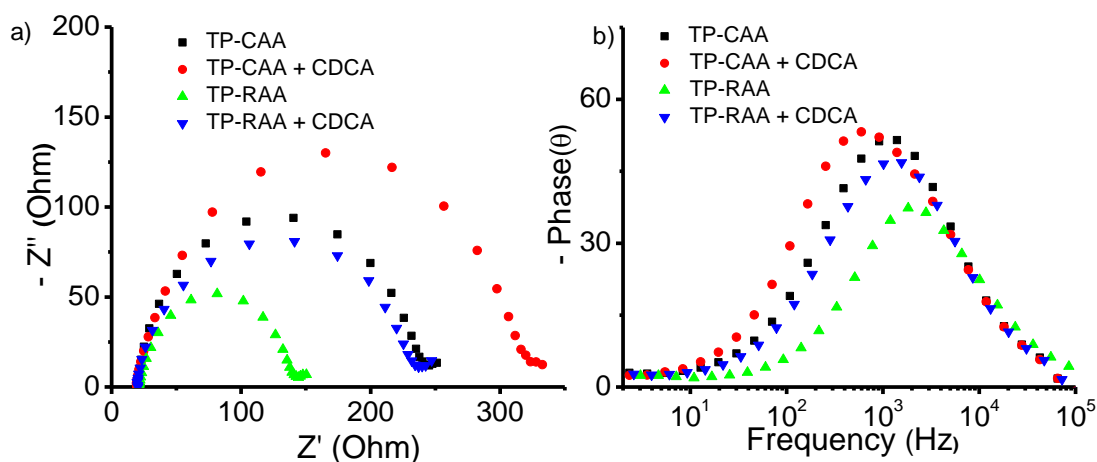
Figure 4.10 (a) EIS Nyquist plot (b) Bode plot for DSSCs based on **TP**-**CAA** and **TP**-**RAA** with and without **CDCA** measured at -0.65 V forward bias in the dark.

As described before, electrochemical impedance spectroscopy is a powerful tool to elucidate the charge transfer and transport processes taking place in DSSCs.[25-29] EIS was carried out to study the effect of binding groups on electron recombination and lifetime. Impedance was measured over the frequency range $0.1 - 10^5$ Hz in dark under a forward bias of -0.7 V. The Nyquist and Bode plots obtained are given in **Figure 4.10**. Analysis of the impedance data in DSSC helps in gaining detailed understanding on interfacial charge transfer processes and electron lifetimes which are summarized in **Table 4.3**.

Table 4.3 Parameters obtained by fitting the impedance spectra using equivalent circuit

Soaking condition	$^a R_S$ (Ω)	$^b R_{rec}$ (Ω)	$^c f_{max}$ (Hz)	$^d \tau_e$ (μs)	$^e k_{eff}$ (ms)$^{-1}$
TP-CAA	20.16	213.5	1158.51	137.45	7.27
TP-CAA+CDCA	19.22	301.4	597.18	266.65	3.75
TP-RAA	21.46	117.7	1830.04	87.01	11.49
TP-RAA + CDCA	20.51	198.2	1287.23	123.70	8.08

The parameters given in **Table 4.3** was calculated following literature procedure.[30] In **Table 4.3**, R_s represents series resistance which is almost the same in all entries as we are using the same electrode material and same electrolyte. R_{rec} corresponds to the larger semicircle in Nyquist plot that portray the charge transfer resistance at TiO_2/dye/electrolyte interface. The radius of the larger semicircle and hence the R_{rec} values decreased in the order **TP-CAA + CDCA** (301.4 Ω) > **TP-CAA** (213.5 Ω) > **TP-RAA + CDCA** (198.2 Ω) > **TP-RAA** (117.7 Ω) which indicates that the device sensitized by **TP-CAA + CDCA** exhibited the largest resistance for recombination between the electrons injected to TiO_2 and electrolyte leading to a better lifetime and photovoltage. These results are in agreement with the V_{OC} values obtained for the devices **TP-CAA + CDCA** (0.75 V) > **TP-CAA** (0.70 V) > **TP-RAA + CDCA** (0.69 V) > **TP-RAA** (0.63 V). In the Bode-phase plot, the maximum peak frequency (f_{max}) was

indicative of the charge recombination rate. The lifetime of injected electrons τ_e were estimated using equation (1) and summarized in **Table 4.3**.

$$\tau_e = 1/(2\pi f_{max}) \qquad (1)$$

Shift of the peak from higher frequency to lower frequency is an indicative of the longer electron lifetime which is highest for **TP-CAA** + **CDCA** since the frequency maximum and Bode plot is inversely related to electron lifetime. The lower frequency corresponds to larger charge recombination resistance and longer electron lifetime in agreement with the values obtained in **Table 4.3** by fitting the impedance data.[30, 31] This points out to effective suppression of back electron transfer between the injected electrons and electrolyte for **TP-CAA** + **CDCA** in comparison to rest of the entries resulting in a lower recombination rate (k_{eff}) giving rise to improved open circuit voltage. The recombination rate follows the order **TP-CAA** + **CDCA** (3.75 ms) < **TP-CAA** (7.27 ms) < **TP-RAA** + **CDCA** (8.08 ms) < **TP-RAA** (11.49 ms). Lower electron lifetime for **TP-RAA** dye in comparison to **TP-CAA** is mainly attributed to the aggregation of the former dye as explained in **Section 4.3.2**, which leads to higher electron recombination rate and reduced lifetime as explained by the equivalent circuit fitted impedance data given in **Table 4.3**. The fitted parameters are in well agreement with the rest of the photovoltaic characterization results.

It must be noted that a few triphenylamine-bithiazole based systems are reported in literature with cyanoacrylic acid as the anchoring group.[14,22,34,35] In

one of the papers, He *et al*. reported a PCE of 7.51%.[34] Our triphenylamine-

bithiazole systems contain alkyl groups on both the thiophene units on either side

of the bithiazole in order to improve solubility and to prevent charge

recombinations. We have also introduced a better acceptor group like rhodanine

acetic acid which helped to cover more area in the visible spectrum by shifting

the onset of absorption. However, the efficiency of the cyanoacrylic acid system

is comparatively lower than the reported system.

   To find the fundamental reason for this observation, we have calculated

dihedral angles of the individual moieties in each molecule (**Figure 4.11**) using

DFT method. The dihedral angles between the bithiazole units and the alkylated

thiophene moieties on either side were considerably higher in both systems. This

could be attributed to the presence of hexyl chains on the thiophenes resulting in

reducing the effective conjugation lengths of the molecules. This leads to blue

shifted absorption spectra of the dyes in comparison to those molecules reported

in literature where the absorption extends up to 620 nm (up to 550 nm in the

present case).[36] Hence it could be concluded that the high dihedral angles in

general played a major role in lowering the efficiency of the present system. So,

the future work will be focussed on improving the efficiencies by reducing the

dihedral angles through rational design. The solubilizing alkyl groups could be

placed on the donor moieties which may not affect the planarity and hence the

effective conjugation lengths of the molecules. But a noticeable aspect in the

case of rhodanine acetic acid system is that even though being an efficient

acceptor leading to bathochromic shift in absorption, this functionality is rarely
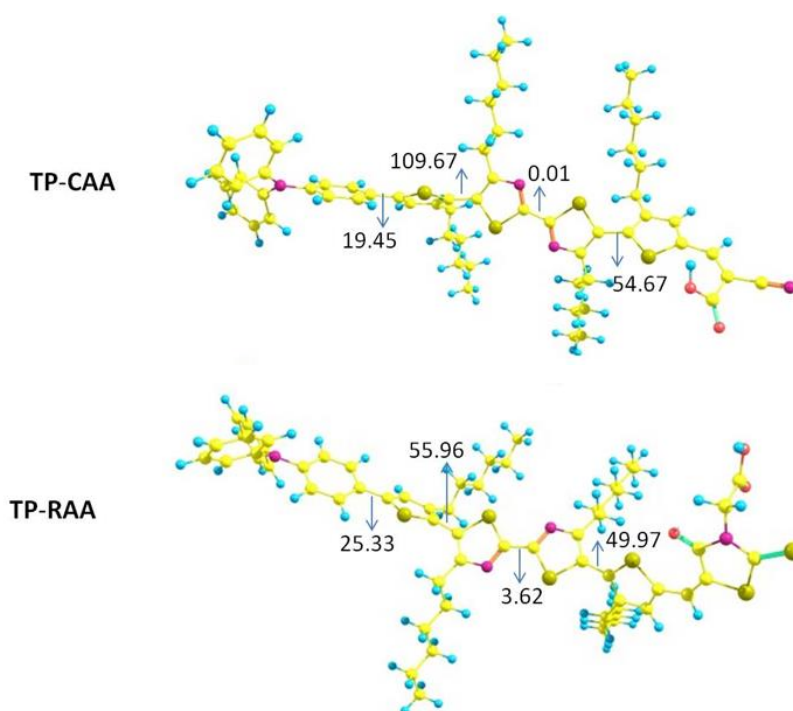
Figure 4.11. Dihedral angle between various units in **TP-CAA** and **TP-RAA** obtained from DFT calculations.

used in dyes due to their enhanced aggregation on semiconductor surface leading

to diminution in the photovoltaic efficiency when compared to cyanoacrylic acid

systems.[7,9,36-38] But in our case we obtained good photovoltaic efficiency values

for rhodanine acetic acid system (almost near to the cyanoacrylic acid system)

because we could prevent the aggregation in this system to a greater extent by

molecularly engineering the π-spacer leading to better performance even at low

co-adsorbent concentrations. This could lead to new ways of tuning the dye

skeleton in a way to minimize the impeding back electron transfer processes. Further, in the case of **TP-RAA** in particular, use of iodide/triiodide electrolyte may not be a suitable choice as it contributes to increase in the recombination rate as reported in literature.[22] The recombination rate can be reduced by using alternate redox shuttles (such as cobalt based electrolytes) instead of the iodide/triiodide electrolyte for molecule with rhodanine based anchoring groups.

4.4. Conclusions

Triphenylamine-bithiazole based two metal-free organic dyes consisting of two different anchoring groups *viz.* cyanoacrylic acid (**TP-CAA**) and rhodanine acetic acid (**TP-RAA**) were designed and synthesized. Detailed photophysical, electrochemical and photovoltaic characterization proved that the structure and nature of the anchoring groups and twist in the molecular structure significantly influenced the PCEs of the DSSC devices. DFT analysis showed that the introduction of hexyl chains on the thiophene units is detrimental to the device efficiencies as they induce twist in the molecular structure and hence reduce the effective conjugation lengths. Compared to that of cyanoacrylic acid, rhodanine acetic acid exhibited better absorption characteristics. However, the higher recombination rates in this molecule as evident from the OCVD and EIS results pulled down the PCE below to that of the former. But the efficiency of rhodanine

acetic acid system remains high when compared to similar systems in literature as a result of lower aggregation resulted from properly engineered π-spacer.

4.5. Experimental section

### 4.5.1. Materials and characterization techniques

The reagents and materials for synthesis were purchased from Sigma-Aldrich, Merck, TCI and Spectrochem chemical suppliers, and are used as received. Air and water sensitive synthetic steps were performed in an argon atmosphere using standard Schlenk techniques. ^{1}H and ^{13}C-NMR spectra were recorded using Bruker-500 MHz spectrometer. The compounds were thoroughly purified using the recycling preparative HPLC system of Japan Analytical Industry Co., Ltd LC-9220 II NEXT SERIES (eluent CHCl$_3$). Absorption spectra were recorded using Shimadzu UV-Visible-2401PC spectrophotometer. Steady-state fluorescence experiments were performed using a SPEX Fluorolog F112X spectrofluorimeter. Cyclic voltammetry experiments were performed using a BAS 50W voltammetric analyser. Density functional theory (DFT) calculations were performed at the B3LYP/6-31G* (d,p) level using Gaussian 09 program.

4.5.3. Synthesis

The dyes were synthesized as shown in **Scheme 4.1**. Suzuki coupling of **5** with (4-(diphenylamino)phenylboronic acid gave **6** which was then reacted with acceptors such as 2-cyanoacetic acid and 2-(4-oxo-2-thioxothiazolidin-3-

yl)acetic acid, to give **TP-CAA** and **TP-RAA**, respectively. The dyes were characterized using analytical techniques such as ^{1}H NMR, ^{13}C NMR and mass spectrometry.

Synthesis of 6:
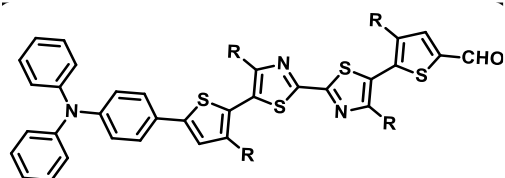
Compound **10** (100 mg, 0.129 mmol), Pd(PPh$_3$)$_4$ (22 mg, 0.02 mmol), K$_2$CO$_3$ (1.02 g, 0.01 mol) in THF (10 mL) and water (5 mL) were heated to 45 ^{o}C under a nitrogen atmosphere for 30 minutes. A solution of 4-(diphenylamino) phenyl boronic acid (70.8 mg, 0.245 mmol) was added slowly and the mixture was heated at reflux for further 2 hours. After cooling to room temperature, THF was evaporated and the mixture was extracted with DCM. The combined organic layers were dried with anhydrous Na$_2$SO$_4$. The solvent was evaporated and the residue was purified by column chromatography on silica gel (Hexane:DCM = 1:1) to give a dark orange solid. (Yield: 80.62 %); ^{1}H NMR (500 MHz, CDCl$_3$) : δ 9.89 (s, 1H), 7.67 (s, 1H), 7.46 (d, 2H, *J*=8.5 Hz), 7.25-7.28 (m, 3H), 7.02-7.13 (m, 10H), 2.70-2.76 (m, 8H), 1.68-1.72 (m, 8H), 1.26-1.33 (m, 24H), 0.84-0.87 (m, 12H); ^{13}C NMR (CDCl$_3$, 150 MHz): 182.77, 161.32, 159.45, 158.10, 157.55, 147.60, 147.41, 144.72, 144.61, 144.54, 143.18, 137.49, 136.20, 129.33, 127.81, 126.45, 126.14, 124.57, 124.03, 123.56, 123.49, 123.46, 123.20, 31.64,

31.61, 31.56, 31.54, 30.58, 30.37, 29.94, 29.84, 29.62, 29.59, 29.20, 29.10, 29.07, 29.03, 28.97, 28.93, 22.58, 22.56, 22.53, 14.07, 14.03; IR ($\bar{\upsilon}$): 2934, 2850, 1683, 1582, 1271, 1158 cm^{-1}; HRMS (*m/z*): (M^{+}+H) calculated for C$_{57}$H$_{69}$N$_3$OS$_4$: 940.4323; Found: 940.4392.

Synthesis of TP-CAA:
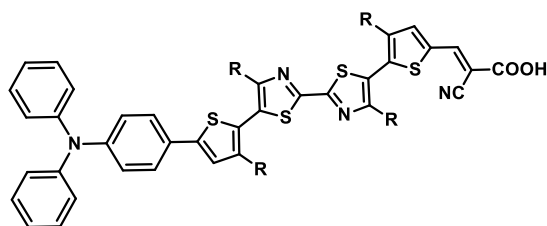
Compound **7** (50 mg, 0.053 mmol), 2-cyanoacetic acid (40.7 mg, 0.4 mmol) and few drops of piperidine in chloroform (4 mL) were heated at 60 °C for 30 h. After cooling to room temperature, the mixture was added to water and extracted with chloroform. The crude product was purified by column chromatography on silica gel (CH$_2$Cl$_2$: EtOH = 9:1 v/v) to give an orange red solid. It was again purified by precipitating from cold methanol. Final purification was done using recycling HPLC using CHCl$_3$ as eluent (Yield: 81%). M. P. 108.5 °C; ^{1}H NMR (500 MHz, CDCl$_3$): δ 8.30 (s, 1H), 7.75 (s, 1H), 7.47 - 7.46 (m, 2H), 7.29 - 7.26 (m, 3H), 7.13 - 7.11 (m, 5H), 7.08 - 7.03 (m, 5H), 2.63 - 2.60 (t, 4H), 2.57 - 2.54 (m, 4H), 1.75 - 1.71 (m, 4H), 1.59 - 1.58 (m, 4H), 1.31 - 1.27 (m, 24H), 0.88 - 0.84 (m, 12H); ^{13}C NMR (CDCl$_3$, 150 MHz): 160.35, 158.34, 157.20, 156.53, 146.54, 146.39, 143.88, 143.65, 143.49, 137.61, 134.89, 128.31, 126.83, 125.42,

125.15, 123.53, 123.00, 122.55, 122.23, 122.16, 98.97, 30.62, 30.58, 30.54,

30.49, 29.55, 29.35, 29.03, 28.81, 28.60, 28.56, 28.17, 28.07, 28.03, 27.99,

27.77, 21.55, 13.05, 13.00; IR ($\bar{\upsilon}$): 3455, 2935, 2848, 2217, 1702, 1589, 1492,

1278 cm^{-1}; MALDI-TOF-MS (*m/z*): M$^+$ calculated for $C_{60}H_{70}N_4O_2S_4$: 1006.438;

Found: 1006.376.

Synthesis of TP-RAA:
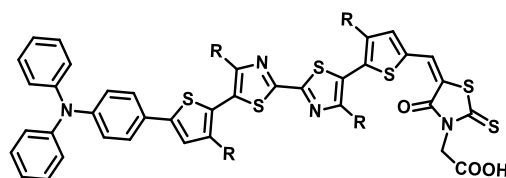
    Compound **7** (50 mg, 0.053 mmol), 2-(4-oxo-2-thioxothiazolidin-3-yl) acetic

acid (91.5 mg, 0.4 mmol) and few drops of piperidine in chloroform (4 mL) were

heated at 60 °C for 12 h. After cooling to room temperature, the mixture was

added to water and extracted with chloroform. Then purified by column

chromatography on silica gel (CH_2Cl_2: EtOH = 9:1 v/v) to give an orange red

solid. It was again purified by precipitating from cold methanol. Final

purification was done using recycling HPLC using $CHCl_3$ as eluent (Yield: 72

%); M. P. 130 °C; ^{1}H NMR (500 MHz, CDCl$_3$) : δ 7.89 (s, 1H), 7.47 - 7.46 (d,

2H , *J* = 8.5 Hz), 7.32 - 7.27 (m, 4H), 7.13 - 7.09 (m, 5H), 7.07 - 7.03 (m, 5H),

4.92 (s, 2H), 2.77 - 2.73 (m, 4H), 2.62 - 2.54 (m, 4H), 1.27 (s, 32H), 0.87 - 0.84

(m, 12H); ^{13}C NMR (CDCl$_3$, 150 MHz): 191.97, 166.93, 161.34, 159.59, 158.24,

157.67, 147.73, 147.54, 145.47, 144.86, 144.70, 137.93, 136.08, 134.69, 129.46,

127.94, 126.58, 126.31, 125.93, 124.70, 124.17, 123.69, 123.59, 123.33, 121.08, 116.50, 53.56, 32.06, 31.78, 31.73, 31.71, 31.67, 31.37, 30.71, 30.54, 30.15, 29.95, 29.83, 29.79, 29.76, 29.49, 29.34, 29.23, 29.21, 29.13, 22.83, 22.71, 22.68, 14.25, 14.20, 14.16; IR ($\bar{\upsilon}$): 3657, 2942, 2860, 2352, 1713, 1592, 1485, 1324, 1202 cm^{-1}; MALDI-TOF-MS (*m/z*): (M$^+$+H) calculated for C$_{62}$H$_{72}$N$_4$O$_3$S$_6$: 1113.392; Found: 1113.713.

4.6. References

1. Sun, S.; Lin, T.; Ho, K. *RSC Adv.* **2015**, *5*, 23810–23825.
2. Wu, J.; Lan, Z.; Lin, J.; Huang, M.; Huang, Y.; Fan, L.; Luo, G. *Chem. Rev.* **2015**, *115*, 2136–2173.
3. Taek, I.; Seok, B.; Kyung, Y.; Jong, M.; Seok, W.; Ho, S.; Soo, M.; Deuk, K.; Yeoun, J.; Hyun, S. *Org. Electron.* **2014**, *15*, 3316–3326.
4. Zhang, L.; Cole, J. M. *ACS Appl. Mater. Interfaces* **2015**, *7*, 3427–3455.
5. Kalyanasundaram, K.; Gratzel, M. *Coord. Chem. Rev.* **1998**, *77*, 347–414.
6. Galoppini, E.*Coord. Chem. Rev.* **2004**, *248*, 1283–1297.
7. Yang, C.; Liao, S.; Sun, Y.; Chuang, Y.; Wang, T.; Shieh, Y.; Lin, W. *J. Phys. Chem. C,* **2010**, *114*, 21786–21794.
8. Soni, S. S.; Fadadu, K. B.; Vaghasiya, J. V; Solanki, B. G. *J. Mater. Chem. A* **2015**, *3*, 21664–21671.
9. Ahn, H. J.; Thogiti, S.; Cho, J. M.; Jang, B. Y.; Kim, J. H. *Electron. Mater. Lett.* **2015**, *11*, 822–827.
10. Lan, T.; Lu, X.; Zhang, L.; Chen, Y.; Zhou, G.; Wang, Z. *J. Mater. Chem. A,* **2015**, *3*, 9869–9881.
11. Qian, X.; Lu, L.; Zhu, Y. Z.; Gao, H. H.; Zheng, J. Y. *Dye. Pigment.* **2015**,

113, 737–742.

12. Pei, J.; Peng, S.; Shi, J.; Liang, Y.; Tao, Z.; Liang, J.; Chen, J., *J. Power Sources* **2009**, *187*, 620–626.

13. Yang, C.; Chen, H.; Chuang, Y.; Wu, C.; Chen, C.; Liao, S.; Wang, T. *J. Power Sources* **2009**, *188*, 627–634.

14. Kanaparthi, R. K.; Kandhadi, J.; Giribabu, L. *Tetrahedron* **2012**, *68*, 8383–8393.

15. He, J.; Wu, W.; Hua, J.; Jiang, Y.; Qu, S.; Li, J.; Long, Y.; Tian, H. *J. Mater. Chem.* **2011**, *21*, 6054–6062.

16. Wang, P.; Humphry-baker, R.; Zakeeruddin, S. M.; Gratzel, M., *J. Am. Chem. Soc.* **2005**, *127*, 808–809.

17. Hamann, T. W.; Jensen, R. A.; Martinson, A. B. F.; Ryswyk, V.; Hupp, J. T.; Hamann, T.,*Energy Environ. Sci.* **2008**, *1*, 66–78.

18. Robson, K. C. D.; Sporinova, B.; Koivisto, B. D.; Schott, E.; Brown, D. G.; Berlinguette, C. P. *Inorg. Chem.***2011**, *50*, 6019–6028.

19. Teng, C.; Yang, X.; Yang, C.; Li, S.; Cheng, M.; Hagfeldt, A.; Sun, L. *J. Phys. Chem. C* **2010**, *114*, 9101–9110.

20. Zhou, N.; Prabakaran, K.; Lee, B.; Chang, S. H.; Harutyunyan, B.; Guo, P.; Butler, M. R.; Timalsina, A.; Bedzyk, M. J.; Ratner, M. A. *J. Am. Chem. Soc.* **2015**, *137*, 4414–4423.

21. Soman, S.; Rahim, M. A.; Lingamoorthy, S.; Suresh, C. H.; Das, S. *Phys. Chem. Chem. Phys.* **2015**, *17*, 23095–23103.

22. Yen, Y.; Lin, T.; Hsu, C.; Chen, Y.; Chou, H.; Tsai, C.; Lin, J. T. *Org. Electron.* **2013**, *14*, 2546–2554.

23. Daphnomili, D.; Landrou, G.; Singh, P.; Thomas, A.; Yesudas, K. *RSC Adv.* **2012**, *2*, 12899–12908.

24. Zhongquan, W.; Jia, C.; Yao, X. *RSC Adv.* **2015**, *5*, 50813–50820.

25.   Zhang, J.; Wu, Y.; Geng, Y.; Fu, Q.; Su, Z. *J. Mater. Chem. A* **2013**, *1*,14000–14007.

26.   Seo, K. D.; Choi, I. T.; Kyu, H. *Chem. - A Eur. J.* **2015**, *21*, 14804–14811.

27.   Wu, G.; Kong, F.; Zhang, Y.; Zhang, X.; Li, J.; Chen, W.; Liu, W.; Ding, Y.; Zhang, C.; Zhang, B. *J. Phys. Chem. C* **2014**, *118*, 8756–8765.

28.   Cisneros, R.; Beley, M.; Fauvarque, J.; Lapicque, F. *Electrochim. Acta* **2015**, *171*, 49–58.

29.   Cheol, B.; Seok, M.; Ju, M.; Hoon, D.; Ahn, K.; Hong, J. *Synth. Met.* **2014**, *188*, 130–135.

30.   Adachi, M.; Sakamoto, M.; Jiu, J.; Ogata, Y.; Isoda, S. *J. Phys. Chem. B* **2006**, *110*, 13872–13880.

31.   Fakharuddin, A.; Ahmed, I.; Wali, Q.; Khalidin, Z.; Yosuff, M. M.; Rajan, J. *Adv. Mater. Res.* **2014**, *925*, 553–558.

32.   Bisquert, J.; Zaban, A.; Greenshtein, M. *J. Am. Chem. Soc.* **2004**, *13*, 13550–13559.

33.   Jia, H.; Zhang, M.; Ju, Z.; Zheng, H.; Ju, X. *J. Mater. Chem. A* **2015**, No. 3, 14809–14816.

34.   Lai, L.; Ho, C.; Chen, Y.; Wu, W.; Dai, F.; Chui, C.; Huang, S.; Guo, K.; Lin, J.; Tian, H. *Dye. Pigment.* **2013**, *96*, 516–524.

35.   He, J.; Guo, F.; Wu, W.; Yang, J.; Hua, J. *Chem. Eur. J.* **2012**, *18*, 7903–7915.

36.   Li, Y.; Chen, C.; Hsu, Y.; Hsu, H.; Chi, Y.; Chen, B.; Liu, W.; Lai, C.; Lin, T. *Tetrahedron* **2010**, *66*, 4223–4229.

37.   Wang, Z.; Liang, M.; Wang, L.; Hao, Y.; Wang, C.; Sun, Z.; Xue, S. *Chem. Commun.* **2013**, *2*, 5748–5750.

38.   Gupta, K. S. V; Singh, S. P.; Islam, A.; Han, L.; Chandrasekharam, M. *Electrochim. Acta* **2015**, *174*, 581–587.

Rhodanine-anchored metal-free dyes: Effect of thiophene spacers on photovoltaic properties

5.1. Abstract

*Three new photosensitizers (**TP, BTP** and **TTP**) with a D-π-A architecture were synthesized in which triphenylamine acts as a donor, thiophene moieties as π-spacers and rhodanine-3-acetic acid as acceptor/anchoring group. Absorption properties were studied in solution and thin film state by adsorbing on to TiO$_2$. The compounds exhibited intense structured absorption band in the UV-vis region from 250-750 nm. Electrochemical properties were studied using cyclic voltammetry experiments, and the HOMO-LUMO energy levels were ascertained. The dyes exhibited a maximum photovoltaic efficiency of 1.62%. Measurement of dihedral angle of these dyes and comparison with an earlier system reported reveals that dihedral angle of the spacer unit plays an important role in determining the photovoltaic efficiency. EIS was carried out to study the effect of π-spacers on electron recombination and lifetime.*

5.2. Introduction

Molecular engineering is one of the successful strategy for tuning the performance of organic photosensitizers for DSSC application.[1] As described before, most of the organic photosensitizers follow D-π-A configuration for better photoinduced electron transfer process.[2-4] The covalently linked donor-π-acceptor system strategy and the choice of electron donor, π-spacer and acceptor molecules anchoring to TiO_2 are important factors which helps in the cascade flow of electron from the donor through the π-spacer to the acceptor.

In this chapter, we have studied the dependence of the anchoring groups on the photovoltaic properties of triphenylamine-bithiazole based metal-free organic dyes. Cyanoacrylic acid is employed as a very common acceptor or anchoring group for attachment to TiO_2.[5] Rhodanine-3-acetic acid, due to its strong electron withdrawing ability, is recently employed as anchoring group in a series of organic dyes reaching a maximum photovoltaic efficiency of 9.03%.[6,7] But this anchoring group is very much less explored with thiophene based systems.

Rajalingam and coworkers synthesized D–π–π–A dyes (**1-4;** chemical structures are shown in **Figure 5.1**) with different π-spacers and analyzed for

their effect on photophysical properties and photovoltaic applications.[8] Triphenylamine moiety was used in these dyes as the electron donor and cyanoacetic acid acts as the electron acceptor. Benzene, furan
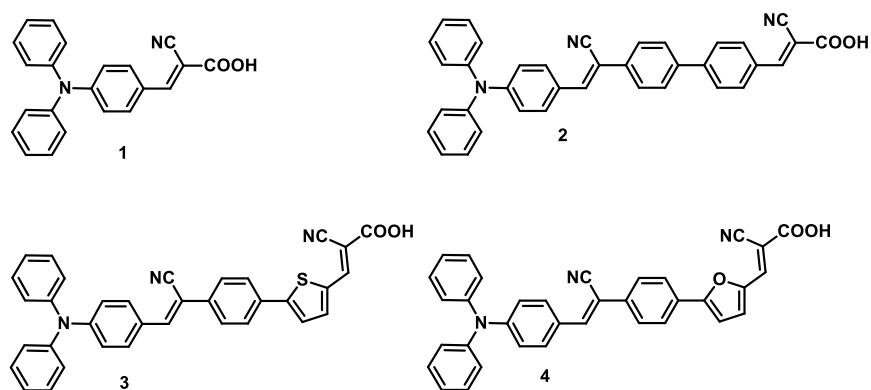
Figure 5.1 Molecular structures of compounds **1-4**.

and thiophene moieties varies by maintaining phenyl acetonitrile as π-spacer. Effect of various π-spacers on photophysical, electrochemical and photovoltaic characteristics have been analyzed. On changing the π-spacer, photovoltaic parameters such as short circuit current density (J_{SC}) and open circuit voltage (V_{OC}) are found to be significantly varied. Maximum absorption was observed for dye **3**, with thiophene linker resulting in high J_{SC} value than other dyes. The photophysical and photovoltaic experiments shows that the phenyl and thiophene spacer produces greater power conversion efficiency than the furan-based dye.
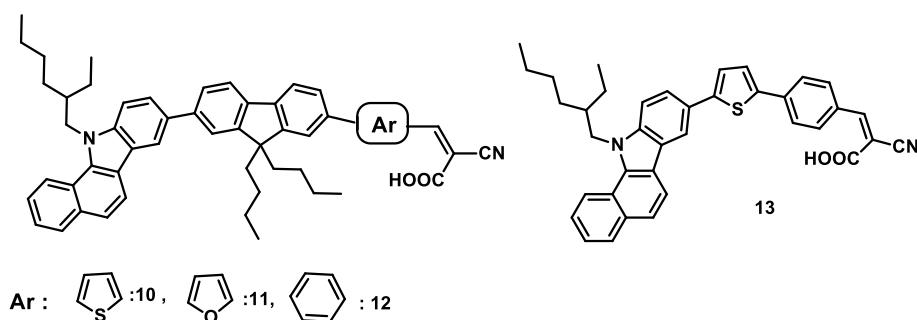
Zhu and coworkers synthesized a series of metal-free panchromatic organic
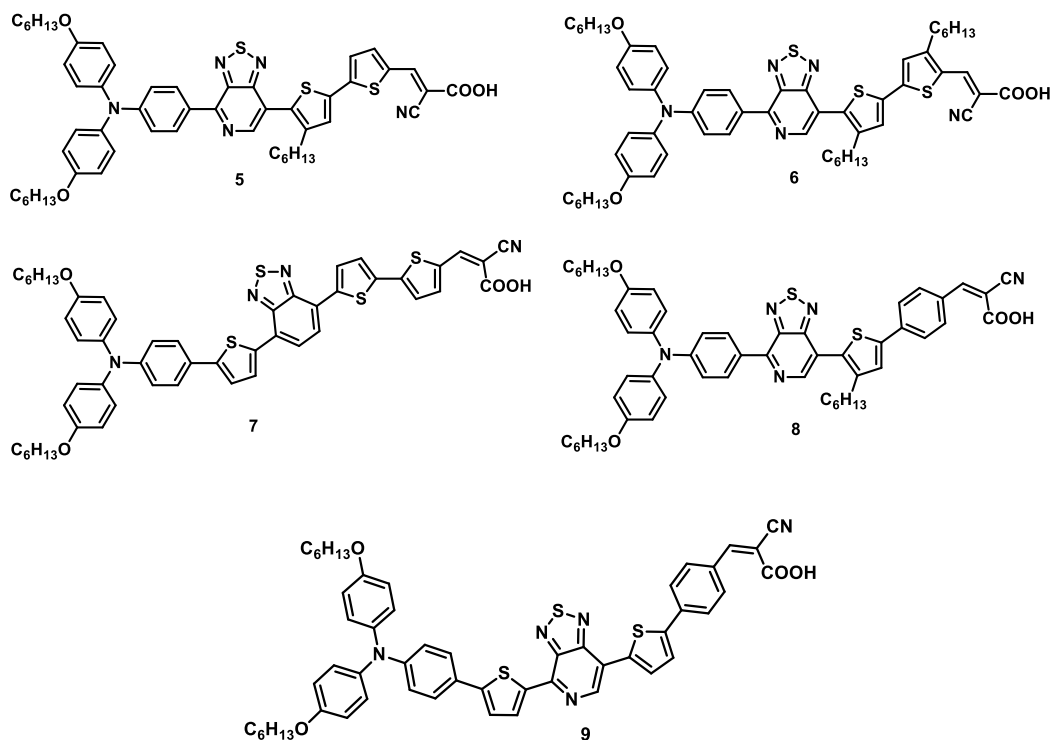
Figure 5.2 Molecular structures of compounds **5-9**.

photosensitizers (**5-9;** chemical structures are shown in **Figure 5.2**) based on a

strong electron deficient thiadiazole[3,4-c]pyridine core for DSSC and studied

the impact of various π-conjugated spacers.[9]The incorporation of π-spacer such

as thiophene, n-hexylthiophene and benzene results in different dihedral angles.

Large steric conformations arise due to higher dihedral angles may break the

effective conjugation in the dye results in separated HOMO and LUMO levels

with sufficient orbital overlaps. This may facilitate the electron transfer from

donor part of the dye molecule to the conduction band of TiO_2. Among the dyes,

higher dihedral angle was observed in **8**. So, largest steric hindrance was

observed in dye **8**, and showed higher photovoltaic properties. This is due to the better charge recombination and inhibition of intermolecular π-π stacked aggregation on the TiO$_2$ surface.


Figure 5.3 Molecular structures of compounds **10-13**.

Bhanuprakash and coworkers synthesized a series of novel metal-free sensitizers (**10-13;** chemical structures are shown in **Figure 5.3**) for DSSC with different π-conjugated spacers.[10] Fluorene-thiophene (BFT), fluorene-furan (BFF), fluorenephenyl (BFB) and thiophene-phenyl (BTB) were the different combination of spacers used in this study. Fluorenephenyl based dye (**12**) showed enhanced intensity and higher molar extinction coefficient. This dye on adsorption on TiO$_2$ exhibits better conjugation due to more planar arrangement results in stronger binding on TiO$_2$ surface. The photovoltaic efficiency of the device with this dye showed highest performance.

In the present study, we employ rhodanine-3-acetic acid as the anchoring group in triphenylamine-based systems. Three different π-spacers such as

thiophene **(TP)**, bithiophene **(BTP)** and thienothiophene **(TTP)** were used. Structures of the molecules are shown in **Scheme 5.1**. The dyes are comparable with respect to donor and anchoring group but differing in the π-spacers. In order to reduce possible intermolecular interactions, suitable alkyl chains are introduced at the thiophene π-bridging units.
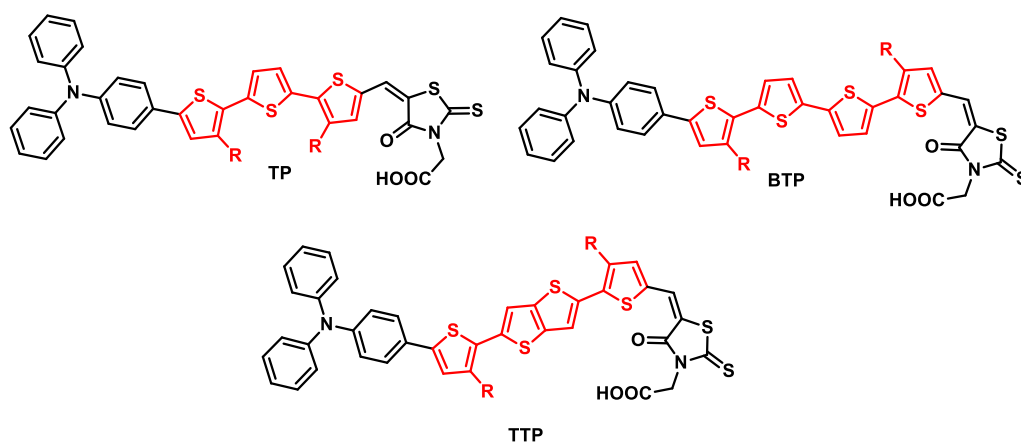
Scheme 5.1 Structure of compounds used in the present study.

5.3. Results and Discussion

5.3.1. Synthesis

The dyes were synthesized starting from the respective stannylated compounds of the π-spacers as shown in **Scheme 5.2**. Compounds **14**-**22** were already reported in the literature.[11-13] The π-spacers were attached with hexylated thiophenes at both ends to increase the solubility using Stille coupling. Then they were formylated and brominated to get the intermediate compounds **20**-**22**. The

intermediate compounds were then coupled with boronylated ester of triphenylamine using Suzuki coupling to give **23**-**25**. Subsequently, they were reacted with the acceptor 2-(4-oxo-2-thioxothiazolidin-3-yl)acetic acid to give **TP**, **BTP** and **TTP**. The dyes were characterized using analytical techniques such as ^{1}H NMR, ^{13}C NMR and mass spectrometry.
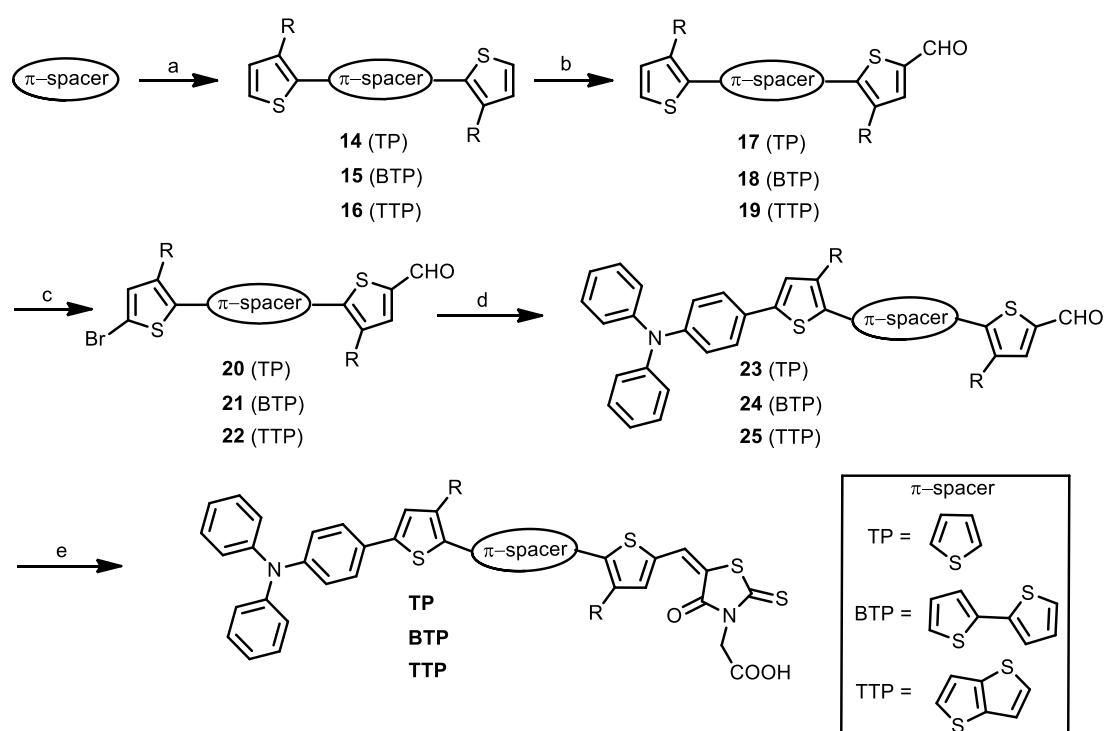
Scheme 5.2 *Synthetic route for the preparation of **TP**, **BTP** and **TTP**. Reagents and conditions: (a) Pd(PPh₃)₄, K₂CO₃, toluene, 24 h, reflux; (b) POCl₃, DMF, dichloroethane, 0 - 60 °C, 12 h; (c) NBS, chloroform, acetic acid, 3 h; (d) 4-(1,3,2-dioxaborinan-2-yl)-N,N-diphenylaniline, Pd(PPh₃)₄, K₂CO₃, toluene, 24 h, reflux; (e) 2-(4-oxo-2-thioxothiazolidin-3-yl)acetic acid, CHCl₃, piperidine, 18 h, reflux.*

5.3.2. Photophysical properties of the dyes

Normalized absorption spectra of the dyes in DCM and adsorbed on thin TiO_2 film are shown in **Figure 5.4a** and **5.4b**, respectively. The compounds exhibited intense structured band in the UV-vis region from 250 nm to around 750 nm. The whole absorption can be attributed to the aromatic π-π* transition as well as the intramolecular charge transfer transitions between the electron donor and acceptor moieties involving the triphenylamine and rhodanine acetic acid, respectively.
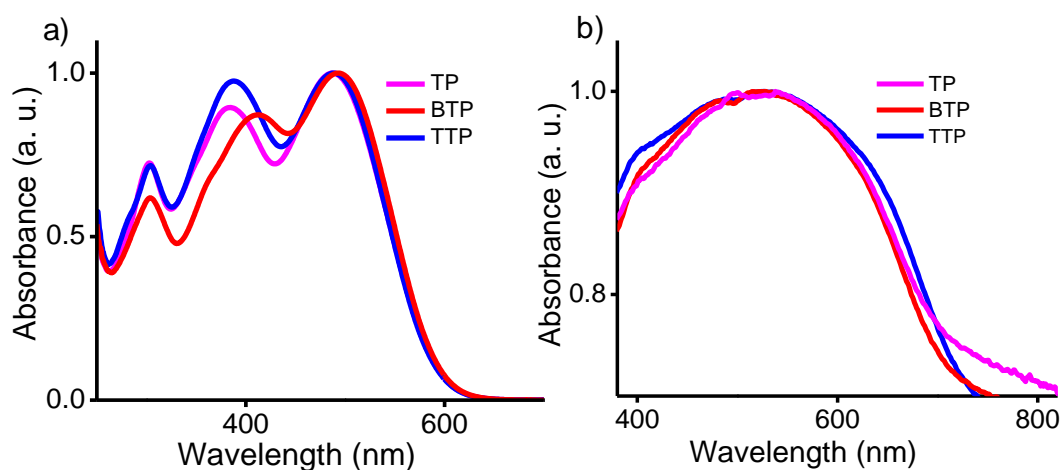
Figure 5.4 Absorption spectra of dyes (a) in solution (DCM 10^{-5} M) and (b) adsorbed on TiO_2 thin film (thickness 12 μm).

TP exhibited the absorption maximum at 503 nm and another peak at higher energy region at 382 nm. In the case of **BTP**, a slight red shift was obtained for λ_{max} (505 nm) for the lower energy peak and a considerable red shift of 39 nm was obtained for the higher energy peak at 421 nm. The red shift in the higher

energy peak reflects the increase in the π-conjugation in the spacer unit in **BTP**.

In the case of **TTP**, a considerable red shift of about 25 nm was observed for the

lower energy peak as well as about 10 nm shift for the higher energy peak

compared to **TP** exhibiting λ_{max} at 529 and 392 nm, respectively. This can be

attributed to the rigid thienothiophene spacer unit, which increases the

conjugation as well as enhance the planarization of the conjugated backbone.

The molar extinction coefficients of **TP**, **BTP** and **TTP** in solution state were

calculated to be 34530, 32950 and 32000 $M^{-1}cm^{-1}$, respectively, which shows

that the dyes have good light harvesting ability in comparison to the conventional

ruthenium complexes, which can help in fabricating thinner devices. The

wavelength corresponding to the onset of the absorption for the dyes were found

to be 630, 660 and 685 nm for **TP**, **BTP** and **TTP**, respectively. The resulting

optical band-gaps were calculated to be 1.96, 1.87 and 1.81 eV, respectively.

The introduction of rigid thienothiophene moiety has resulted in considerable

reduction of bandgap.

Thin film electronic absorption spectra of dyes adsorbed on TiO_2 were

recorded by immersing DCM solutions of the dyes in TiO_2 films of 12 μm

thickness for 12 h. The corresponding absorption profiles are shown in **Figure

5.4b**. The structured absorption in solution state was changed to a broad

absorption which was almost similar in all the three dyes with a bathochromic

shift with λ_{max} at about 535 nm. The bathochromic shift implies that *J*-aggregates of dyes are formed on TiO₂ surface and the dyes adsorb efficiently to the semiconductor surface.

5.3.3. Electrochemical properties of the dyes
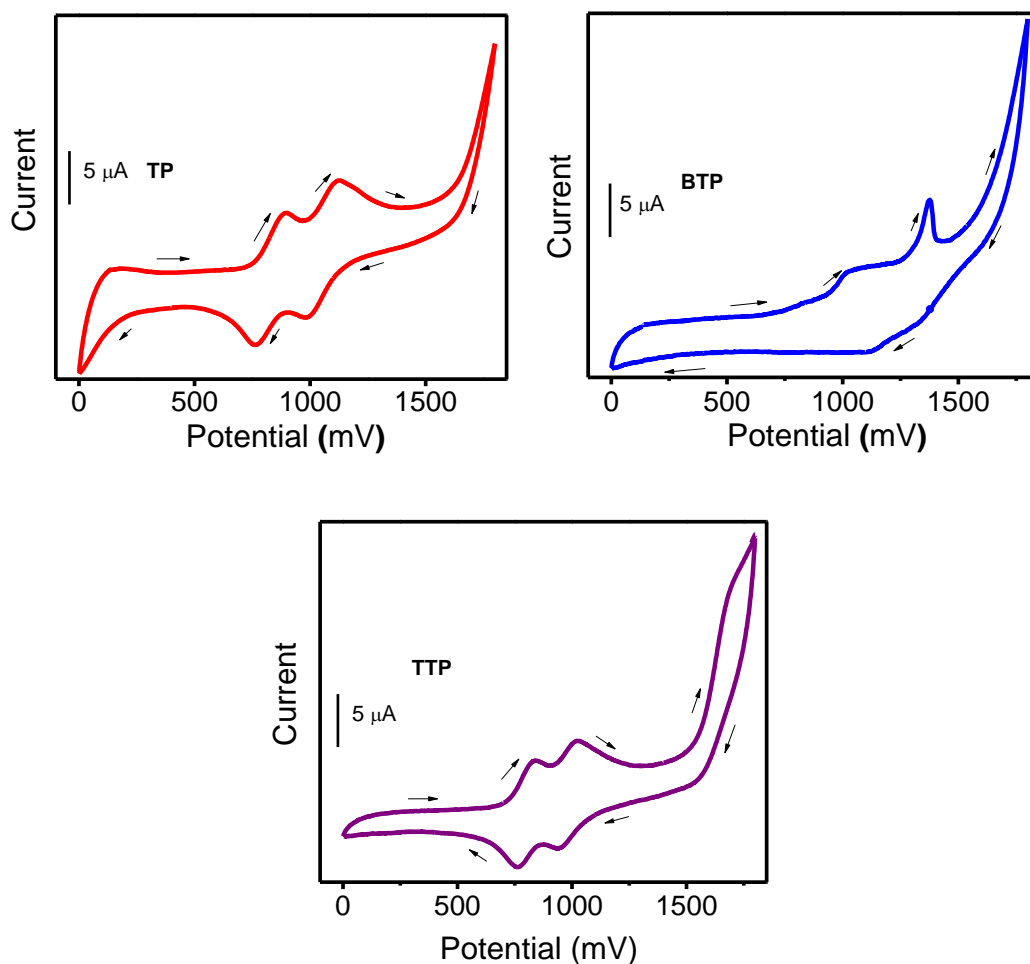
**Figure 5.5** Cyclic voltammogram vs Ag/AgNO₃ of **TP**, **BTP** and **TTP** (0.3 mM conc.).

To evaluate the thermodynamic possibility of electron transfer from the excited dye molecules to the conduction band of TiO₂, cyclic voltammetric

experiments were performed in DCM solution using 0.1 M tetrabutylammonium hexafluorophosphate as the supporting electrolyte, Pt as the counter electrode and $Ag/AgNO_3$ as the reference electrode (**Figure 5.5**). The reference electrode was calibrated by using a ferrocene/ferrocenium (Fc/Fc^+) redox couple as an external standard.

The first half wave potential of **TP** was obtained at 0.82 V *vs.* $Ag/AgNO_3$ and 0.33 V *vs.* Fc/Fc^+. All the potentials measured were converted to NHE considering Fc/Fc^+ as +0.765 V *vs.* NHE in DCM.[15] The ground state oxidation potential of **TP** was calculated to be 1.09 V *vs.* NHE, which corresponds to the HOMO level. Similarly, a value of 0.99 V and 0.80 V *vs.* $Ag/AgNO_3$ was obtained which corresponds to the HOMO level of 1.26 and 1.06 V *vs.* NHE for **BTP** and **TTP**, respectively**.** HOMO value was lowest for **TTP** which shows that the dye undergoes easy oxidation, which must be due to the strong electron donating thienothiophene unit. The band gap energies (E_{0-0}) were estimated to be 1.96, 1.87 and 1.81 eV for **TP**, **BTP** and **TTP**, respectively using the method described previously. The excited state potentials of the dyes were calculated from E_{HOMO} - E_{0-0} and the values obtained were -0.87, -0.61 and -0.75 V *vs.* NHE for **TP**, **BTP** and **TTP** respectively, which corresponds to its LUMO level.

The HOMO and LUMO electronic levels of the dyes should match with the conduction band edge of TiO_2 and the redox potential of the iodine for using the

dyes in DSSC devices. Moreover, the energy gap between the LUMO level of the dyes and the conduction band of TiO_2 should be at least 0.2 eV.[16] Analyzing the HOMO and LUMO values, we can see that there is sufficient driving force for electron transfer from **TP** and **TTP** to the conduction band edge of TiO_2, which comes around 0.41 and 0.25 eV, respectively. But the energy gap between the LUMO of **BTP** and conduction band of TiO_2 is only 0.16 eV, which is less than the needed driving force. Detailed absorption, emission and electrochemical parameters of the dyes are shown in **Table 5.1**.
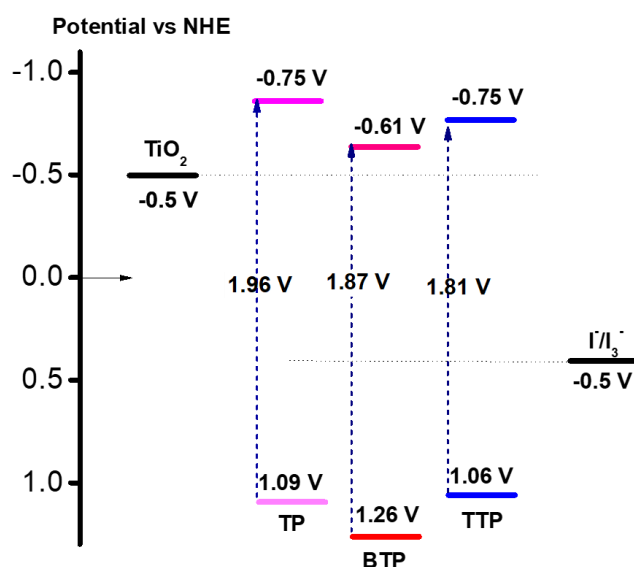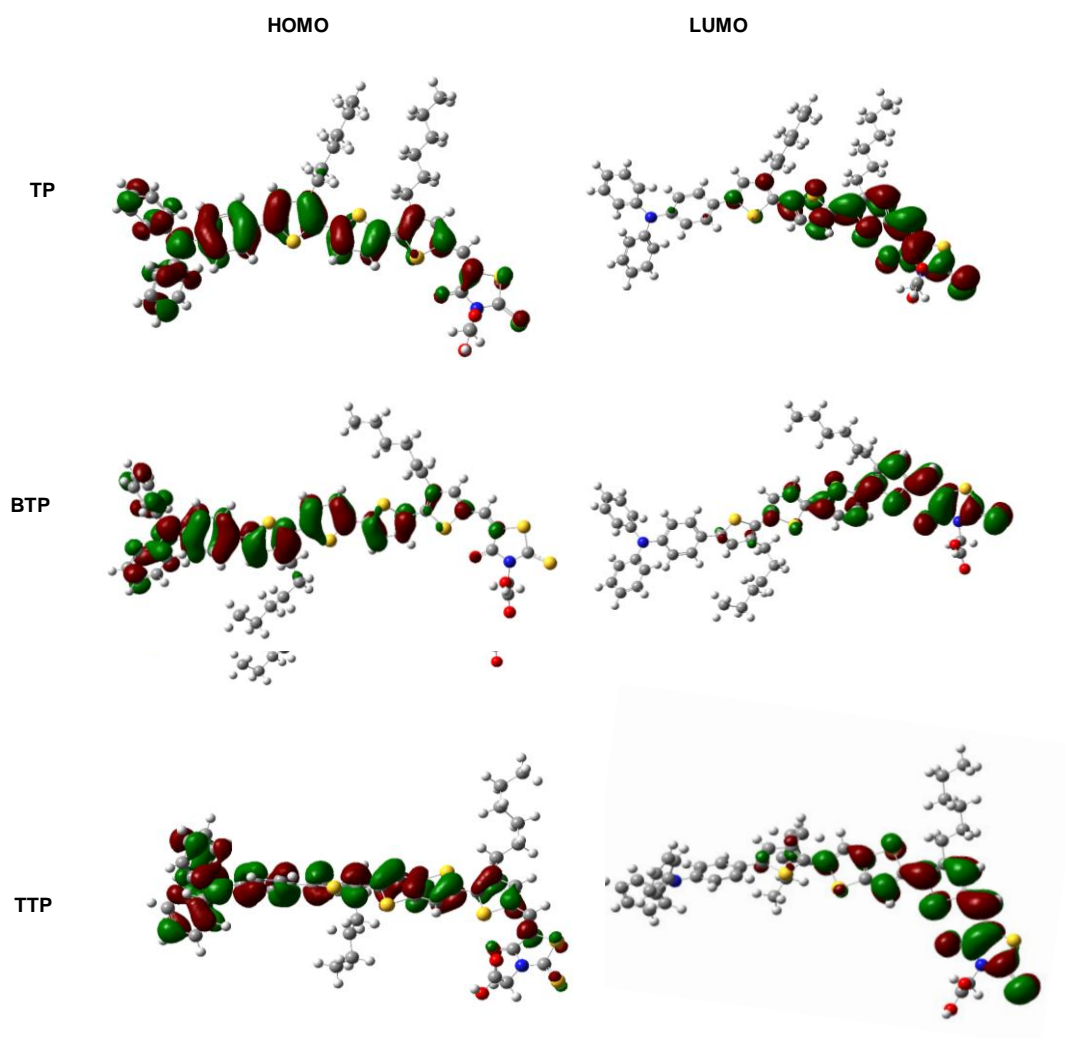

Figure 5.6 Scheme showing the energetics of TiO_2/dye/redox electrolyte interface.

Table 5.1 Absorption, emission and electrochemical parameters of **TP**, **BTP** and **TTP** in DCM.

Dyes	λ_{abs} (nm)	ε ($M^{-1}cm^{-1}$)	E_{0-0} (eV)	E_{HOMO} (V vs NHE)	E_{LUMO} (V vs NHE)

|					
TP	382,503	34530	1.96	1.09	-0.87
BTP	401,505	32950	1.87	1.26	-0.61
TTP	392,530	32000	1.81	1.06	-0.75

5.3.4. DFT Calculations

Figure 5.7 Distribution of the HOMO and LUMO of the dyes in the energy minimized state.

Density functional theory (DFT) calculations at the B3LYP/6-31G* level were performed to understand the electronic structure of the dyes using Gaussian 09 program. The optimized HOMO and LUMO topologies for the dyes are shown in **Figure 5.7**. HOMO is mainly located on the triphenylamine unit extending to the spacer unit, while the LUMO is mainly located on the rhodanine unit with slight extension to the spacer unit. There is an overlap of HOMO and LUMO orbitals along the π-bridge thus facilitating the electronic communication between the donor and acceptor moieties.

5.3.5. Photovoltaic properties

DSSCs were fabricated using these dyes as photosensitizer in presence of **CDCA** as co-adsorbent. The electrolyte composition consists of mixed solution of 0.6 M BMII, 0.1 M LiI, 0.05 M I$_2$ and 0.5 M TBP.
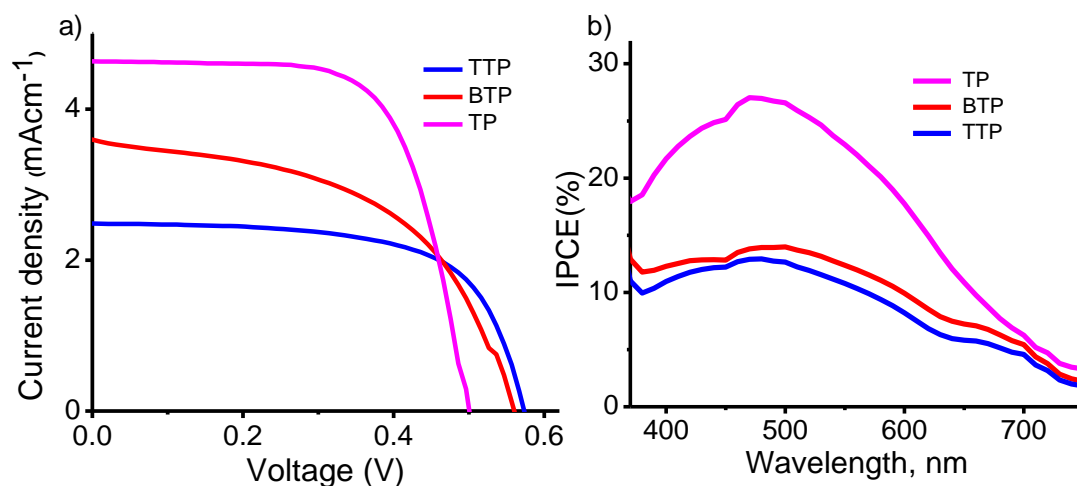
Figure 5.8 (a) Current-voltage characteristics (b) IPCE of DSSCs sensitized by dyes in the presence of **CDCA**, under AM1.5 irradiation.

Photocurrent-voltage (*J-V*) characteristic curves for the devices based on these dyes in the presence of **CDCA** are shown in **Figure 5.8a** and corresponding IPCE are shown in **Figure 5.8b**. The detailed parameters such as short circuit current density (J_{SC}), open-circuit voltage (V_{OC}), fill factor (*FF*) and photovoltaic conversion efficiency (η) are summarized in **Table 5.2**. The efficiency of **TP** based device exhibits a slightly higher value (PCE = 1.5%; J_{SC}: 4.61 mA cm^{-2}, V_{OC}: 0.5 V, *FF*: 0.65) than the other devices. Under the same fabrication conditions, **BTP** (PCE = 1.02%; J_{SC}: 3.6 mAcm^{-2}, V_{OC}: 0.56 V, *FF*: 0.51) and **TTP** (PCE = 0.98%; J_{SC}: 2.48 mAcm^{-2}, V_{OC}: 0.57 V, *FF*: 0.64) exhibits lower efficiency compared to **TP**. On increasing the length of spacer unit from thiophene to bithiophene unit, the open circuit voltage was increased slightly, whereas, the J_{SC} and *FF* values were reduced leading to a reduction in the photovoltaic efficiency. Changing the spacer unit from thiophene to a rigid thienothiophene unit the J_{SC} value was considerably reduced although not much change was observed in the V_{OC} and *FF* values.

Table 5.2 Photovoltaic performance parameters of the dyes.

Dye	J_{SC} (mAcm^{-2})	V_{OC} (V)	FF	η (%)
TP	4.61	0.5	0.65	1.5
BTP	3.6	0.56	0.51	1.02
TTP	2.48	0.57	0.64	0.98

Illumination: 100 mWcm^{-2} simulated AM 1.5G solar light; composition of electrolyte: 0.6 M BMII, 0.1 M LiI, 0.05 M I$_2$, 0.5 M TBP.

Incident photon-to-current conversion efficiencies of the devices in the presence of **CDCA** are shown in **Figure 5.8b**. The results of IPCE measurements were in accordance with the photovoltaic performances. Solar cells based on **TP** exhibited action spectra in the range of 380-700 nm with the highest IPCE value of 27% at 480 nm, **BTP** with highest value of 14% and **TTP** 12% at 480 nm with **CDCA**. Although all the three dyes exhibited a broader action spectrum, the IPCE values were relatively low, which resulted in lower photocurrent densities.
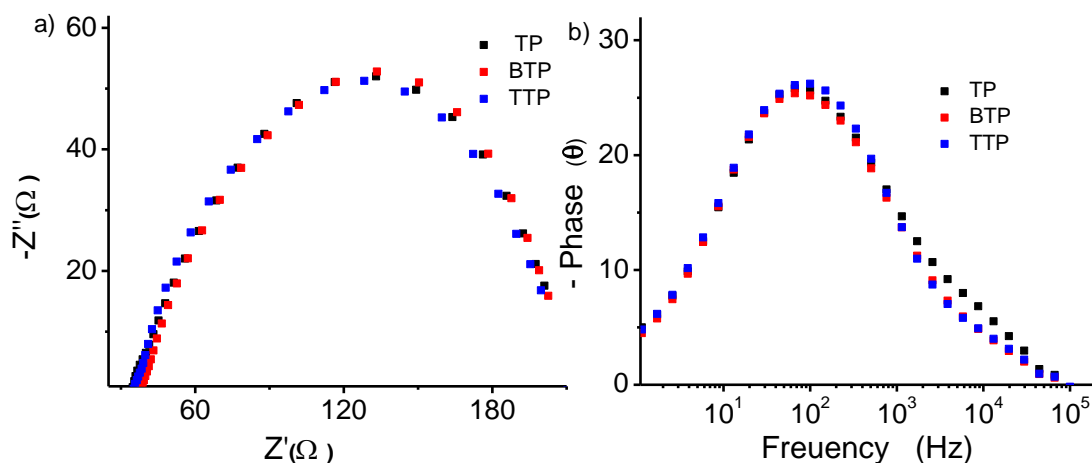
Figure 5.9 (a) EIS Nyquist plot and (b) Bode plot for DSSC devices made from dyes measured at -0.65 V in forward bias in the dark.

EIS was carried out to study the effect of binding groups on electron recombination and lifetime. Impedance was measured over the frequency range of 0.1-10^5 Hz in dark under a forward bias of -0.7 V. The Nyquist and Bode plots obtained are given in **Figure 5.9**.

Table 5.3 Parameters obtained by fitting the impedance spectra using equivalent circuit

Dye	$^a R_s$ (Ω)	$^b R_{rec}$ (Ω)	$^c f_{max}$ (Hz)	$^d \tau_e$ (μs)	$^e k_{eff}$ $(ms)^{-1}$
TP	34.79	180	66.60	2387.7	0.418
BTP	38.06	172	66.66	2391	0.418
TTP	34.99	174	99.9	1594	0.627

Analysis of the impedance data of the devices helps in gaining detailed understanding on interfacial charge transfer processes and electron lifetimes which are summarized in **Table 5.3**. The parameters given in **Table 5.3** were calculated from following literature procedures.[22] In **Table 5.3**, R_s represents series resistance which is nearly the same in all the three dyes as we are using the same electrode material and same electrolyte. R_{rec} corresponds to the larger semicircle in Nyquist plot that portray the charge transfer resistance at TiO$_2$/dye/electrolyte interface. The radius of the larger semicircle and hence the R_{rec} values decreased in the order **TP** (180 Ω) > **TTP** (174 Ω) > **BTP** (172 Ω) which indicates that the device sensitized by **TP** exhibited the largest resistance for recombination between the electrons injected to TiO$_2$ and electrolyte. **TTP** and **BTP** exhibited almost similar values. In the Bode-phase plot, the maximum peak frequency (f_{max}) was indicative of the charge recombination rate. The lifetime of injected electrons τ_e were estimated and the obtained values were summarized in **Table 5.3**. Shift of the peak from higher frequency to lower frequency is indicative of the longer electron lifetime which is highest for **TP** and **BTP** since the frequency maximum and Bode plot is inversely related to

electron lifetime. The lower frequency corresponds to larger charge recombination resistance and longer electron lifetime, which is in agreement with the values shown in **Table 5.3** by fitting the impedance data.[24] This points out to the effective suppression of back electron transfer between the injected electrons and electrolyte for **TP** in comparison to rest of the entries resulting in a lower recombination rate (k_{eff}) giving rise to improved photovoltaic efficiency. The recombination rate follows the order **TP** = **BTP** (0.418 ms) < **TTP** (0.627 ms). Higher electron recombination rate and reduced lifetime of **TTP** compared to other two dyes leads to the lower photovoltaic performance of **TTP** as explained by the equivalent circuit fitted impedance data given in **Table 5.3**. The fitted parameters are in well agreement with the rest of the photovoltaic characterization results.
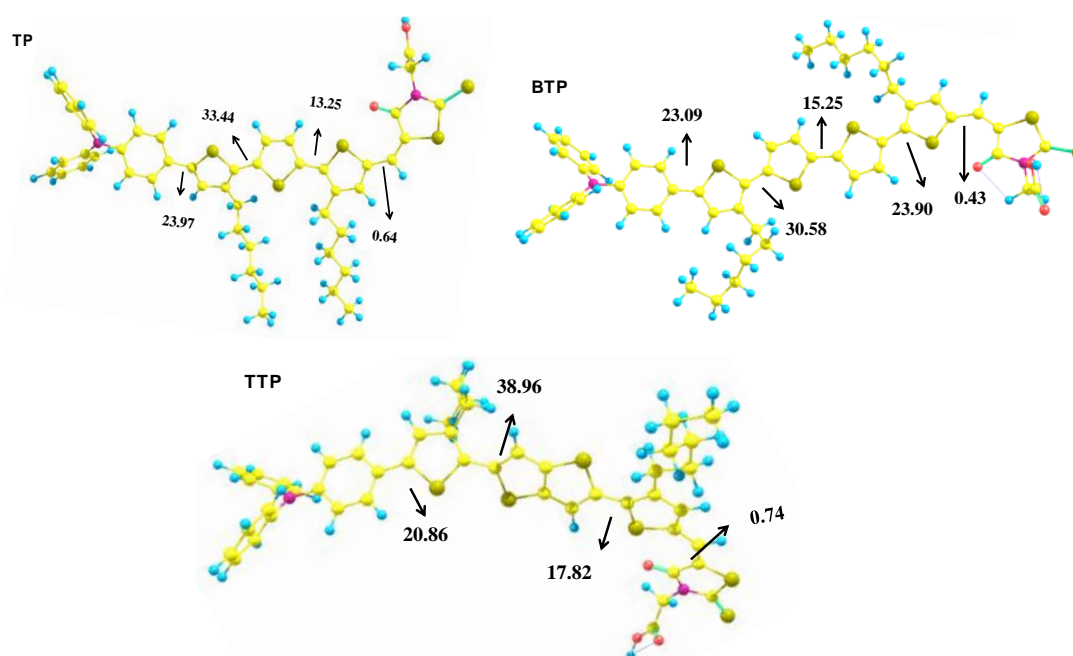
Figure 5.10 Dihedral angle between various units in dyes obtained from DFT calculations

In the previous chapter, in a triphenylamine-bithiazole-rhodanine based system (**Scheme 4.2**), we have obtained a photovoltaic efficiency of 4.4% (**Table 4.2**).[25] In the present system, although the absorption properties were much improved compared to the earlier bithiazole based systems, the photovoltaic efficiency was less. This may be attributed to the lower driving force for electron transfer in the present systems (for **TP**: 0.41 eV, **BTP**: 0.16 eV, **TTP**: 0.25 eV). In addition to that, we examined the dihedral angle of these molecules. The present systems exhibit lesser dihedral angles between the bonds connecting donor, spacer and acceptor, whereas, very high dihedral angles were obtained for the previous systems. Hence aggregation may be prevented in the earlier systems whereas aggregation may not be easily prevented in the present triphenylamine-thiophene based systems which may lead to the lowering of photovoltaic efficiencies.

5.4. Conclusions

Triphenylamine-rhodanine acetic acid based three metal-free organic dyes were designed and synthesized in which the spacer thiophene units were varied *viz.* thiophene (**TP**), bithiophene (**BTP**), thienothiophene (**TTP**). Detailed photophysical, electrochemical and photovoltaic characterization of DSSC devices were carried out. Absorption properties showed that the molecules have

strong absorption with high extinction coefficients in the UV-visible region leading to a better matching with the solar spectrum. Bandgaps were determined from the absorption spectra. From the electrochemical experiments, HOMO and LUMO values of the compounds were determined. Although the absorption properties were better with the bithiophene and thienothiophene derivatives, the photovoltaic properties were found to be better for the thiophene derivative.

5.5. Experimental section

5.5.1. Materials and characterization techniques

The reagents and materials for synthesis were purchased from Sigma-Aldrich, Merck, TCI and Spectrochem chemical suppliers, and are used as received. Air and water sensitive synthetic steps were performed in an argon atmosphere using standard Schlenk techniques. ^{1}H and ^{13}C-NMR spectra were recorded using Bruker-500 MHz spectrometer. The compounds were thoroughly purified using the recycling preparative HPLC system of Japan Analytical Industry Co., Ltd LC-9220 II NEXT SERIES (eluent $CHCl_3$). Absorption spectra were recorded using Shimadzu UV-Visible-2401PC spectrophotometer. Steady-state fluorescence experiments were performed using a SPEX Fluorolog F112X spectrofluorimeter. Cyclic voltammetry experiments were performed using a BAS 50W voltammetric analyser. Density functional theory (DFT) calculations were performed at the B3LYP/6-31G* (d, p) level using Gaussian 09 program.

For the DSSC device fabrication, same method was followed as described in the section **3.5.2**.

5.5.2. Synthesis

Synthesis of 23:
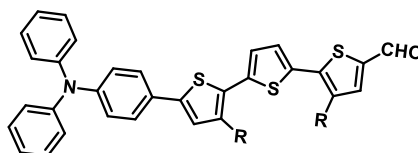
4-(1,3,2-dioxaborinan-2-yl)-N,N-diphenylaniline (94.29 mg, 0.28 mmol), **20** (100 mg, 0.190 mmol), and $Pd(PPh_3)_4$ (2.1 mg, 0.019 mmol) were added to a mixture of degassed toluene (15 mL) and aqueous 2 M K_2CO_3 under nitrogen atmosphere. The mixture was stirred at 110 °C for 48 h. After completion of reaction as monitored by TLC, the mixture was cooled to room temperature, and poured into deionized water (200 mL). The aqueous layer was extracted with dichloromethane. The combined organic layers were washed with water and dried over sodium sulphate. The organic layer was concentrated under vacuum, to obtain an orange coloured solid. The crude product was purified by column chromatography on silica gel (Hexane - Chloroform: 1:1) (Yield: 80.62 %); ^{1}H NMR (500 MHz, $CDCl_3$) : δ 9.827 (s, 1H), 7.596 (s, 1H), 7.460-7.442 (d, 2H, *J* = 9 Hz), 7.288-7.271 (m, 3H), 7.251-7.243 (m, 2H), 7.132-7.113 (m, 5H), 7.077-

7.032 (m, 5H), 2.851-2.773 (m, 4H), 1.714-1.254 (m,16H), 0.909-0.875 (m, 6H);

^{13}C NMR (CDCl$_3$, 125 MHz): 181.55, 181.51, 146.39, 141.57, 140.28, 139.22, 139.11, 138.06, 137.67, 128.32, 126.84, 125.37, 124.83, 124.37, 123.59, 122.48, 122.20, 52.39, 30.68, 30.61, 29.52, 29.28, 28.70, 28.47, 28.26, 28.16, 21.61, 21.58, 13.07, 13.05; HRMS (*m/z*): (M$^+$) calculated for C$_{43}$H$_{45}$NOS$_3$: 687.27; Found: 687.26.

Synthesis of 24:
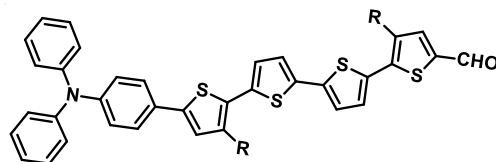
24 was synthesized employing similar procedure as **23** using 4-(1,3,2-dioxaborinan-2-yl)-N,N-diphenylaniline (216 mg, 0.66 mmol), **21** (200 mg, 0.33 mmol), and Pd(PPh$_3$)$_4$ (3.8 mg, 0.033 mmol Yield: 82%); ^{1}H NMR (500 MHz, CDCl$_3$): δ 9.819 (s, 1H), 7.586 (s, 1H), 7.434-7.452 (m, 2H), 7.283-7.111 (m, 10H), 7.066-7.027 (m, 6H), 2.765-2.838 (m, 4H), 1.663-1.703 (m, 8H), 1.254-1.577 (m, 8H), 0.881-0.916 (t, 6H); ^{13}C NMR (CDCl$_3$, 125 MHz): 174.55, 169.41, 167.07, 165.41, 147.57, 143.02, 141.65, 140.55, 139.30, 129.48,129.28,127.93, 126.55, 125.50, 124.76, 123.64, 123.37, 119.21, 117.41, 46.58, 46.13, 45.80, 45.29, 34.32, 32.07, 31.84, 31.76, 31.58, 30.76, 30.46, 30.35, 30.17, 29.83, 29.59, 29.50, 29.42, 29.28, 27.72, 27.47, 25.05, 23.21,

22.83, 22.77,21.51, 20.70, 20.40, 20.10, 19.85, 14.56, 14.25 ; MALDI-TOF-MS

(*m/z*): M$^+$calculated for C$_{47}$H$_{47}$NOS$_4$: 769.25; Found: 769.25.

Synthesis of 25:
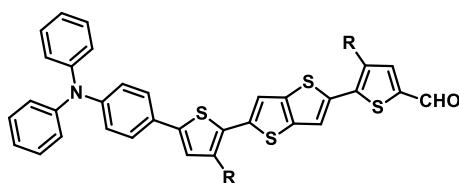
4-(1,3,2-dioxaborinan-2-yl)-N,N-diphenylaniline (42 mg, 0.12 mmol), **22** (50

mg, 0.086 mmol), and Pd(PPh$_3$)$_4$ (0.9 mg, 0.0058 mmol); (Yield: 92%); ^{1}H NMR

(500 MHz, CDCl$_3$): *δ* 9.750 (s, 1H), 7.526 (s, 1H), 7.378-7.361 (m, 2H), 7.324

(s, 1H), 7.207-7.174 (m, 5H), 7.053- 7.034 (m, 4H), 7.004-6.952 (m, 5H), 2.775-

2.701 (m, 4H), 1.347-1.176 (m, 16H), 0.832-0.786 (m, 6H); ^{13}C NMR (CDCl$_3$,

125 MHz): 181.49, 146.51, 146.38, 141.88, 140.50, 140.39, 139.70, 139.64,

139.60, 138.67, 138.03, 137.95, 134.86, 128.32, 128.00, 126.71, 125.37, 124.31,

123.58, 122.45, 122.20, 118.48, 116.23, 30.68, 30.60, 29.61, 29.33, 28.68, 28.61,

28.40, 28.27, 28.15, 21.61, 21.58, 13.07, 13.04; MALDI-TOF-MS (*m/z*): M$^+$

calculated for C$_{60}$H$_{70}$N$_4$O$_2$S$_4$: 743.24; Found: 743.23.

Synthesis of TP:
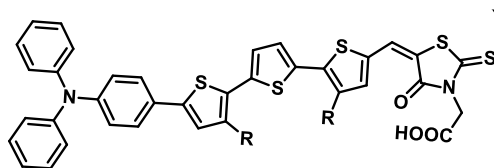
Compound **23** (50 mg, 0.072 mmol), rhodanine-3-acetic acid (139 mg, 0.727 mmol) and few drops of piperidine in chloroform (4 mL) were heated at 60 °C for 12 h. After cooling to room temperature, the mixture was added to water and extracted with chloroform. It was then purified by column chromatography on silica gel (CH$_2$Cl$_2$: EtOH=9:1 v/v) to give a blackish red solid. It was again purified by precipitating from cold methanol (Yield : 60%); ^{1}H NMR (500 MHz, CDCl$_3$): δ 7.807 (s, 1H), 7.426-7.413 (d, 2H, J = 6.5 Hz), 7.266-7.246 (m, 2H), 7.175-7.114 (m, 5H), 7.100-7.038 (m, 9H), 4.857(s, 1H), 2.579 (m, 5H), 1.395-1.254 (m, 16H), 0.883-0.842 (m, 6H); ^{13}C NMR (CDCl$_3$, 150 MHz): δ 175.06, 158.95, 147.52, 147.43, 142.54, 141.26, 141.06, 140.30, 138.52, 137.91, 134.82, 134.08, 129.35, 128.57, 128.23, 127.79, 127.44, 126.38, 126.13, 125.86, 125.43, 124.62, 123.51, 123.23, 100.00, 58.86, 31.71, 31.63, 30.50, 30.25, 29.77, 29.48, 29.29, 29.23, 23.91, 22.64, 22.62, 19.69, 14.12, 14.08, 13.60; MALDI-TOF-MS (*m/z*): (M$^+$+H) calculated for C$_{48}$H$_{48}$N$_2$O$_3$S$_5$: 860.2268; Found: 860.2263.

Synthesis of BTP:
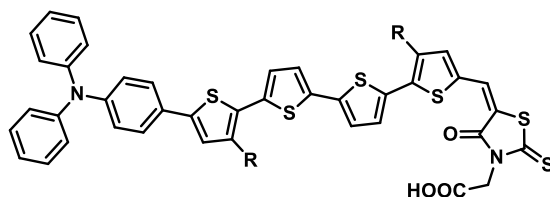
BTP was synthesized employing a similar procedure as TP employing compound **24** (100 mg, 0.129 mmol), rhodanine-3-acetic acid (191.2 mg, 1.29 mmol) and chloroform (4 mL). Purification is done by column chromatography on silica gel (CH$_2$Cl$_2$: EtOH = 9:1 v/v) to give a blackish red solid. Final purification is done by precipitating from cold methanol (Yield: 60%); ^{1}H NMR (500 MHz, CDCl$_3$): δ 7.837 (s, 1H), 7.456-7.439 (d, 2H), 7.288-7.272 (m, 4H), 7.202-7.172 (m, 3H), 7.131-7.115 (m, 5H), 7.070-7.032 (m, 6H), 4.900 (m, 2H), 2.836-2.773 (m, 4H), 1.705-1.254 (m, 16H), 0.904-0.900 (m, 6H); MALDI-TOF-MS (*m/z*): (M$^+$+H) calculated for C$_{52}$H$_{50}$N$_2$O$_3$S$_6$: 943.21; Found: 943.72.

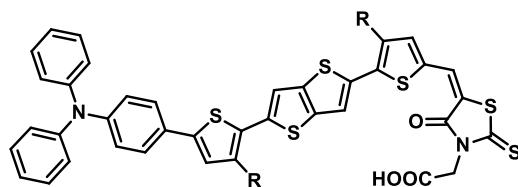*Synthesis of TTP:*

TTP was synthesized employing a similar procedure as TP employing compound **25** (100 mg, 0.129 mmol), rhodanine-3-acetic acid (191.2 mg, 1.29 mmol) and chloroform (4 mL). Purification is done by column chromatography on silica gel (CH$_2$Cl$_2$: EtOH = 9:1 v/v) to give a blackish red solid. Final purification is done by precipitating from cold methanol (Yield : 60%); ^{1}H NMR (500 MHz, CDCl3) : δ 7.90 (s, 1H), 7.468-7.429 (m, 6H), 7.124-7.045 (m, 12H), 4.896 (s, 2H), 2.841-2.79 (m, 4H), 1.677-1.254 (m, 16 H), 0.890-0.77 (m, 6H); ^{13}C NMR (CDCl$_3$, 150 MHz): δ 174.55, 169.41, 167.07, 165.41, 147.57, 143.02,

141.65, 140.55, 139.30, 129.48,129.28,127.93, 126.55, 125.50, 124.76, 123.64, 123.37, 119.21, 117.41, 46.58, 46.13, 45.80, 45.29, 34.32, 32.07, 31.84, 31.76, 31.58, 30.76, 30.46, 30.35, 30.17, 29.83, 29.59, 29.50, 29.42, 29.28, 27.72, 27.47, 25.05, 23.21, 22.83, 22.77,21.51, 20.70, 20.40, 20.10, 19.85, 14.56, 14.25; MALDI-TOF-MS (*m/z*): (M+) calculated for $C_{50}H_{48}N_2O_3S_6$: 916.20; Found: 916.19.

5.6. References

1. Wu, Y.; Zhu, W.; Zakeeruddin, S. M.; Gratzel, M. *ACS Appl. Mater. Interfaces* **2015**, *7*, 9307–9318.
2. Wu, Y.; Zhu, W. *Chem. Soc. Rev*. **2013**, *42*, 2039–2058.
3. Preat, J.; Jacquemin, D.; Perp, E. A. *Energy Environ. Sci*. **2010**, *22*, 891–904.
4. Hagfeldt, A.; Boschloo, G.; Sun, L.; Kloo, L.; Pettersson, H. *Chem. Rev.* **2010**, *110*, 6595–6663.
5. Gratzel, M. *Acc. Chem. Res.***2000**, *33*, 269–277.
6. Zhang, L.; Cole, J. M. *ACS Appl. Mater. Interfaces* **2015**, *7*, 3427–3455.
7. Yang, C.; Liao, S.; Sun, Y.; Chuang, Y.; Wang, T.; Shieh, Y.; Lin, W. *J. Phys. Chem. C* **2010**, *114*, 21786–21794.
8. Sivanadanam, J.; Ganesan, P.; Madhumitha, R.; Nazeeruddin, M.; Rajalingam, R. *J. Photochem. Photobiol. A Chem.* **2015**, *299*, 194–202.
9. Hua, Y.; He, J.; Qin, C.; Han, L.; Zhao, J.; Chen, T.; Wong, W.; Wong, W.; Zhu, X. *J. Mater. Chem. A* **2015**, *3*, 3103–3112.
10. Paramasivam, M.; Chitumalla, R. K.; Singh, S. P. *J. Phys. Chem. C* **2015**, *119*, 17053–17064.
11. Saravanan, C.; Liu, C.; Chang, Y.; Lu, J.; Hsieh, Y.; Rwei, S.; Wang, L. *ACS Appl. Mater. Interfaces* **2012**, *4*, 6133–6141.

12. Kanato, H.; Takimiya, K.; Otsubo, T.; Aso, Y.; Nakamura, T.; Araki, Y.; Ito, O. *J. Org. Chem.* **2004**, *69*, 7183–7189.

13. Yue, J.; Sun, S.; Liang, J.; Zhong, W.; Lan, L.; Ying, L.; Huang, F.; Yang, W.; Cao, Y. As Featured In : *J. Mater. Chem. C* **2016**, *4*, 2470–2479.

14. Wang, P.; Humphry-baker, R.; Zakeeruddin, S. M.; Gratzel, M. *J. Am. Chem. Soc.* **2005**, *127*, 808–809.

15. Robson, K. C. D.; Sporinova, B.; Koivisto, B. D.; Schott, E.; Brown, D. G.; Berlinguette, C. P. *Inorg. Chem.***2011**, *50*, 6019–6028.

16. Wu, Y.; Zhu, W. *Chem. Soc. Rev.* **2013**, *42*, 2039–2058.

17. Wu, G.; Kong, F.; Zhang, Y.; Zhang, X.; Li, J.; Chen, W.; Liu, W.; Ding, Y.; Zhang, C.; Zhang, B. *J. Phys. Chem. C* **2014**, *118*, 8756–8765.

18. Cisneros, R.; Beley, M.; Fauvarque, J.; Lapicque, F. *Electrochim. Acta* **2015**, *171*, 49–58.

19. Cheol, B.; Seok, M.; Ju, M.; Hoon, D.; Ahn, K.; Hong, J. *Synth. Met.* **2014**, *188*, 130–135.

20. Adachi, M.; Sakamoto, M.; Jiu, J.; Ogata, Y.; Isoda, S. *J. Phys. Chem. B* **2006**, *110*, 13872–13880.

21. Fakharuddin, A.; Ahmed, I.; Wali, Q.; Khalidin, Z.; Yosuff, M. M.; Rajan, J. *Adv. Mater. Res.* **2014**, *925*, 553–558.

22. Jia, H.; Zhang, M.; Ju, Z.; Zheng, H.; Ju, X. *J. Mater. Chem. A* **2015**, *3*, 14809–14816.

23. Bisquert, J.; Zaban, A.; Greenshtein, M. *J. Am. Chem. Soc.* **2004**, *13*, 13550–13559.

24. Jia, H.; Zhang, M.; Ju, Z.; Zheng, H.; Ju, X. *J. Mater. Chem. A* **2015**, *3*, 14809–14816.

25. Panicker, J. S.; Balan, B.; Soman, S.; Nair, V. C. *Sol. Energy* **2016**, *139*, 547–556.

LIST OF PUBLICATION

1. Thiophene-bithiazole based metal-free dye as DSSC sensitizer: Effect of co-adsorbents on photovoltaic efficiency; **Jayanthy S. Panicker**, Bijitha Balan,* Suraj Soman,* Tanwistha Ghosh and Vijayakumar C. Nair; *J. Chem. Sci.* **2016**, *128*, 101-110.

2. Understanding structure-property correlation of metal free organic dyes using interfacial electron transfer measurements; **Jayanthy S. Panicker**, Bijitha Balan,* Suraj Soman,* and Vijayakumar C. Nair; *Solar Energy* **2016**, *139*, 547-556.

3. Synthesis and optoelectronic properties of thiophene based semiconducting oligomers; Bijitha Balan,* **Jayanthy S. Panicker**, Shinji Nagasawa, Akinori Saeki* and Vijayakumar C. Nair; *Chem. Select,* **2016**, *1*, 6872-6879.

4. Self-assembled organic materials for photovoltaic application; Tanwistha Ghosh, **Jayanthy S. Panicker** and Vijayakumar C. Nair*; *Polymers* **2017**, *9*, 112.

5. Investigation on the effect of thiophene based electron donor π-spacers on the photovoltaic properties of rhodanine-anchored metal-free dyes for DSSC; **Jayanthy S. Panicker**, Bijitha Balan,* Suraj Soman,* Sourav C. Pradhan, Tanwistha Ghosh, Narayanan Unni and Vijayakumar C. Nair*; (*To be communicated*)

6. Fumaronitrile-triphenylamine derivative for electrochromic device application; **Jayanthy S. Panicker,** Sajitha Surendarn, Bijitha Balan, Biswapriya Deb, and Vijayakumar C. Nair* (*Manuscript under preparation*).